Jukka Manninen

STRUCTURAL CONTROL OF THE OROGENIC GOLD DEPOSITS IN KULLAA, SW FINLAND

Geologian pro gradu -tutkielma

Turku 2020

TURUN YLIOPISTO
Department of Geography and Geology, Geology section

MANNINEN, JUKKA: Structural control of the orogenic gold deposits in Kullaa, SW Finland.

MSc thesis, 81 p. + 4 appendix pp.
Geology and mineralogy
May 2020

The Pomarkku block in SW Finland comprises four known orogenic gold mineralizations in the vicinity of Kullaa municipality. Previous studies have focused on the geochemical features of the mineralizations whereas the structural setting and interpretation on both regional and target-scale has remained ambiguous. The primary objective in this study is to define the controlling structures for the known mineralizations and compare them with the tectonic evolution in Southern Finland. The secondary objective is to define the age of peak metamorphism in the area. New structural measurements and field observations were collected from the study area and were used with geophysical data to divide the study area into seven internally coherent structural domains, each comprising distinctive structural features. Domains I-III host ENE-WSW -orientations whereas Domains IV-VII host NE-SW -oriented structures. The ENE-WSW -oriented structures in the northern part of the study area comprise of L- and L>S-tectonites with coaxial strain accounting for the formation of these structures whereas non-coaxial strain is concentrated in narrow zones. Gently overturned fold geometries with fold axes plunging towards ENE and WSW are characteristic for the northern part. The central part of the study area hosts the gold mineralizations in NE-SW -oriented structures formed under NW-SE -oriented transpressional regime. Non-coaxial strain and S>L -tectonites dominate the central parts of the study area where the characteristic folds are upright and attributed to non-coaxial deformation with associated lithological changes and heterogeneity. Two NE-SW -oriented vertical strike-slip zones with apparent right-lateral kinematics and the intervening high-strain zone forms the main structural framework in the central area. Geochemical classification of plutonic units displays dominant granodioritic to dioritic composition. The trace element analysis indicates distinct subduction-type patterns. Age determinations from the leucosome close to the Välimäki prospect yielded concordia ages of 1886.8 ± 6.1 Ma for the zircon and 1799.2 ± 3.8 Ma for the monazite. The zircon ages represent the peak metamorphism in the area and associated migmatization. Approximately 90 Ma younger monazite ages represent a later thermal pulse and the formation of monazite grains is correlated with hydrothermal activity. Two mineralization events are identified: i) the c. 1885 Ma peak metamorphic event and ii) the younger, 1.80 Ga hydrothermal event. Emplacement of foliation-parallel veining is correlated to peak metamorphism. The younger event at an ESE-WNW compressional regime led to reactivation of NE-SW-oriented structures in the brittle-ductile boundary and emplacement of auriferous veins in narrow shear zones and secondary tensional fractures.

Keywords: structural geology, strain partitioning, geochronology, geochemistry, orogenic gold

TURUN YLIOPISTO
Maantieteen ja geologian laitos, geologian osasto

MANNINEN, JUKKA: Structural control of the orogenic gold deposits in Kullaa, SW Finland.

Pro gradu -tutkielma, 81 s. + 4 liites.
Geologia ja mineralogia
Toukokuu 2020

Pomarkun lohko sisältää neljä tunnettua kultamineralisaatiota Kullaan kunnan alueella. Aikaisemmat tutkimukset alueella ovat keskittyneet geokemiallisiin piirteisiin, kun taas rakennegeologinen viitekehys sekä tulkinta on jäänyt epäselväksi. Tutkimuksen ensisijainen tavoite on määrittää kultamineralisaatioita kontrolloivat rakenteet ja rinnastaa nämä Etelä-Suomen tektonisen kehityksen kanssa. Toissijainen tavoite on määrittää alueellisen metamorfisen huipun ikä. Tutkimusalueelta kerättiin uusia rakennegeologisia mittauksia sekä kenttähavaintoja, joita hyödynnettiin yhdessä geofysikaalisen aineiston kanssa alueen jaottelussa rakennegeologisiin yksilöllisiin alayksiköihin. Alayksiköt I-III koostuvat ENE-WSW -suunnista ja alayksiköt IV-VII NE-SW -rakenteellisista suunnista. ENE-WSW -suuntaiset rakenteet tutkimusalueen pohjoisosissa koostuvat L- ja L>S -tektoniiteista, jotka ovat muodostuneet koaksiaalisen muodonmuutoksen seurauksena, kun taas ei-koaksiaalinen muodonmuutos on jakautunut kapeisiin vyöhykkeisiin. Loivasti ylikääntyneet poimurakenteet, joiden poimuakselit kaatuvat loivasti ENE ja WSW -suuntiin, ovat tunnusomaisia alueen pohjoisosille. Kultamineralisaatiot tutkimusalueen keskiosissa ovat asemoituneet NE-SW -suuntaisiin, NW-SE -suuntaisen transpressionaalisen vaiheen aikana muodostuneisiin rakenteisiin. Ei-koaksiaalinen muodonmuutos ja S>L -tektoniitit dominoivat tutkimusalueen keskiosia ja alueelle tyypilliset pystyasentoiset poimurakenteet rinnastettiin ei-koaksiaaliseen muodonmuutokseen yhdessä litologisen heterogeenisyyden kanssa. Kaksi oikeakätistä NE-SW -suuntaista pystysuoraa sivuttaissiirrosta ja niiden välinen korkean muodonmuutoksen vyöhyke muodostavat rakenteellisen viitekehyksen alueen keskiosille. Plutoniset yksiköt ovat geokemiallisen koostumuksen perusteella granodioriittisesta dioriittisia ja hivenaineanalyysi osoitti selkeitä subduktiotyypin piirteitä. Leukosomin ikämääritys tuotti concordia-iän 1886.8 ± 6.1 Ma zirkoni-mineraaleille ja 1799.2 ± 3.8 Ma monatsiitti-mineraaleille. Zirkoni-iät edustavat alueellista metamorfista huippua sekä migmatisoitumista. Noin 90 Ma nuoremmat monatsiitti-iät edustavat myöhäisempää termistä pulssia, jossa monatsiittien muodostuminen rinnastettiin hydrotermiseen aktiivisuuteen. Tutkimuksessa tunnistettiin kaksi mineralisaatiotapahtumaa, jotka ovat i) 1885 Ma metamorfinen huippu sekä ii) nuorempi, 1.80 Ga hydroterminen tapahtuma. Liuskeisuuden suuntaisen juonituksen asettumisen todettiin korreloivan metamorfisen huipun kanssa. Nuorempi, ESE-WNW -suuntainen kompressionaalinen tapahtuma hauras-duktiili -rajapinnalla johti NE-SW -suuntaisten rakenteiden reaktivoitumiseen ja kultapitoisten juonien asettumiseen kapeisiin hiertosaumoihin ja avautuneisiin rakoihin.

Avainsanat: rakennegeologia, muodonmuutoksen jakautuminen, geokronologia, geokemia, orogeeniset kultamalmit

Table of Contents

1. Introduction

1.1. Orogenic gold

Orogenic gold deposits can be described as a coherent group characterized by several geochemical and geological features, such as the tectonic setting and active fluid flow (Goldfarb et al., 2000). The deposits have formed during collisionary or accretionary tectonic events in a convergent setting (Groves et al., 1998). The most consistent characteristic feature of the orogenic deposit type is the spatial association of the deposits to the metamorphic terranes and the presence of crustal-scale shear zones with the related second and third order structures (Groves et al., 1998). McCuaig and Kerrich (1998) note that the orogenic gold deposits are epigenetic and form during peak metamorphism or soon after it, following a clockwise P-T-t -path. Other distinctive feature to orogenic gold deposits is hydrothermal alteration related to the presence of ore-bearing fluids (Groves et al., 1998).

1.1.1. Hydrothermal fluids and alteration

Whereas the tectonic setting of accretionary to collisional orogenic terranes is a generally agreed feature with very few exceptions, other related features such as the fluid pathways, metal and fluid source, relative timing, and the depositional mechanisms has been controversial (Groves et al., 2018). According to Sibson et al. (1988), brittle and ductile faults and shear zones act as pathways for auriferous fluids. As the fluid pressure in these structures reaches or exceeds the lithostatic pressure, the usually high-angle reverse fault reactivates causing fracture permeability to increase, resulting into fluid flow towards the surface (Sibson et al., 1988). A slightly different model is used in strike-slip settings, in which dilational jogs are formed in the step-over setting, creating pressure minimums and open spaces for fluid transportation and precipitation (Sibson, 1987).

In most studies, the source for the gold-bearing fluid has been defined as metamorphic (Goldfarb & Groves, 2015) although the source is largely controversial. Two primary sources for the auriferous fluids have been defined: (i) metamorphic; fluids are released during metamorphism from underlying basins (Goldfarb & Groves, 2015) and (ii) magmatic; de-volatilization of the sedimentary unit overlying in the subducting slab and following felsic intrusions (Groves & Santosh, 2016). A third model of metamorphic-magmatic fluid mixing has also been proposed (e.g. Molnár et al., 2016; Neumayr et al., 2008; Walshe et al., 2003). Goldfarb & Groves (2015) note that this mixing model should be ruled out due to the over pressurisation of the ore-bearing fluid and as a consequence

the metamorphic fluids would be driven out of the system, not mixed with the fluids from the magmatic source. However, the source of the fluids from an exploration perspective is somewhat irrelevant as the gold mineralizations are a widespread feature in an orogenic belt (Groves et al., 2018). The key factor from an exploration point of view is in the placement of economically viable deposits in the hosting structures (Hronsky & Groves, 2008).

In orogenic settings, gold is transported as a reduced sulphur complex with low-salinity H_2O-CO_2±$CH4$±N_2 ore fluids (Groves et al., 1998; Groves et al., 2000). As the metamorphic grade is strongly correlated to the alteration mineralogy, the fluid solution transporting the gold also changes with the metamorphic facies. In greenschist facies, gold is transported as $Au(HS)^-_2$ and under amphibolite facies as $AuHS^0$ (e.g. Mikucki & Groves, 1990). According to McCuaig & Kerrich (1998), the destabilization of the gold-bearing fluid and following deposition of gold can take place in numerous processes: i) cooling of the fluid; ii) oxidation of the fluid; iii) reduction of the fluid; iv) increasing the pH of the fluid and v) lowering the ∑S in the fluid. These precipitation events can occur by one or several methods: i) P-T -changes in the plumbing system; ii) chemical reactions with the wall rock; iii) momentary pressure fluctuations and following phase inequilibrium; iv) fluid mixing and v) chemsorption (McCuaig & Kerrich, 1998).

The hydrothermal fluids discussed above flow through the host rock in the vicinity of fluid pathways forming alteration zones with widths up to hundreds of meters in suitable host lithology (Bierlein & Maher, 2001) although in some orogenic gold deposits significant alteration is non-existent (Goldfarb et al., 2005). As the fluids move towards the surface in suitable pathways (Figure 1), they approach thermal, isotopic and chemical equilibrium with the host rock forming alteration zones in the host rock (McCuaig & Kerrich, 1998). This metasomatic alteration is controlled by two processes: the fluids flow along fractures/microcracks of different scales or the ions flow through static pore fluids. The hydrothermal alteration forms lateral zones parallel with the fluid conduit with variable alteration mineralogy in the proximal and distal parts of the zone (Eilu & Groves, 2001). The alteration mineralogy is dependent on the fluid/rock ratios together with the geometry of the plumbing system and associated deformation mechanisms dictating the fluid access to the wall rock (McCuaig & Kerrich, 1998).

1.1.2. Structural features

The structural geometry of orogenic gold deposits is dominantly in the second- and third order structures controlled by the regional structures whereas the associated large-scale crustal shear zones or faults have controlled the fluid flow in the region (Groves et al., 2000). The gold deposits are most commonly a down-plunging, continuous feature extending from hundreds of meters up to 2.5 kilometres (Groves et al., 2000). The hosting structures are most commonly ductile to brittle (Figure 1), highly variable in type, such as reverse, oblique or strike-slip faults or fracture arrays commonly hosting a syn- or post mineralization displacement (Groves et al., 2000; Ojala et al., 1993). Flat-lying extensional quartz veins and mutually cross-cutting steep fault-related veins form during cyclic fault-valve fluid pressure fluctuations, forming common features in many deposits (Sibson et al., 1988; Miller et al., 1994).

According to Groves et al. (2018), the relative timing for the precipitation of auriferous fluids within the structural evolution of the orogenic belt is a crucial constraint. The relationship between the tectonic evolution and the precipitation of gold has to be taken into account as the pre-existing structural features formed during earlier tectonic events can be reactivated during the transition from compressional to transpressional (Groves et al., 2018). Therefore, the pre-existing reactivated structures can also be mineralized in addition to syn-gold structures, highlighting the importance of structural geometry instead

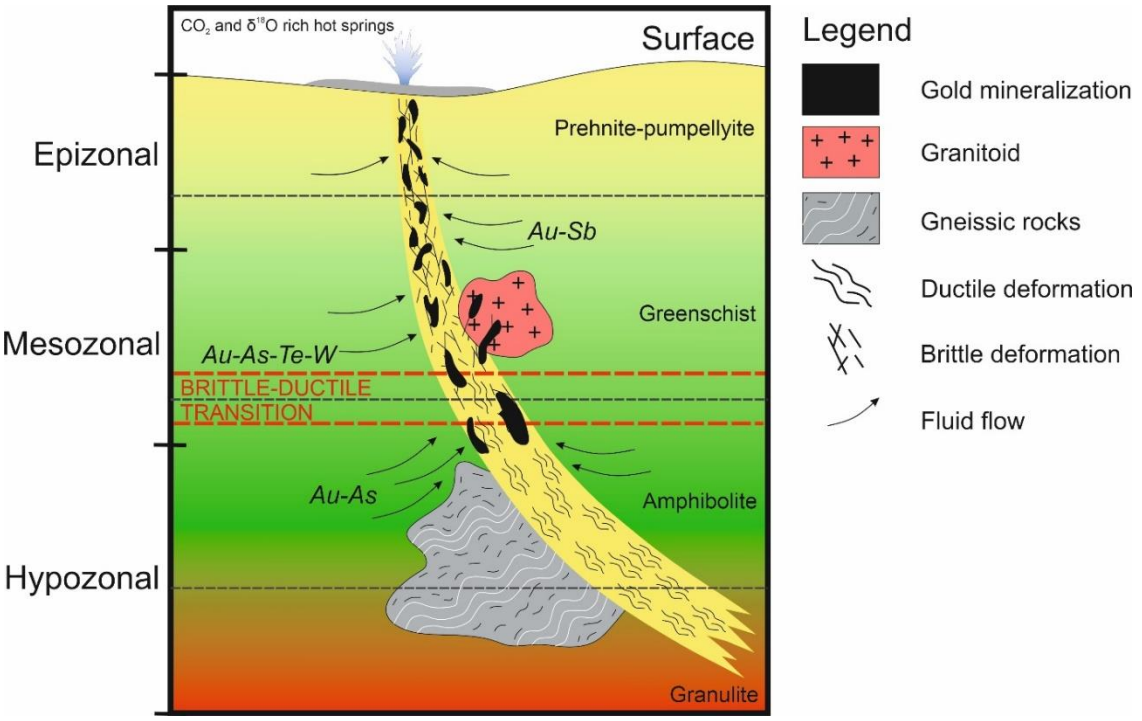

Figure 1: Schematic diagram of orogenic gold deposits in different metamorphic and deformation conditions and the change in gold-associated mineralogy. Modified after Goldfarb & Groves (2015).

of structural history (Groves et al., 2000). This is also crucial within the Svecofennian domain as the crustal evolution consists of several overprinting deformation stages and thermal peaks which should be taken into account (Lahtinen et al., 2011).

1.2. Orogenic gold and tectono-thermal evolution in Finland

The Archean and Paleoproterozoic greenstone belts in Eastern Finland and Lapland display the greatest potential for economic gold deposits (Eilu et al., 2003). The period of time during which orogenic gold deposits are formed cover a large time span, beginning in the Archean roughly at 2.75 Ga (Eilu et al., 2003). These prospects are situated in the Karelian craton where the N-S striking Hattu schist belt hosts several deposits, such as the active gold mine Pampalo (Nurmi & Sorjonen-Ward, 1993; Eilu et al., 2003) and increasing interest in the exploration due to several occurrences of orogenic gold prospects in the area (Kalliomäki et al., 2019). The majority of orogenic gold deposits are however located within the Paleoproterozoic crust, in the Central Lapland greenstone belt (CLGB), the Kuusamo greenstone belt and the Svecofennian domain in Southern Finland (Eilu et al., 2003; Sundblad, 2003). The most remarkable is the Suurikuusikko gold deposit within the CLGB, the biggest gold mine in Europe (Wyche et al., 2015). Within the Svecofennian domain, several known gold deposits including the active Jokisivu mine have been recognized and the recent discoveries of new gold-critical areas highlights the prospectivity of the area.

90 % of the known deposits in Finland are defined as orogenic as they area spatially associated with quartz veins within shear and fault zones though several other types of gold mineralizations, e.g. metamorphosed epithermal and paleoplacer deposits are also recognized (Eilu et al., 2003; Saalmann et al., 2009). For example, Saalmann et al. (2010) has shown that the Jokisivu gold prospect (Figure 2; B) has been impacted by several deformation stages and two high-temperature peaks associated with active fluid flow and gold precipitation. According to Saalmann et al. (2009), previous studies in Finland have however focused on the prospect-scale geochemical and mineralogical features instead of the structural relationships between the gold deposits. As a result, the genetic model within Svecofennian domain for gold mineralizations does not exist (Saalmann et al., 2009). These genetic models can provide a profitable tool for mineral exploration purposes in targeting new areas by enabling a more systematical search (Lahtinen et al., 2011; Saalmann et al., 2009).

The 1.90–1.80 Ga Svecofennian orogeny consists of a single continuous accretionary event in which an island arc complex obliquely collided against the Archean craton (Pajunen et al., 2008), forming suitable tectonic environment for the formation of orogenic gold deposits. Both compressional and extensional tectonics were present and high-temperature – low-pressure -events are correlated to the extensional tectonic settings. Pajunen et al. (2008) divided the Svecofennian orogeny into five events: E1) Collisional event between the island arc system and Archean continent at 1.90–1.88 with N-S contraction; E2) The island arc system collapsed, formation of associated sedimentary rocks and volcanism at 1.88–1.87, strong vertical shortening; E3) N-S oriented collision at 1.88–1.87 and transition into NE-SW transpression and related NW-SE oblique extension; E4) Southern Finland Granitoid zone formed in oblique extensional regime, NE-SW oriented transpression at 1.87-1.80 Ga; E5) Post-tectonic magmatism related to fading of the Svecofennian orogeny at ESE-WNW contraction.

1.3. Study area

Previous research in Kullaa, the present study area, SW Finland has mainly focused on the geochemical features of the mineralizations and the tectonic evolution together with the structural control of the deposits at both regional and target scales have remained ambiguous. In this study we focus on the structural controls of the mineralizations and structural evolution of the study area. The primary objective is to define the controlling structures for the known gold mineralizations utilizing the field data, geophysical data and thin sections for kinematic indicators. The structural setting and the formation of the orogenic gold mineralizations will be related to the evolution of Svecofennian orogeny. The secondary objective is to define the age of the peak metamorphism in the study area. This data provides a good point of comparison to the complex crustal evolution of the area and precipitation of gold in the controlling structures. Whole-rock analyses from plutonic rocks will be utilized in comparing the geochemical features to other of similar kind in the metamorphic belts in Southern Finland.

The study area is located within the Pomarkku block in SW Finland (Figure 2) and is characterized by several known gold occurrences (Kärkkäinen et al. 2016 and references therein) and a complex tectonic history (e.g., Pietikäinen 1994). The SW side of the Pomarkku block is bordered by the crustal-scale Kynsikangas shear zone with sinistral strike-slip kinematics. The more ambiguous Kankaanpää shear zone with gently dipping structural features borders the Pomarkku block in NE. It belongs to the central part of the 1.90–1.80 Ga Svecofennian orogeny and it has been suggested that it is the western

continuation of the high-grade Pirkanmaa Belt (Kähkönen 2005, Nironen et al. 2016, Lahtinen et al. 2017). Metamorphic grade in the study area is within upper amphibole facies (Hölttä & Heilimo, 2017). Northern part of the Pomarkku block consists of nearly linearly E-W trending structures whereas the southern part comprises of more complex, NE-EW trending structures associated with the gold mineralizations.

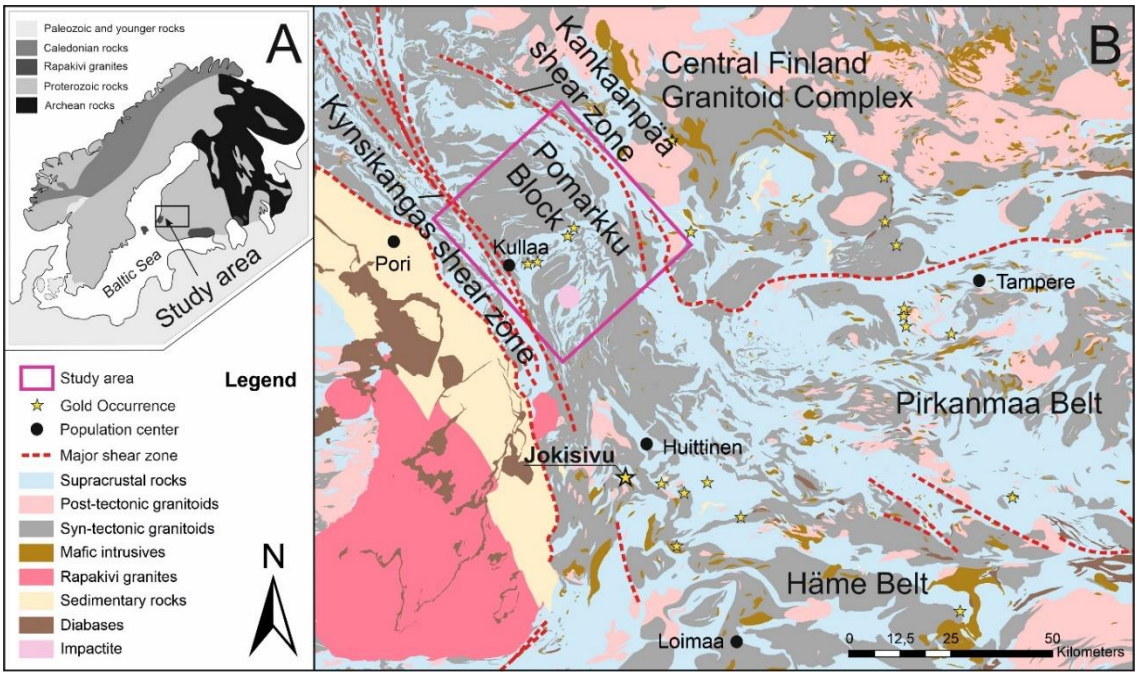

Figure 2: A) Generalized overview of the Fennoscandian Shield. **B)** Generalized lithological map of the study area and SW Finland. Geological data modified after ©Geological Survey of Finland. Modified after Kara et al., 2018.

The study is part of a joint-project between the Geological Survey of Finland (GTK) and the University of Turku focusing on the spatial distribution of the known gold occurrences and their genetic linkage to the evolution of the regional-scale structures and lithologies in SW Finland. The study area has been utilized for a small-scale gold exploration since 1950s by Outokumpu Company (Eilu & Pankka 2009) and more extensively after late 1990s by the Geological Survey of Finland (Kärkkäinen et al. 2012).

2. Geological background

2.1. Fennoscandian shield

The East European Craton (EEC) comprises three crustal segments: Sarmatia, Volgo-Uralia and Fennoscandia (Figure 3). Sarmatia consists of several Archean microcontinents intervened by 2.2–2.1 Ga Paleoproterozoic belts (e.g. Shchipansky & Bogdanova, 1996) and the less known, dominantly Archean Volgo-Uralia is mostly covered by younger lithological units (Bogdanova et al., 2008). The Fennoscandian shield comprises dominantly Archean and Proterozoic gneisses and greenstones with complex tectonic histories. The formation of EEC initiated when the Sarmatian and Volgo-Uralian segments formed Volgo-Sarmatian procraton at 2.10–2.05 Ga (Bogdanova et al., 2008) and formed into its final shape when the Volgo-Sarmatian procraton collided with the Fennoscandian craton at 1.8–1.7 Ga, forming the unified craton (Bogdanova et al., 2008). The original sutures between the three crustal segments were reactivated by rifting, marking the aulacogens at the segment boundaries (Figure 3).

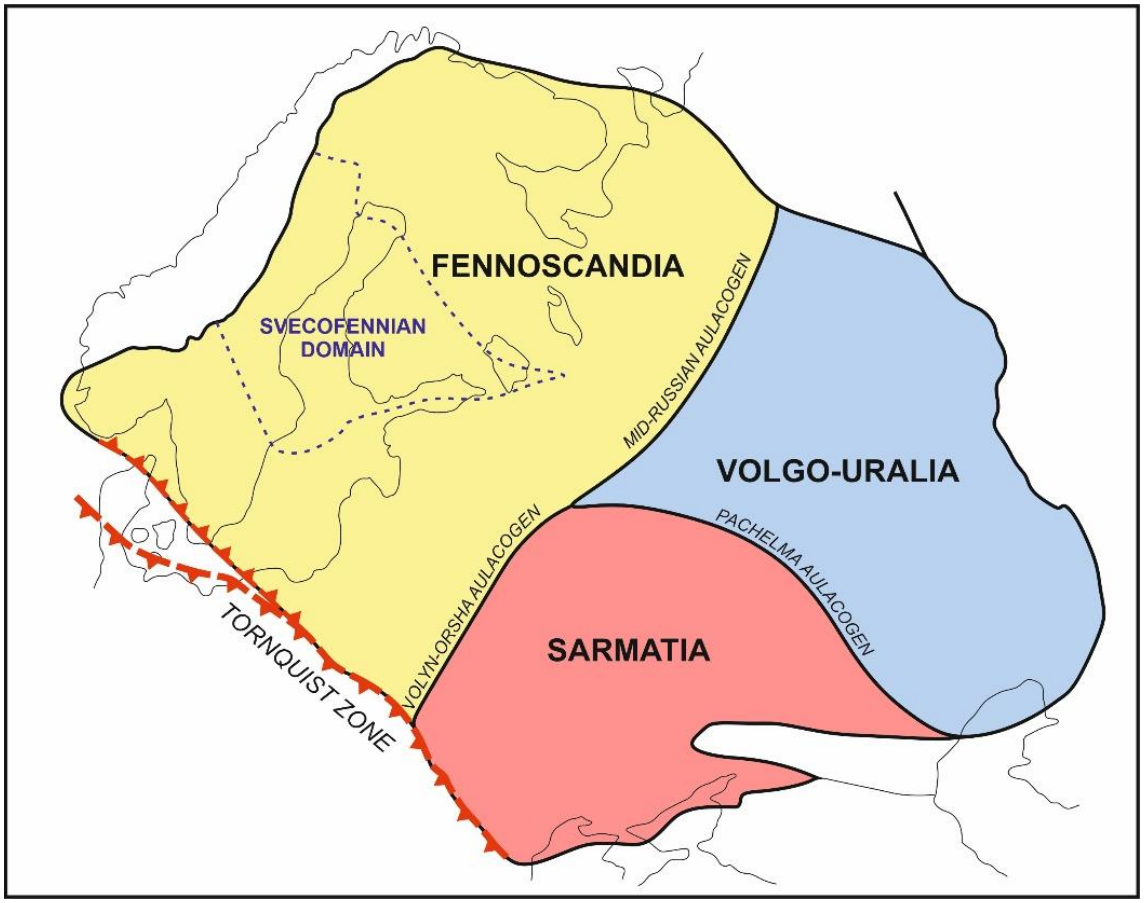

Figure 3: The East European Craton (EEC) and the crustal segments, the Svecofennian domain outlined. Modified after Gorbatschev & Bogdanova (1993).

The Fennoscandian crustal segment, comprising roughly half of the EEC, hosts four domains of different ages: the Archean (3.5–2.5 Ga), Svecofennian (1.95–1.79 Ga) and Sveconorwegian (1140–960 Ma) domains and the Transscandinavian Igneous Belt (TIB, 1.81–1.65 Ga). In short, the Fennoscandian shield includes both rifting and accretionary tectonic events. The accretionary orogenic events of the Paleoproterozoic Era in Fennoscandia can be divided into the 1.94–1.86 Ga Lapland-Kola orogeny (Daly et al., 2006) and the Svecofennian orogeny (e.g. Nironen, 1997).

2.2. Svecofennian orogeny

The Svecofennian domain covers the central and southern parts of Finland and can be subdivided into seven subdomains: the Vaasa and Central Finland Granitoid complexes and the Savo, Tampere, Pirkanmaa, Häme and Uusimaa belts (Figure 4). The Svecofennian rocks are bordered from the Archean rocks in the NE by a NW-SE -trending complex suture zone (Figure 4). According to Lahtinen et al. (2009b), the Svecofennian orogeny can be divided into the linear Lapland-Savo, Svecobaltic and Nordic orogens and the equidimensional Fennian orogeny. The *Lapland-Savo* -orogeny, first of the major accretionary events, can be divided into two segments, the northern and southern segments (Lahtinen et al., 2009b). Northern segment formed during the collision of

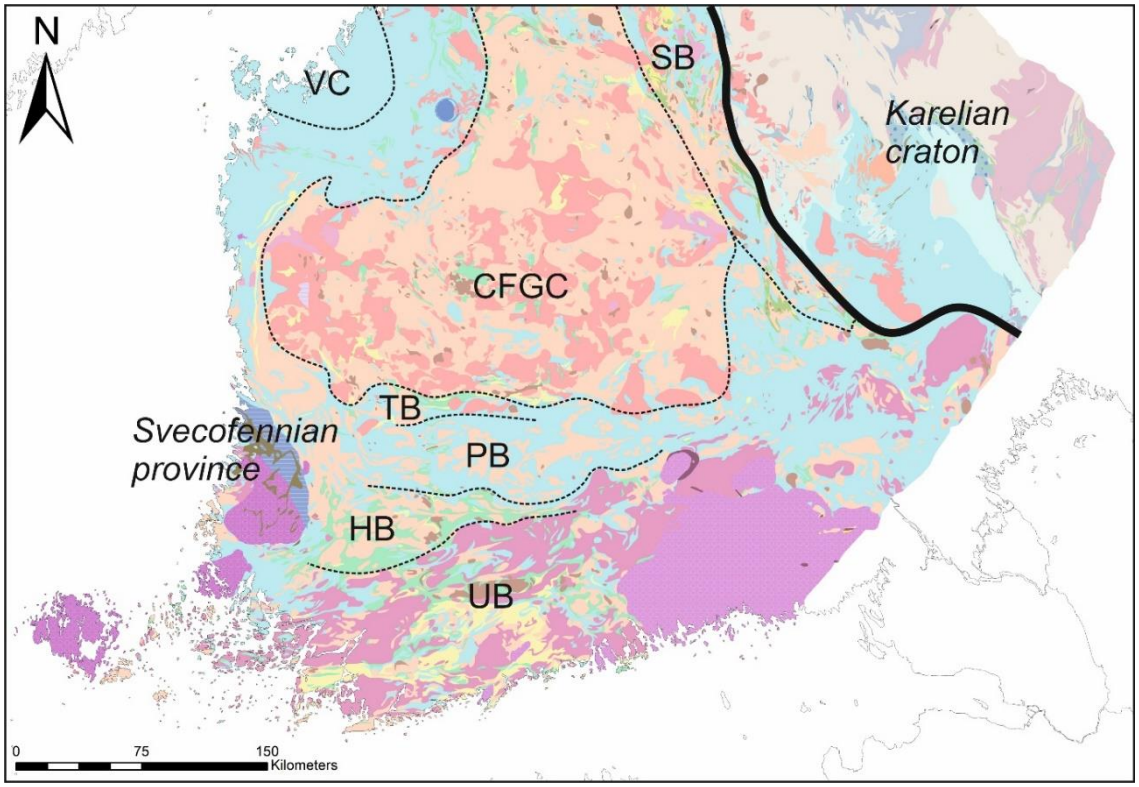

Figure 4: Locations and outlines of major Svecofennian complexes and metamorphic belts. Solid black line indicates the Raahe-Ladoga suture zone between the Karelian craton and Svecofennian province. CFGC = Central Finland Granitoid Complex, VC = Vaasa Complex, SB = Savo Belt, TB = Tampere Belt, PB = Pirkanmaa Belt, HB = Häme Belt, UB = Uusimaa Belt. Modified after Korsman et al., (1997).

Archean Norrbotten and Karelian cratons. The southern segment represent the collision of the Keitele microcontinent and associated island arc complex to the Archean Karelian craton. The rocks formed during this collisional stage at 1.92–1.89 Ga form the Savo Belt, characterized by juvenile volcanic arc material that forms the suture zone between the Archean and Paleoproterozoic rocks (Lahtinen et al., 2005; Lahtinen et al., 2009b). The Central Finland Granitoid Complex formed in the southern segment, on the Keitele microcontinent (Lahtinen et al., 2009b)

The aforementioned Keitele-Karelia collision initiated a shift in the plate motions. According to Lahtinen et al. (2009b), two almost simultaneous subduction environments formed associated with the Bergslagen microcontinent; the northwards-oriented zone at the Keitele-Karelia collage and the second one in the southern margin of the Bergslagen microcontinent. At the collisional stage of the Keitele-Karelia and Bergslagen, the *Fennian orogeny* (1.89–1.86 Ga) initiated, forming the metamorphic Tampere, Pirkanmaa, Häme and Uusimaa belts located in Southern Finland and analogous domains in Sweden, e.g. the Skellefte district. The Fennian orogeny was followed by the transpressional *Svecobaltic orogeny* at 1.83–1.79 Ga, a collisionary event between the Sarmatia and Fennoscandia (Lahtinen et al., 2005; Lahtinen et al., 2009b). Volcanic rocks of this setting are not present in Finland, indicating a continent-continent collision. The Svecobaltic orogeny represent a tectonic inversion, sited in the newly formed crust during the Fennian orogeny (Lahtinen et al., 2005). The Svecobaltic orogeny was followed by the *Nordic orogeny* at 1.82–1.79 Ga, reworking the crust at an N-S and NE-SW orientation. Two models for the Nordic orogeny comprise a continent-continent collision with the Amazonia (Lahtinen et al., 2005) and an accretionary, advancing Andean-type orogeny associated with retro-arc fold-and-thrust -belts (Lahtinen et al., 2009b).

The model by Lahtinen et al. (2005) consisted of a microcontinent-continent -collision followed by a subduction reversal, representing a break in the subduction. A contrasting model of tectonic switching was introduced by Hermansson et al. (2008) that accounts the accretionary event at 1.91–1.85 Ga in central Sweden with a continuous subduction environment with the migrating subduction hinge creating a setting with fluctuating extension and compression related to one progressive orogeny. Volcanism in the extensional back-arc setting, caused by the retreating subduction hinge, accounting for the accretionary environment. The first extensional back-arc setting took place at 1.91–1.89 Ga due to the retreating subduction hinge. This setting was followed by an event at 1.89–1.87 Ga during which the retreating of the hinge slowed down and eventually

changed direction, resulting into a compressive setting in the back-arc, dominating at 1.87–1.86. The compressive setting then rapidly changed into an extensional at 1.86 Ga, again caused by the migrating subduction hinge into a retreating motion. The key differences between the models of Hermansson et al. (2008) and Lahtinen et al. (2005) displayed in Figure 5.

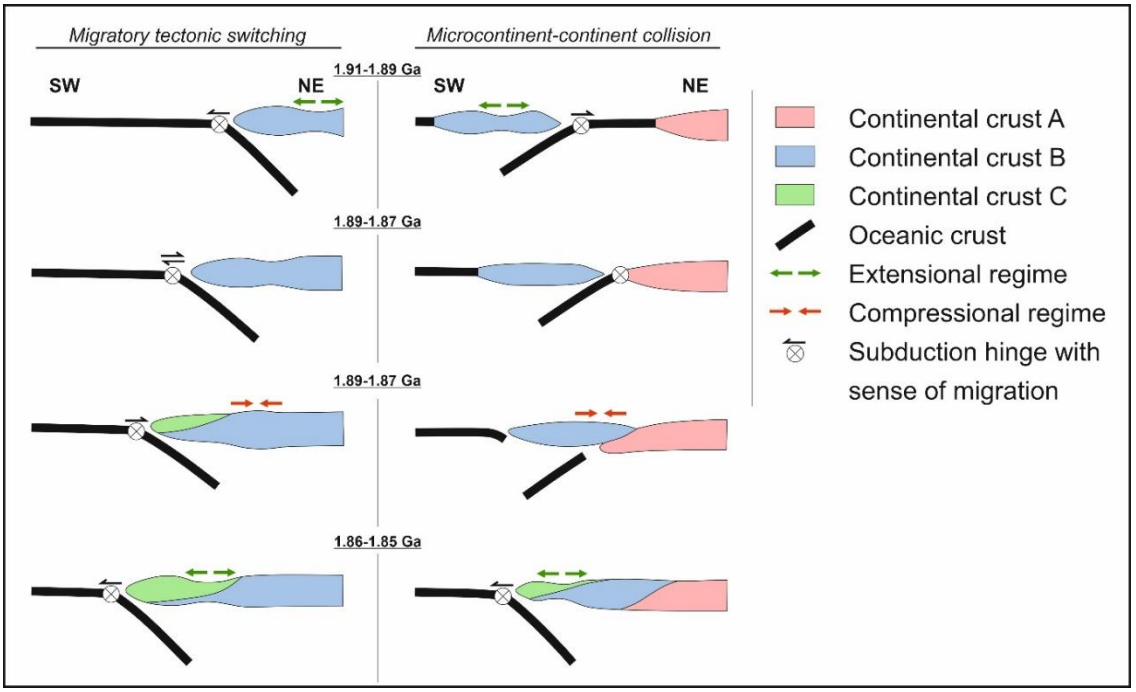

Figure 5: Two different tectonic models from central Sweden. Migratory tectonic switching represent the continuous subduction environment with migrating subduction hinge according to Hermansson et al. (2008). Microcontinent-continent collisionary model after Lahtinen et al. (2005). Modified after Hermansson et al. (2008).

As the Lapland-Savo, Svecobaltic and Nordic orogens are linear in shape, the Fennian orogeny displays an equidimensional shape. According to Lahtinen et al. (2014), the Fennian orogen experienced buckling at the end or at the later stages of Fennian orogeny at 1.87 Ga (Figure 6). The collision between the southern Svecofennia and the Tampere-Skellefte arc system, forming the Fennian orogeny, caused uplift of the arc system which resulted into most competent behaviour during buckling. The switch in the principal orientation of stress took place within the lower part of the continental plate. This change in the orientation of principal stress initiated the formation of oroclines, reshaping the Fennian orogen and other units within the Svecofennian domain from linear shape to equidimensional (Figure 6) and led to the formation of Bothnian coupled oroclines. The Fennian orogen most likely had a continuation towards NW and SE, but the later Svecobaltic orogeny at 1.83–1.79 Ga and associated NW-SE -oriented convergence overprinted the continuations of the Fennian orogeny, resulting into contraction of the southern limb of the Bothinan oroclines.

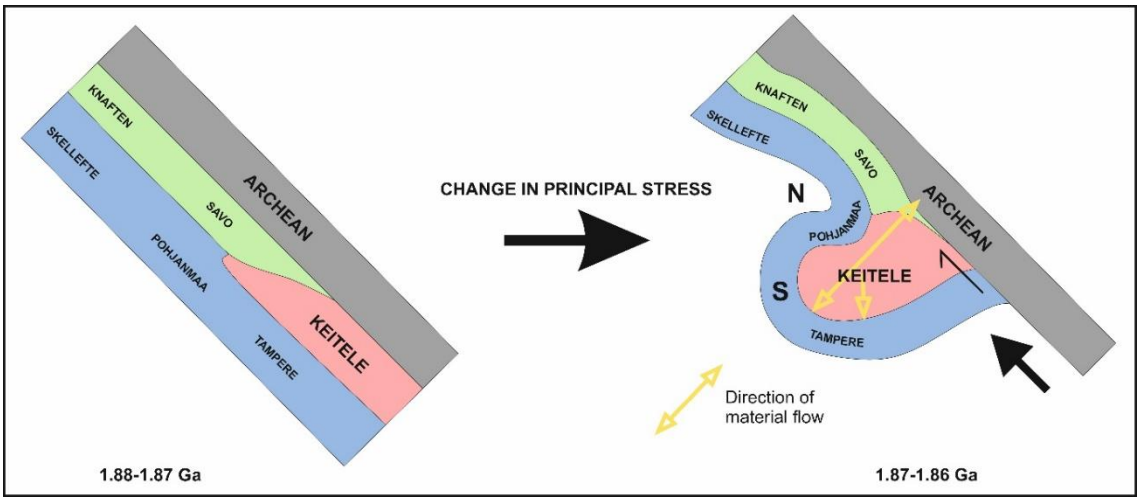

Figure 6: A thematic illustration of buckling in the Fennoscandian domain and the formation of Bothnian oroclines. Modified after Lahtinen et al. (2014).

2.3. Pirkanmaa Belt

According to Lahtinen et al., (2005), the collision between Keitele and Karelia led to a subduction reversal, initiating a northward subduction, sited at the southern edge of the Keitele-Karelia -collage. The newly formed subduction zone formed the volcanic and volcanoclastic rocks in the Tampere Belt, formed in a mature island arc or active continental margin environment (Kähkönen, 1987, 2005). The Pirkanmaa Belt is interpreted to represent the accretionary prism in the same complex, consisting mostly of migmatites and gneisses of turbiditic origin together with 1.89–1.87 Ga plutonic rocks, predominantly granodioritic in composition. Complex deformation (Kilpeläinen, 1998) consisting of early thrusting and associated subhorizontal folding, followed by extensional setting and almost simultaneous upright folding in a low-P, high-T -environment in an upper amphibole facies (Hölttä & Heilimo, 2017), peaking at 1.88 Ga (Mouri et al., 1999).

The border between the Pirkanmaa Belt and Tampere Belt in the north (Figure 7) displays both gradual and fault-controlled changes (Kilpeläinen, 1998) and Nironen (1989) described thrust faulting with S-side-up -kinematics. The border between the Pirkanmaa Belt and Häme Belt in the south (Figure 7) is interpreted to represent the suture zone between the Central Svecofennian Arc Complex (CSAC, Figure 7), containing the Central Finland Granitoid Complex, Tampere and Pirkanmaa belts, and Southern Svecofennian Arc Complex (SSAC, Figure 7), containing the Häme and Uusimaa belts (Korsman et al., 1997). The internal structures of the Pirkanmaa Belt are characterized by foliation parallel with the primary bedding which was followed by a ductile deformation

forming fold patterns with E-trending, subvertical axial planes. Faults within the Pirkanmaa Belt occur as a conjugate sets with respect to the E-trending axial planes and the thrust-type contact with the Tampere Belt (Figure 7, Korsman et al., 1997).

Two mineralization districts are sited in the Pirkanmaa Belt: the Pirkkala-Valkeakoski Au-zone and the Vammala Ni-Cu -zone (Saltikoff et al., 2006) (Figure 7). All of the gold deposits represent an orogenic style and the most notable deposits are the Kaapelinkulma, Hopeavuori and Palokallio deposits (Figure 7). The Kaapelinkulma is an open-pit type mine opened in 2018 in which the gold is hosted by a sheared quartz diorite (Dragon Mining 2020). Gold in the Hopeavuori deposit is located in quartz veins within narrow shear zones (Sotkamo Silver, 2020). The Palokallio prospect is similar in nature with the Kaapelinkulma deposit, hosting the gold in a sheared mafic intrusive (Grönholm & Voipio, 2012). The Vammala Ni-Cu -zone (see Saltikoff et al., 2006) and references therein) is the second prominent zone within Pirkanmaa Belt, including the nowadays closed mines of Stormi and Kylmäkoski. These deposits are sited in the mafic-ultramafic intrusions of Vammala suite in the migmatitic gneisses (Figure 7).

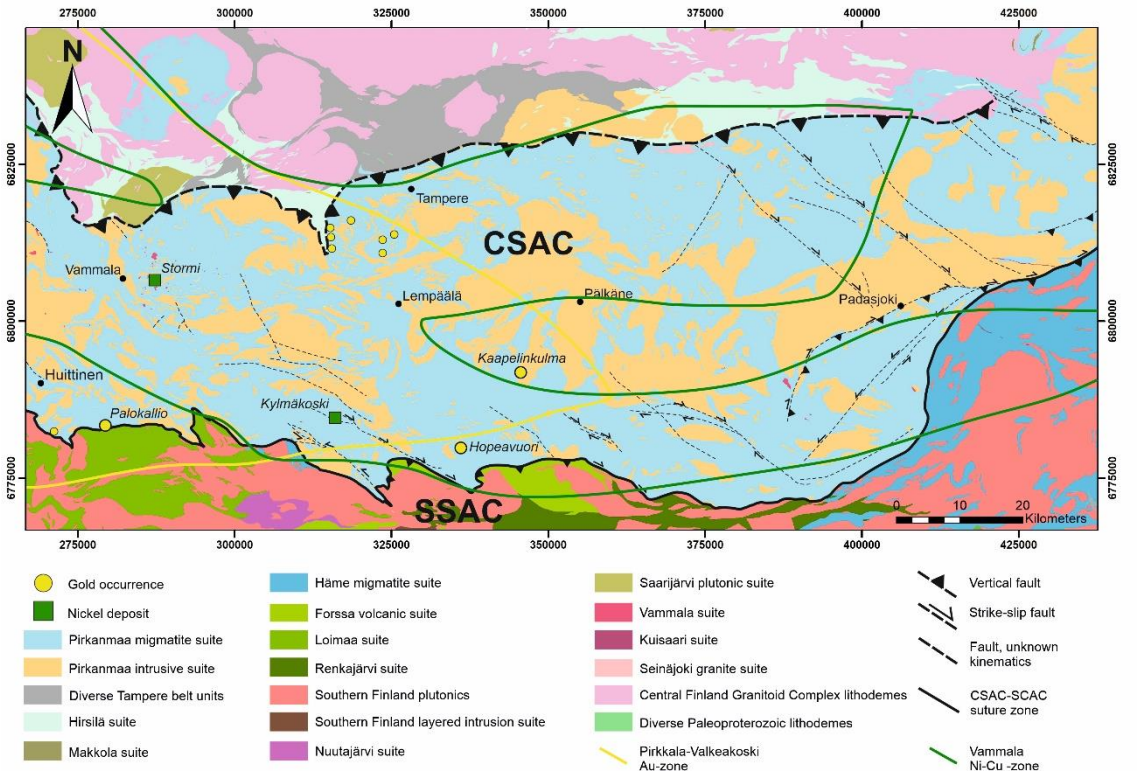

Figure 7: Generalized geological map of the Pirkanmaa belt, modified after Korsman et al. (1997). Gold occurrences from Mineral Deposits of Finland © Geological Survey of Finland. CSAC = Central Svecofennian Arc Complex, SSAC = Southern Svecofennian Arc Complex.

2.4. Pomarkku block

The study area is sited within the Pomarkku block, representing the western continuation of the Pirkanmaa Belt. The Pomarkku block is sited between the Satakunta sandstone basin and the Central Finland Granitoid Complex (Figure 2). The lithology of the Pomarkku block consists mostly of plutonic units displaying dominantly of granodioritic to dioritic composition. Migmatized supracrustal sedimentary units, typical for Pirkanmaa Belt, along with small amounts of supracrustal mafic to intermediate volcanic units are present (Figure 9). The metamorphic grade is typically within upper amphibolite facies conditions (Hölttä & Heilimo, 2017) but the timing of the peak conditions is unknown. Four known gold deposits are located in the Pomarkku block within a spatially restricted area (Figure 2) and the previous studies reaching to 1950's have mainly focused on the geochemical exploration. Studies with structural emphasis has been done by Pietikäinen (1994) and Pajunen et al. (2001) but these focussed on the regional structural evolution and consequently lack the interpretation of gold-critical structures and the association to the regional geological setting.

The Pomarkku block is bordered by two crustal-scale shear zones, the Kynsikangas shear zone to the SW and the Kankaanpää shear zone to the NE (Pietikäinen, 1994; Pajunen, 2001). A recent study by Reimers et al. (2018) concluded that deformation within the Kynsikangas shear zone was partitioned into two different deformation regimes. The NW-SE oriented pure shear-dominated transpressional ductile regime formed the map-scale structures in the KySZ. The E-W oriented brittle compressional setting caused localized thrusting of the central segment of KySZ over the eastern segment of the Kynsikangas shear zone. The structures on the SW margin of Pomarkku block were affected by the drag of shearing from the Kynsikangas shear zone during NW-SE -oriented transpressional regime instead of a previously formed structure (Reimers, 2018). The Kankaanpää zone in the NE margin of the Pomarkku block displays linear features plunging gently towards NE and oblique dextral kinematics (Pajunen et al., 2001). The internal structures of the Pomarkku block display E-W trending foliations and axial planes with vergence towards N in the northern part of the block and shift into NE-SW orientation with vertical to subvertical axial planes in the southern part of the study area.

2.4.1. Diamond drilling of gold targets

All four gold targets have been drilled during previous studies. The Välimäki, Kultakallio and Saarijärvi targets were drilled by the Geological Survey of Finland (Lehto &

Kärkkäinen, 2006; Kärkkäinen et al., 2016) and the Silmusuo target by Outokumpu Oy (Vormisto, 1956). Drill core data from the targets lacks structural measurements and is therefore of relatively low relevance in this study. Locations of drill holes in Välimäki, Kultakallio and Silmusuo targets are illustrated alongside new structural field measurements in Figures 31, 33 and 35.

A total of 14 drill holes has been made to the Välimäki prospect (Figure 31) oriented at 120/40 (Lehto & Kärkkäinen, 2006). The structural data lacks from the drill cores, but the gold mineralizations are sited in thin quartz veins, located in narrow shear zones and as a parallel feature with respect to foliation (Lehto & Kärkkäinen, 2006). These gold-critical zones are narrow and scattered in nature with highest gold rates at 12.7 ppm (R309, 15.00–16.00 m) and 13.9 ppm (R309, 21.00–22.00 m) (Lehto & Kärkkäinen, 2006). In the Kultakallio prospect, eight drill holes (R318–R325) were drilled during previous studies with a total length of 517.50 meters (Kärkkäinen et al., 2016). The drillholes in the Kultakallio prospect are oriented towards SSE (R318, R319) and NNW (R320–R325) (Figure 33), plunging roughly at 45 degrees in both orientations (Kärkkäinen et al., 2016). Shearing, both mylonitic and as breccia zones, was observed to be roughly parallel with the drillholes oriented towards SSE (Kärkkäinen et al., 2016).

Three drillholes were made on the Saarijärvi prospect (R315–R317), drilled at an orientation of 135 degrees, plunging between 40–60 degrees (Kärkkäinen et al., 2016). The drill core displayed foliation parallel to the drilling orientation in holes R315 and R317 (Kärkkäinen et al., 2016). At the end of the hole R315, the foliation cut the core at an angle of 45 degrees (Kärkkäinen et al., 2016). In the hole R316, narrow shear zones were associated with mineralization (Kärkkäinen et al., 2016). Quartz veining of two generations was observed: parallel with the foliation and locally tightly folded sets of quartz veins and younger, cutting veins (Kärkkäinen et al., 2016).

Drilling in the Silmusuo prospect was carried out by Outokumpu Oy. Two holes were drilled to the vicinity of the gold-critical boulders (SS-001, SS-002) and six more holes roughly 2.2 kilometres to the ESE (Vormisto, 1956). The detailed data from these holes is absent, but the presence of graphite and associated tectonic relationship, in addition to absence of gold is identified (Vormisto, 1956). The drillholes SS-001 and SS-002, dipping towards NW at an angle of 40 degrees, reached the depths of 162.21 (SS-001) and 155.04 (SS-002) metres. No tectonic features were recorded from these holes but rapidly changing lithologies is a common feature in the drill holes (Vormisto, 1956).

3. Research material and methods

3.1. Background material and analysis

Raster-shaped RGB-colour-scaled aeromagnetic geophysical map data produced by the Geological Survey of Finland on a pixel density of 10 x 10 m has been the most important background material for this study. The data has been exploited on estimations in the structural trends especially in the areas of few to absent outcrops. In 2003, GTK carried out a more detailed, low-altitude geophysical survey with line spacing of 100 m at the altitude of 30 m (Lohva & Jokinen, 2012). Similar detailed surveys have proven to be useful in Southern Finland in identifying gold-critical structures, such as shear zones that intersect mafic-intermediate intrusive units (Lohva & Jokinen, 2012). In the Kullaa region, the more detailed data is being used to identify the internal structural features and the structural trends, critical to the gold mineralizations, especially in the areas of low exposure.

Field data comprising of linear and planar structural measurements collected by the Geological Survey of Finland and Outokumpu Oy was used in interpreting the orientations in the northern part of Pomarkku block. Although the geophysical data was the most important source of information for the planning of mapping, the previous observations were also exploited during the planning. Bedrock of Finland 1:200 000 has been exploited during the mapping process especially tracking down the mafic units in the study area. All map data used in this study is displayed in Transverse Mercator projection EUREF-FIN-TM35FIN.

3.2. Bedrock mapping

Although previously collected field data by the Geological Survey of Finland and Outokumpu Oy cover a large area, the lack of detailed observations in scale and the debatable reliability of previously collected field data provide a good reason for a complementing and more detailed study. Most of the data was collected within the Pomarkku block and the bordering Kankaanpää shear zone. Required background data was collected during regional mapping in a broader scale within the Pomarkku block and in the bordering Kankaanpää shear zone in NE. The main focus in the regional-scale mapping was to observe linear and planar features to recognize deformation zones, fold geometries and apparent strain variations.

In addition to regional mapping, more detailed mapping was focused in the vicinity of previously known gold targets (Figure 8) in an attempt to compare the structural characteristics of the known gold-critical prospects. Linear and planar structural measurements and more detailed features such as veining, small-scale shearing, mineralizations and in some occasions dominant fracture sets were observed on the detailed mapping areas in order to provide a framework to evaluate the structural control of the individual deposits.

The northern part of the Pomarkku block hosts roughly E-W -trending, flat lying structures whereas the structures in the vicinity of the known gold deposits have NE-SW, more vertical structural trends (Figure 16). With the regional data and old observations from the northern part and the detailed structural data in the gold-critical areas, the aim is to divide the Pomarkku block into structural domains and visualize the transition in the structural trends using lower hemisphere projections and cross sections. A more detailed form line map from the area of detailed mapping visualizes the structural complexity in the gold-critical area. Structural measurements and features will be correlated to domain-scale structures. With these elements, the final objective is to form an understanding of the controlling structures for the mineralized prospects.

During the field work, a total of 180 linear and 281 planar measurements were taken from 286 localities (Figure 2). A total of 120 rock samples from which 79 are oriented samples were taken. Some of the data is collected approximately 40 kilometres south from the study area in an attempt to define the transition in regional geology between the Pomarkku block and the Pirkanmaa Belt and will not be utilized in this study. Bedrock observations were saved using the Kapalo software in a Panasonic Toughbook with integrated GPS, provided by the GTK. The accessibility in the area is good as the amount of forest roads is substantial. The number of exposures within the Pomarkku block is generally good with some limitations set mostly by the wetlands. Välimäki gold target has a good amount of bedrock exposures whereas the number of outcrops in the Kultakallio, Saarijärvi and Silmusuo targets is more constrained.

3.3. Thin sections

The purpose of the thin section study is to identify microtextures, particularly kinematic indicators in polarized microscopy. The main focus is on the kinematic indicators within the ductile deformation regime together with other indicators of deformation, e.g. dynamic recrystallization of quartz. These can be utilized in defining the kinematic

features and the deformation conditions within the Pomarkku block and correlating them with the regional structural setting and development of different structures in the study area. A total of 73 thin sections from 64 localities were made from which 63 thin sections are oriented (Figure 8). A cut-mark was made on every oriented thin section which was then correlated to a point of the compass. This method preserves the original orientation of the sample during the thin section preparation process. The oriented thin sections are cut in a way that the examined surface is perpendicular to the foliation and parallel to the lineation. This enables the inspection of kinematic indicators assuming they are parallel with the lineation. The thin sections were made in the Department of Geography and Geology in the University of Turku by the author under the guidance of laboratory technician Arto Peltola. All the thin sections are polished, allowing future geochemical analyses if needed.

3.4. Geochemical analyses

The main objective on the geochemical analysis is on the classification of plutonic rocks and their linkage to the regional geology and the Svecofennian crustal evolution together with the age determination. Gold-critical samples were also recognized using the geochemical analysis. A total of 30 samples (Figure 8) within the Pomarkku block from which 14 are of plutonic origin were sent to geochemical analysis. The rocks were cut to a suitable size during which the homogeneity and purity was ensured. The samples were then sent to Bureau Veritas Mineral Laboratories in Vancouver, Canada. At the laboratory, the samples were first crushed, split and pulverized after which a total whole rock characterization was done. Aqua Regia digestion was then done to the samples and in between these two analyses the samples were heated to measure the loss on ignition (LOI). Fluoride was analysed with a specific ion electrode.

3.5. Age determination

A granitic leucosome sample (JUMA-2018-5.1) from a paragneiss host rock was collected from the Välimäki gold target (Figure 8). The goal is to determine the age of the peak metamorphism, providing an age that can be linked to the Svecofennian crustal evolution and other gold deposits in the southern Finland. The age dating sample was separated as a heavy mineral separation course work in the Department of Geography and Geology, University of Turku by student Anssi Arminen in collaboration with the author. Both zircons and monazites were extracted from the sample.

The sample was first cut using a rock saw and then crushed using a rotary guillotine press. The slabs were then set into a crusher. The sample was then pulverized and sieved using a Swing mill and a 250 µm sieve. The powder was then panned removing the light mineral fraction. The magnetic minerals were then removed using a magnet and a paper slip, followed by a heavy liquid (Diiomethane, CH_2I_2) separation in which the desired heavy fraction sinks to the bottom of a funnel. The following electromagnetic separation was done using three different currents with Franz isodynamic mineral separator. The remaining mineral fraction was then handpicked using a human hair. The picked zircons and monazites were put on lines on a double-sided tape. Epoxy was cast on top of the tape and mineral grains and the sample was then finalized by polishing, cutting the mineral grains in half.

The cast epoxy button was covered in carbon at the Finnish Geosciences Research Laboratory (SGL=Suomen geotieteiden tutkimuslaboratorio) before the SEM imaging to prevent the sample from charging when shooting it with electrons. SEM images of the zircons and monazites were taken at the SGL by JEOL TM JSM-7100F Field Emission Scanning Electron Microscope (FE-SEM). In FE-SEM, the image is created by bombarding the sample with electrons. The composition of the material affects the amount of backscattering and as a result the heavier elements appear light on the image and vice versa. As a result, BSE images of the zircons and monazites was obtained. Suitable grains for the U/Pb age dating was selected based on these images. The grains were then analysed with the Nu instruments^{TM} AttoM Single Collector High Resolution ICP-MS (SC-ICP-MS) equipped with a Photon Machines^{TM} deep UV excimer laser (193 nm wavelength). The data was then analysed using Glitter! (Van Achterbergh, 1999) analytical software package at the SGL.

3.6. Micro-XRF

Two gold-critical samples (JUMA-2018-5.1, JUMA-2018-107.1; Figure 8) were analysed with Bruker Tornado M4 micro-XRF spectrometer with 2 SDD detectors. The samples analysed were the counterparts from thin section preparation, which were levelled to be suitable for the analysis. A series of different elements were then analysed, e.g. Au and As. The goal in this section is to identify if the gold is present as a native gold or in the crystal lattice. Micro-XRF is also highly suitable for visualizing the presence of gold. The results of the Micro-XRF -analysis is presented in Appendix 4 displaying the distribution of the elements of interest.

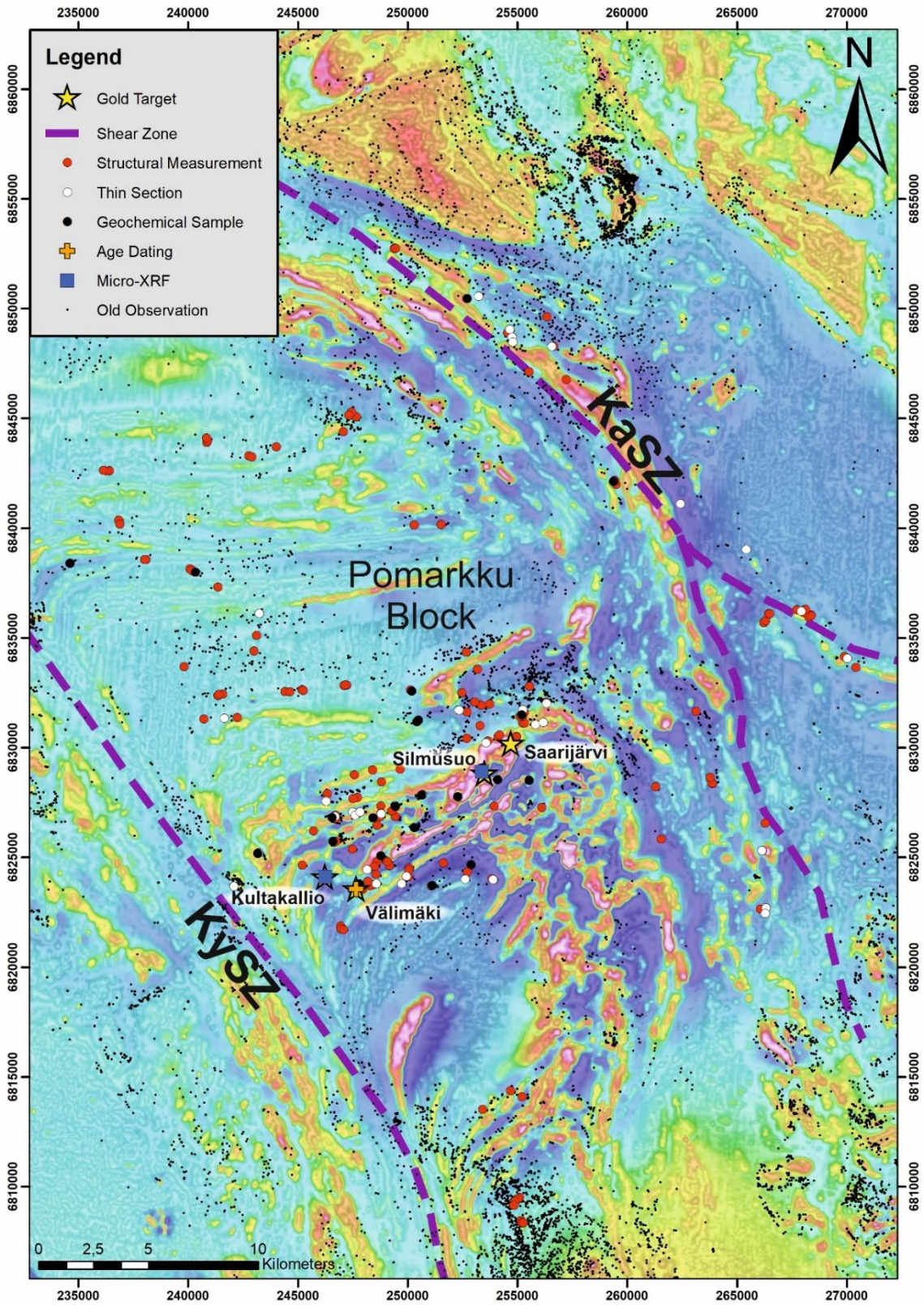

Figure 8. Observations from the Pomarkku block. Overlapping point data, layer order (bottom to top): old observation; structural measurement (n: 225); thin sections (n: 64); geochemical samples (n: 30); age dating (n: 1); micro-XRF (n: 2). KySZ = Kynsikangas Shear Zone, KaSZ = Kankaanpää shear zone. Tilt derivate (TDR) processed aeromagnetic map ©Geological Survey of Finland.

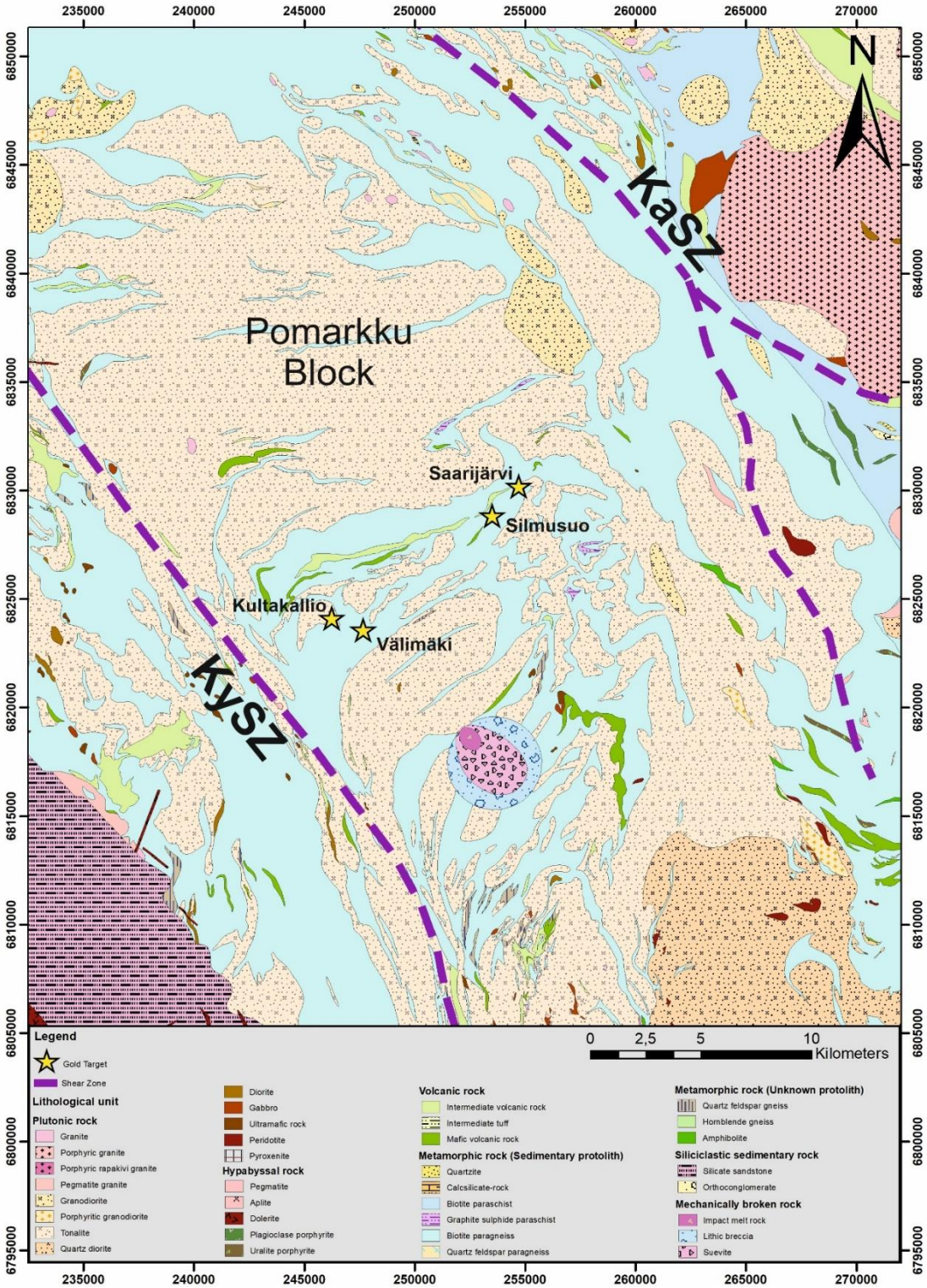

Figure 9: Lithological map of the study area with gold targets and main shear zones indicated. KySZ = Kynsikangas Shear Zone, KaSZ = Kankaanpää Shear Zone. Bedrock of Finland - DigiKP 1:200 000, ©Geological Survey of Finland.

4. Results

4.1. Lithology of the Kullaa area

The classification of rocks is based on field observations, which for the plutonic rocks have been supplemented by whole-rock analyses. The study area consists mainly of supracrustal and plutonic rocks with some supracrustal volcanic rocks also observed. The syntectonic plutonic rocks are mostly granodioritic or dioritic of their composition based on the whole-rock analysis and their grade of migmatization also varies greatly. The composition of the volcanic rocks varies from mafic to intermediate. Pegmatitic dikes in the study area are associated with localized shearing or higher grade of migmatization (Figure 13). The grade of migmatization in the supracrustal paragneisses is controlled by the composition of the protolith; pelitic sequences melt easier, with respect to sections of psammitic composition, due to the presence of clay minerals and are therefore more prone to host partial melts. The presence of partial melts is associated with the regional lithology and strain variations within the study area. Partial melts in plutonic units are present in the southern parts of the study area, associated with the presence of supracrustal paragneisses melts formed in these units together with an increase in strain (for reference see cross sections, Figures 29 and 30).

4.1.1. Supracrustal rocks

The dominant mineral assemblage of the supracrustal paragneisses are biotite, feldspar and quartz. The weathered surface is on average light grey whereas the fresh surface has a darker tint. The high-grade, partially molten host displays relative amounts of melts ranging from 0 to over 50 %. The composition of paragneisses varies across compositional banding, defined by the pelitic and psammitic layers and this apparently primary feature is common and very well visible in several outcrops. The pelitic parts of the paragneisses are systematically more migmatized due to the presence of biotite and other clay minerals that lower the melting temperature compared to the psammitic layers. This represents the strongest controlling feature in the grade of migmatization in the study area. Stromatic texture is a common feature in the pelitic sections (Figure 10; B) formed during partial melting of the rock. The psammitic layers are significantly more homogenous and less deformed than the pelitic parts. Garnet porphyroblasts are a fairly common and are usually located in the leucosomes or pegmatitic dikes but their occurrence is not solely confined to these units. The age determination sample JUMA-2018-5.1 was taken from a leucosome in the vicinity of Välimäki gold target.

Figure 10: **A)** Strongly migmatized paragneiss with pegmatitic parts locally folding the foliation, indicating competence differences between the pegmatitic and pelitic sections. JUMA-2018-94. N: 6821640, E: 247030. **B)** Cut surface of a paragneiss with folded leucosome and stromatic texture. JUMA-2018-97.1. N: 6824122, E: 249930.

The structural features, such as foliation and crenulation folding, are usually very well visible in the biotite-rich parts. The leucosomes and pegmatitic dikes commonly fold the foliation of these biotite-rich layers in a small scale (Figure 10; A) and occur parallel to foliation most of the time. Pegmatitic dikes, when syntectonic with the main foliation and within the psammitic layers, form mullion and boudinage structures reflecting the competence contrast between these units. Ptygmatic folding of leucosome veins (Figure 22, C) in the study area is restricted to paragneisses and is observed in multiple locations.

Most of the observations from supracrustal volcanic rocks occur as an apparently continuous chain within a limited area 3–3.5 kilometres north of the Välimäki and Kultakallio gold targets and are interpreted as a continuous lithological unit. The dominant mineral assemblage in these rocks is plagioclase, hornblende and quartz (Figure 11). The volcanic rocks are characterized by compositional metamorphic layering on the outcrop surface where more mafic sections are clearly elevated from the more felsic parts (Figure 12; A). Other units of intermediate volcanic rocks were also observed during the regional mapping in the northern part of the study area but the lithological features differ significantly from the metavolcanics in the vicinity of gold prospects as this volcanic units displays no compositional metamorphic banding and is less deformed.

Mafic parts in the more felsic matrix are commonly tightly folded with asymmetric fold geometrics (Figure 12, A). Garnet porphyroblasts are also a common feature (Figure 11;

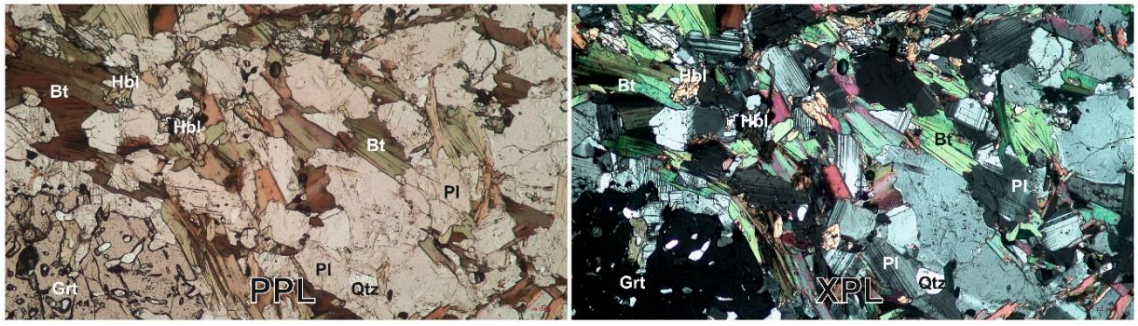

Figure 11: Plane- (PPL) and cross-polarized (XPL) images of an intermediate volcanic rock. JUMA-2018-7, N: 6826873, E: 246700.

Figure 12, B), appearing as layers of both mafic and more felsic compositions. Quartz veins parallel with the foliation together with folded quartz veins with parallel axial plane with the foliation was observed. Pegmatitic dikes associated with shearing and as a parallel feature with foliation were also observed within this unit. Sulphide mineralizations were locally observed in the pegmatitic dike in the contact of the host rock and the dike as a massive sulphide layer with the sulphide amounts gradually increasing towards the contact. Sulphides were also concentrated on the pressure minimas in boudinaged layers.

Figure 12: A) Intermediate volcanic rock with tight folding visible in the more mafic sections. The folded mafic parts have their axial surfaces parallel with the foliation. JUMA-2018-28, N: 6826972, E: 247430. **B)** Cut surface of an intermediate volcanic rock rich in garnet porphyroblasts. Sample JUMA-2018-7.1, N: 6826847, E: 246656.

4.1.2. Plutonic rocks

The plutonic rocks in the study have a varying composition ranging from granitic to gabbroic with dominant granodioritic to tonalitic composition. The mineral assemblage

Figure 13: A) Strongly foliated and moderately migmatized orthogneiss with a discrete sinistral shear band localized along pegmatitic quartz-feldspar melt. JUMA-2018-95. N: 6823693, E: 249613. **B)** Cut surface of a weakly foliated granodioritic rock. Sample JUMA-2018-20.1, N: 6823923, E: 252547.

is most commonly plagioclase, quartz and amphibole in varying proportions. The weathered surface is usually greyish brown and the weathered surface has a darker shade of grey. The strength of the migmatization is on average weaker in the plutonic rocks than in the supracrustal paragneisses as the relative amount of leucosome is ranging typically from 0 to 30 %, strongly controlled by the relative positioning of the plutonic unit in the study area. The migmatization is a more pervasive feature in the plutonic rocks due to homogenous composition (Figure 13; A) and is more commonly parallel with the foliation. Foliation is not as well visible in the plutonic rocks when compared to paragneisses, but the lineation is generally well visible in amphibole grains. Partial melts from the host rocks are a common feature in localized shear zones (Figure 5; A). Garnet porphyroblasts are in the leucosomes. The composition of plagioclase was determined using the Michel-Levy method. A granodioritic sample JUMA-2018-13.1 displayed an extinction angle of 25 degrees, giving An-content An_{46}: andesine (Figure 14, B). Sericite alteration is common in the feldspar minerals (Figure 14, A).

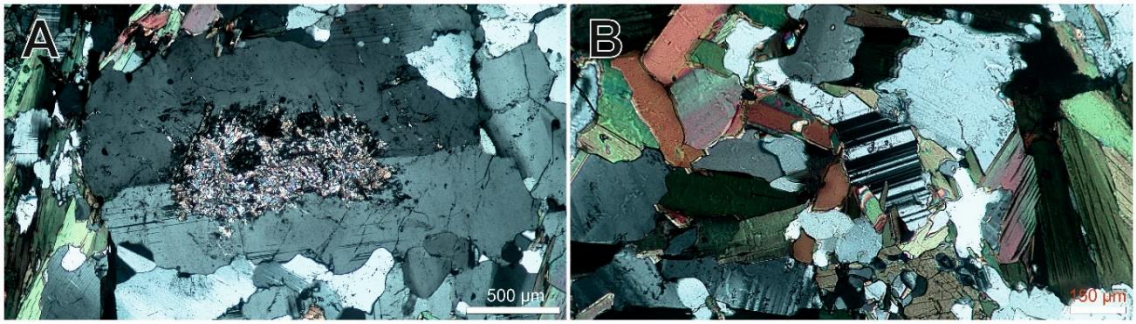

Figure 14: A) Sericite alteration in a plagioclase grain. JUMA-2018-13, N: 6825725, E: 246600. **B)** An andesitic plagioclase grain. Extinction angle: 25 degrees; An_{46}, andesine. JUMA-2018-13, N: 6825725, E: 246600.

4.1.3. Pegmatites

The pegmatitic dikes in the study area are found in all lithological units throughout the Pomarkku block. The dominant composition of the dikes is quartz feldspar with few exceptions (Figure 15, B: Figure 21, E). Dikes in the supracrustal paragneisses are dominantly sited in the pelitic sequences but appear also as a cutting feature. Plutonic units host the dikes dominantly parallel with the foliation when present. Volcanic units hosting pegmatitic dikes display deflection of the foliation towards the contact between the dike and the host rock, indicating pre- to syntectonic formation of the dikes with respect to the main foliation (Figure 15, A).

Figure 15: A) Pegmatitic quartz-feldspar-epidote dyke displaying deflection of foliation towards the dyke, hosted by psammitic paragneiss. **B)** A close-up of a lens of similar composition next to the compass. JUMA-2018-78, N: 6827822, E: 250670.

4.2. Structural geology

4.2.1 Structural domains

The study area was divided into seven structural domains based on the obtained structural data, geophysical properties of the crust, old observations and previously interpreted shear zones (Kärkkäinen et al., 2016) within the Pomarkku block. Each domain represents fairly uniform structural features with noticeable differences to adjacent domains, forming the basis for the structural division. Observations in the vicinity of the crustal-scale Kynsikangas and Kankaanpää shear zones were outlined in all domains except Domain VII, avoiding the distortions in the structural interpretations. Overall, the structural trends in the northern part are ENE-WSW -trending, characterized by subvertical foliation and flat-lying linear features compared to the southern part of the study area, hosting also vertical planar features but an overall more scattered linear properties (Figure 16).

The two northernmost Domains (I &II) are fairly similar, characterized by E-W/ENE-WSW trending planar structures and sub-horizontal linear features. Domains III and VI represent semi regional-scale fold structures gently plunging towards ENE. Domain IV consists to ENE-WSW trending planar structures with dominant vertical orientation and strongly polarized linear features. Domain V hosts three of the known gold occurrences and is characterized by high magnetic anomalies, intense deformation and vertical to subvertical, NE-SW trending, dominantly SE-dipping coherent planar features. Linear features display more scattering and dominantly plunge towards E-NE. Only few structural observations were made in the Domain VII and old observations were used instead in the stereographic projections. Domain VII hosts two sets of planar features, NE-SW -trending and ESE-WSW -trending sets with linear data plunging towards E to NE. Foliation measurements indicated in the text are dip degree/dip (xxx/xx). Locations of shearing observations with images presented are located in Figure 16.

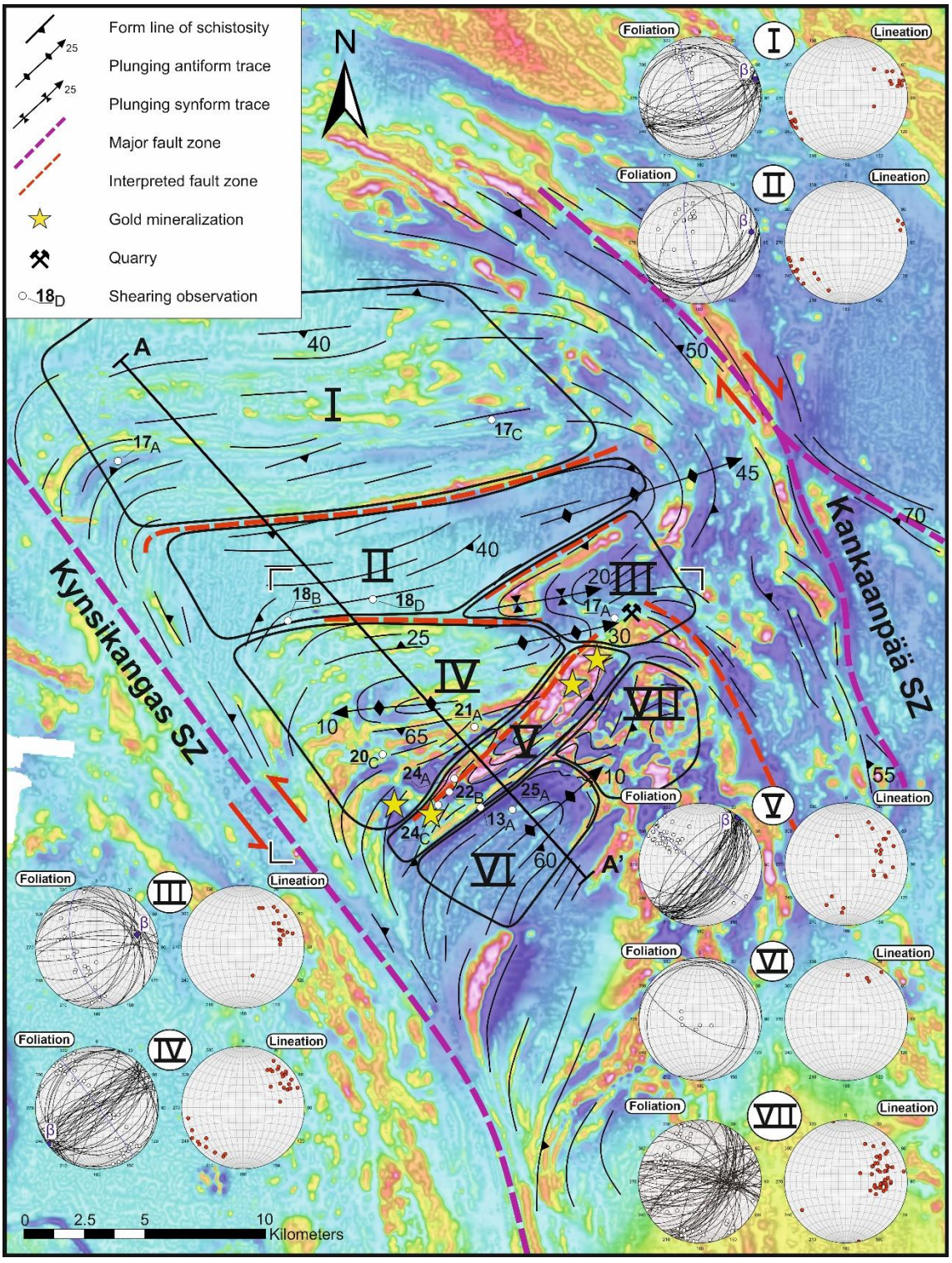

Figure 16: Form line map of the study area with tilt derivate (TDR) processed aeromagnetic map ©Geophysical Survey of Finland on the background. Sub-division into structural domains presented with lower hemisphere stereographic projections from each structural domain displaying planar (foliation) and linear (lineation and fold axis) features along with statistical β-axis. Black line indicates the positioning of cross section A-A' from the study area and the corners of the detailed form line map have been marked. Locations of illustrated shearing observations have been marked.

4.2.1.1 Domain I

The dominant structural trends in the northernmost Domain are ENE-WSW trending foliations with vertical to subvertical dip towards SSE. Some observations have similar strikes, but dip towards NNW in a very gentle manner. These measurements are most likely taken from the proximity of a fold hinge, accounting for the opposing dip direction. The dominant dip direction with fluctuating dip degree indicates asymmetric, gently overturned folding with vergence towards NNW within Domain I. Even though the foliation data displays a lot of scatter, the poles for the foliation data form a distinct girdle and the β-axis plunges towards ENE. The dip of the foliation ranges between 5 to 86 degrees with an average dip of 52 degrees, and define a statistical β-axis of 071/06 for the fold patterns in Domain I. The linear features in this Domain are very strongly polarized and display sub-horizontal plunges. Linear features in the western part of Domain I plunge towards WSW are very tightly stacked and display plunges ranging between 0 and 10 degrees. Linear features in the eastern part of Domain I plunge towards ENE are also dominantly very tightly packed but display slightly steeper dip degrees in a range between 4 and 51 degrees averaging at 20 degrees. A total of 33 foliation measurements and 21 linear measurements were taken from this subarea.

The intensity and the style of the tectonic fabric varies greatly within Domain I as the supracrustal paragneisses display clear foliation whereas several plutonic rocks are dominantly L-tectonites. Hornblende in the plutonic rocks appear as clusters and displays the linear features very clearly whereas the foliation remains ambiguous on many occasions. Open folding of the dominant foliation in an outcrop scale is a representative feature within this subarea, but the fold axis of this feature remained unsolved in most cases but is likely parallel with the linear features in the region (Figure 17, B). Axial planar foliation of this folding is non-existent. Smaller scale folding is also present, best visible as folding of the leucosomes in supracrustal paragneisses and folding of veins in both plutonic and supracrustal units.

Migmatization is present and within Domain I limited to supracrustal paragneisses only. Veining is dominantly parallel with the foliation but appears also as a cutting feature in various angles towards the foliation. Veins consist of quartz and feldspars, commonly displaying a pegmatitic texture. Veins of several generations are present based on the orientations of the veins and deformation of older vein generations. Older generations are folded in the same stress field with the dominant foliation with fold axis parallel to lineation and axial plane foliation parallel with the dominant foliation. One observation

of crenulation foliation with a strike of 130 degrees was made, representing later deformation stages and parallel with the crustal-scale shear zones. Within the same outcrop, leucosome was boudinaged in the corresponding stress field as the crenulation foliation.

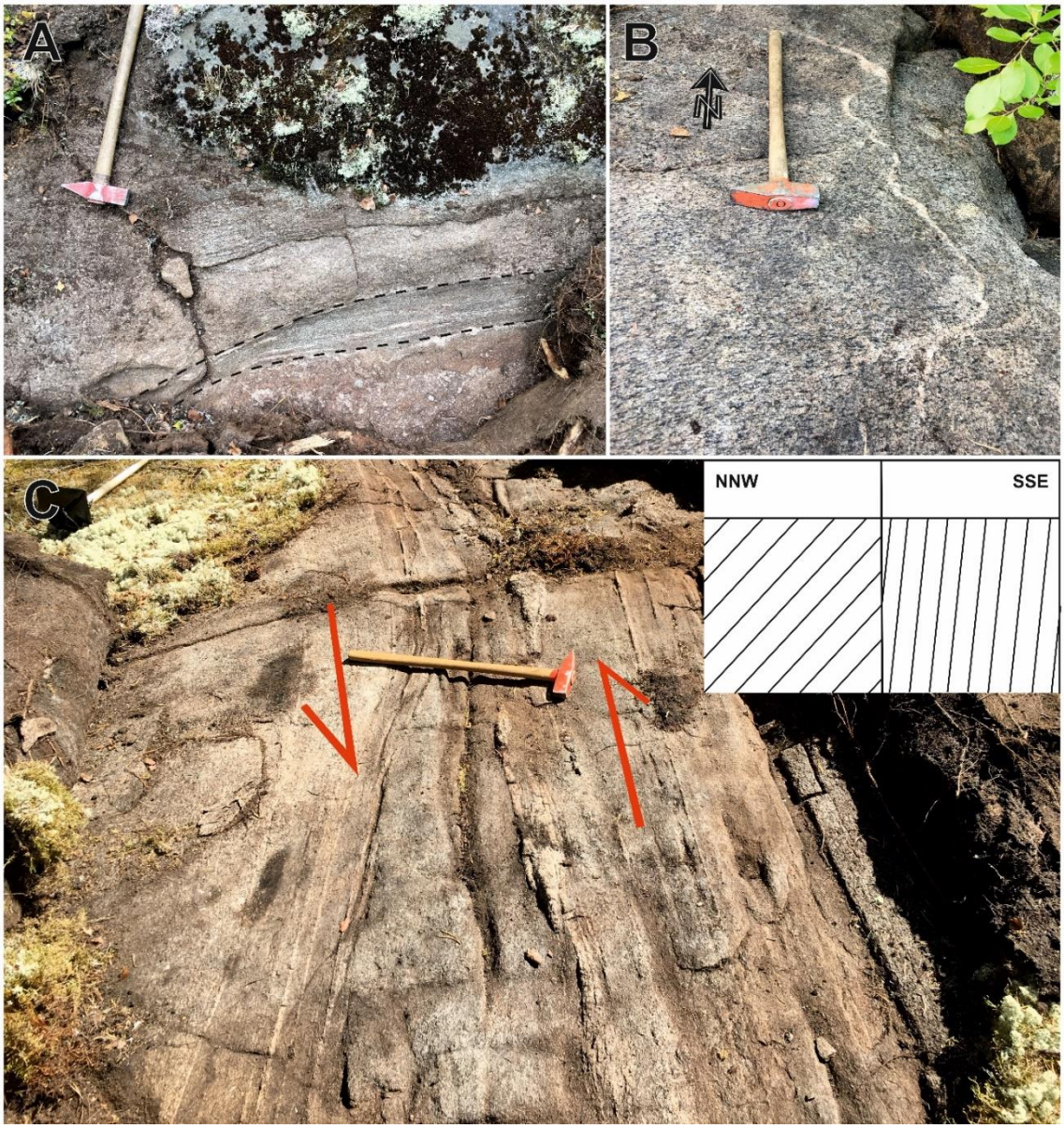

Figure 17: Characteristic structures for Domain I. **A)** Intensively sheared hornblende granodiorite displaying a low-angle shear zone, the zone of most intense shearing outlined. View towards N. TALE-2018-31. N: 6838398, E: 234617. **B)** Hornblende granodiorite, hornblende grains displaying the strong lineation, feldspar vein openly folded, fold axis parallel with lineation. TALE-2018-65. N: 6842629, E: 236154. **C)** A sheared zone displaying nearly vertical planar fabric on the S-side and moderately dipping planar features on the N-side with apparent left-lateral kinematics. A schematic illustration of the planar fabrics on the upper right corner. View towards ENE. TALE-2018-39. N: 6840150, E: 250315.

Shearing was observed in three localities within Domain I. One observation of localized shearing is from an outcrop that has been slightly affected by the Kynsikangas shear zone by transposing the dominant foliation. The shearing in this outcrop is highly localized in zones and strong, displaying flat-lying motion with no clear kinematics (Figure 17, A).

Other two observations are located in the eastern side of Domain I, but the dominant foliation has not been affected by the kinematics of the Kankaanpää shear zone, though the transposition towards the orientation of Kankaanpää shear zone starts to take place abruptly just one kilometer towards east. The shearing in one of these two localities is highly localized along a vertical ENE-WSW trending shear zone displaying sinistral kinematics based on the bending of the sheared layer. The shearing is sub-parallel with the dominant vertical foliation, vertical structures (dip: 86°) are dominant south of the shear and more gently dipping (dip: 47°) to the north (Figure 17, C). The lineation is oriented towards ENE plunging at 22 degrees, indicating slightly oblique kinematics with dominant strike-slip component. The second sheared unit on the eastern side of Domain I has no clear kinematics and displays weak recrystallization of quartz.

4.2.1.2 Domain II

Domain II host foliation structures in similar ENE-WSW -orientation as Domain I (Figure 16), but the dip degree is more moderate and homogenous, ranging between 16 to 59 degrees, averaging at 41 degrees, defining the statistical β-axis of 079/14 for the fold patterns in Domain II. The lack of fluctuation in the dip degrees is most likely related to the lithological difference with respect to Domain I and associated lack of competence differences. Domain II consist almost completely of plutonic rocks whereas both supracrustal and plutonic units are present within Domain I. In the geophysical data, Domain II does not display any clear structural continuations, reflecting lithological homogeneity. Linear features display similar polarization as in Domain I, but are more concentrated towards SW due to the predominance of observations within the SW part of the Domain, characterized by the WSW plunges (Figure 16). Linear features plunging towards ENE have a plunge ranging between 3 to 10 degrees whereas the features plunge towards SW-WSW range between 2 to 29 degrees. A total of 20 foliation measurements and 17 linear measurements were taken from this subarea.

The plutonic rocks within Domain II host stronger foliation compared to the L-tectonites within Domain I. Hornblende occurs in similar clusters as in Domain I, displaying linear features very clearly. Similar open folding of dominant foliation with respect to Domain I is also characteristic within this Domain (Figure 18, A). Axial plane foliation is non-existent for this open folding, but in few localities veins of quartz-feldspar composition have possibly formed parallel with the axial plane. Elongated biotite grains, parallel with the axial plane were observed with an orientation of 156/69, fairly similar to the observed crenulation foliation with a strike of 130 degrees in Domain I. Smaller scale folding

features are more absent due to the lithological differences, but tight folding was also observed within this Domain (Figure 18, C).

Partial melting and related migmatization of plutonic rocks (Figure 18, D) was observed within this Domain whereas this feature was present only in supracrustal rocks in Domain I. Partial melts are dominantly oriented parallel with the foliation but also localized into shear zones when present (Figure 18, D). Veins in this Domain are composed of quartz-feldspar, quartz-only or granitic veins and display variable thicknesses. Veins parallel with foliation are commonly folded asymmetrically displaying both sinistral and dextral asymmetries, related to larger scale fold structures and associated parasitic folding on the fold limbs. Several vein observations have a rough N-S -strike and a conjugate set of quartz veins with strikes of 054 and 118 degrees was observed. A conjugate fracture set with strikes of 050 and 137 degrees was observed, latter having a quartz filling.

Figure 18: Characteristic structures for Domain II. **A)** Open folding in hornblende-biotite granodiorite. TALE-2018-53. N: 6832369, E: 241365. **B)** Sheared hornblende-biotite quartz diorite with psammitic paragneiss enclaves. TALE-2018-51. N: 6831341, E: 241651. **C)** Tight folding in a granodiorite. JUMA-2018-34. N: 6832576, E: 250191. **D)** Migmatized orthogneiss with granodioritic protolith displaying ductile sinistral shearing in a conjugate orientation with respect to the Kynsikangas shear zone. JKKA-2018-7. N: 6832613, E: 245237.

Evidence for small scale shearing is increasingly present within Domain II. Two observations within Domain II display more intensive shearing. The strongest shearing is observed within a hornblende-biotite quartz diorite with psammitic paragneiss enclaves

(Figure 18, B), displaying feldspar porphyroclasts in more fine-grained matrix in an orientation of 140/50, hosting recrystallization of quartz. Garnet porphyroblasts are also present in this outcrop. Second observation of shearing is from an orthogneiss protolith hosting multiple parallel sinistral shear zones at a conjugate angle with respect to Kynsikangas shear zone (Figure 18, D).

4.2.1.3 Domain III

Domain III distinguishes from Domains I and II as the foliation data displays large-scale folding structures, clearly visible in the geophysical data (Figure 16). Northern part of Domain III hosts a large synform structure and towards SE smaller antiform-synform -pairs (Figure 16, Figure 28) associated with the lithological transition from plutonic rocks to supracrustal paragneisses and the associated change in competence. The dip of foliation within this Domain varies greatly, ranging between 20 to 90 degrees, averaging at 50 degrees, defining a statistical β-axis of 073/32 for the synform and associated smaller fold patterns in Domain III. By contrast, linear features are slightly more scattered and have a steeper plunge with respect to Domains I and II. Linear features trend towards E-NE, plunging in the range of 16 to 39 degrees, averaging at 32 degrees, an anomalous SSE-plunging linear feature counted out. Linear features within the large synform structure are oriented towards NE whereas the linear measurements taken south of the synform trend towards E-ENE. A total of 23 foliation measurements and 23 linear measurements were taken from this subarea.

Domain III consist of both plutonic and supracrustal units, plutonic rocks dominating in quantity. Supracrustal units are situated in the area displayed as a positive magnetic anomaly in the southern part of Domain III (Figure 16) and plutonics are sited within the non-magnetic parts. Plutonic rocks host clearly visible foliation and lineation, commonly in the hornblende aggregates similar to that in Domains I and II. Two generations of foliation were observed within one outcrop (Figure 19, E). The interpreted younger, weaker foliation (005/80, dip direction, dip) displays non-folded leucosome parallel with the foliation. The older, stronger foliation oriented at 072/41 has folded leucosome parallel with the foliation that has been folded.

Folding within Domain III is characterized by asymmetrical, both sinistral (Figure 19, A) and dextral features. Open folding, representative for Domains I and II is also present within this Domain but is not as characteristic. Asymmetrical folding of plutonic rocks observed in a quarry has the axial planar foliation oriented at 041/45, parallel with the

crenulation foliation and elongated biotite grains observed within Domains I and II. Folding has a vergence towards SW, indicating the thrust kinematics of the Kankaanpää shear zone (Figure 19, B).

Partial melting and associated migmatization is present in a similar manner as in Domain II. Leucosome is dominantly parallel with the foliation and is also located within cutting shear zones and boudin necks (Figure 19, C and D). Pelitic sections of supracrustal paragneisses are more strongly affected by partial melting than the psammitic sections. Characteristic veining within Domain III is similar to Domain II as the veins are located both parallel with the foliation and also as a cutting feature and the leucosome composition ranges from quartz to quartz-feldspar. Pyrite mineralization was observed in a folded quartz vein, pyrite concentrating especially in the fold hinges. The host for the mineralized rock was an in-situ tonalite boulder, located in the rock quarry. Fracturing with fluid filling was observed in two localities. First of these two fluid-filled fracture systems is hosted by paragneiss and has several fracture orientations, reflecting the impact of heterogeneous protolith. The second fracture set has a strike of 010, perpendicular to the orientation of the very homogenous E-W -trending granodiorite host rock.

Shearing was observed in two localities within Domain III, both hosted by migmatized orthogneiss. These observations are similar in nature, both representing small-scale, semi ductile deformation environments in which leucosome intruded into the shear zone (Figure 19, D). The kinematics and the orientation of the shearing is uniform in both observations, representing apparent left-lateral (sinistral), E-W -trending shearing in which the dominant host-rock foliation transposes towards the shear zone.

Figure 19: Characteristic structures for Domain III. **A)** Sinistral asymmetrical folding of a leucosome in a paragneiss host rock. JUMA-2018-105. N: 6831046, E: 255833. **B)** Asymmetrical folding of tonalite in the proximity of Kankaanpää shear zone, vergence towards SW. JUMA-2018-47. N: 6832070, E: 256327. **C)** Boudinages in an orthogneiss with granodioritic protolith. JUMA-2018-55. N: 6831425, E: 255243. **D)** Sinistral shearing in an orthogneiss with granodioritic protolith, leucosome intruded to the shear zone. JUMA-2018-55. N: 6831425, E: 255243. **E)** Two generation of foliation. Black dashed lines represent the younger foliation acting as an axial plane feature for the folded leucosome. Transparent white plane represents the older, stronger foliation plane. JUMA-2018-106. N: 6831158, E: 256183.

4.2.1.4. Domain IV

The structural pattern of Domain IV differs from Domains I and II as the foliation strikes NE-SW compared to the ENE-WSW -strikes dominant within in the Domains I and II (Figure 16). Dip degree of the foliation within Domain IV transforms from moderate in northern parts to steeper attitudes in southern part (Figure 29), ranging between 5 to 90

degrees, averaging at 61 degrees, defining the statistical β-axis of 233/02 for fold patterns in Domain IV. Foliation within Domain IV dips both towards NW and SE with no visible polarization, presenting no distinctive vergence in folding visible in Domains I and II. Linear features within Domain IV present similarly polarized and clustered features as Domains I and II. The linear features display similar rotation as the foliation in Domain IV, plunging towards NE and SW compared to the ENE and WSW orientations within Domains I and II. Linear features plunging towards NE have a plunge ranging between 6 to 43 degrees whereas linear features plunging towards SW range between 4 to 23 degrees. The linear features plunging towards NE are more tightly clustered with respect to trend but show more variation in plunge when compared to linear features plunging towards SW. Linear features plunging towards SW display opposite features as they are more tightly clustered with respect to plunge but display greater variation in trends (Figure 16). A total of 48 foliation and 40 linear measurements were taken from this subarea.

The intensity of the foliation is related to lithological features, similar to Domains I and II. Plutonic rocks generally display weaker features and the strength of the foliation was observed to increase towards a lithological contact. Domain IV consists of several antiform-synform -pairs as anticline and syncline traces dip both towards NE and SW (Figure 28). Open folding of the dominant foliation, characteristic for Domains I and II, is also present in Domain IV and is characterized by sinistral or unclear kinematics. Crenulation foliation of biotite grains within pelitic sequences in a paragneiss host rock was observed to correspond with the stress orientation of open folding. Tight folding is characteristic within Domain IV in which the axial plane of the foliation is same as the dominant foliation. Both sinistral and dextral tight folding is present, most likely linked to the presence of a larger scale folding and limb-related fold symmetries.

Several observations of boudinage within Domain IV were made with varied boudin structures. Typical pinch-and-swell -structures are common (Figure 20, B) and are present when the boudinaged structure is parallel with the foliation, indicating syntectonic formation as the principal stress regime for the formation of boudin structures and main foliation is analogous. A key outcrop in Domain IV displays shearband boudins with synthetic shearbands with respect to the dominant dextral kinematics and clockwise rotation of the boudins. Quartz veins have intruded into the shearbands, indicating presence of tectonic fluids during this event. Garnet porphyroblasts (Figure 20, A) with diameters varying from few millimeters up to several centimeters are common and can

be found in every lithological unit, usually located within a leucosome melt or as a layer-bound feature, reflecting compositional variation in the host rock.

Figure 20: Characteristic structures for Domain IV. **A)** Cm-scale garnet porphyroblast cluster in an intermediate volcanic host rock. JUMA-2018-7. N: 6826873, E: 246700. **B)** Pegmatitic layers parallel with the foliation of granodioritic host rock boudinaged in a syntectonic manner. JUMA-2018-15. N: 6825740, E: 246728. **C)** Clockwise rotation of more competent leucosome-rich layers in a supracrustal paragneiss host rock. Dextral shearing setting, forming antithetic shearband boudins with quartz filling in the N-S oriented shearbands (Goscombe et al., 2004). JUMA-2018-10. N: 6826207, E: 245718.

Migmatization is present in plutonic rocks and supracrustal paragneisses, commonly as a layer-bound feature but is absent in the volcanic rocks, indicating higher required melting temperature for this lithological unit. Partial melting of the host rock was observed to be strongest in nature in the proximal parts of pegmatitic veins, possibly associated with the fluid transportation in the pegmatitic melt and decreasing the melting temperature in the host rock.

Veining within Domain IV is more intensive than in Domains I and II and appears in several scales, from millimeter to tens of centimeters in diameter. Whereas the pegmatitic veining within plutonic rocks and supracrustal paragneisses commonly represent partial melting of the host rock, two observations of a pegmatitic veins in a psammitic paragneiss

host rock and in an intermediate metavolcanic host rock were made (Figure 15; Figure 21, F). Both of these observations display deflection of the dominant foliation towards the contact of the vein, as the vein has acted as a more competent unit during deformation.

Quartz veining was observed in eight different localities from which five observations host quartz veins of two different generations (Figure 21, C), including the Kultakallio gold target. The interpreted older generation of quartz veins are parallel with the foliation and display open folding together with the host rock with moderate dip degrees. These veins are sited in the fold hinges of tight folding and associated weakness zones within one outcrop, parallel with the foliation. These vein sets are relatively thick, displaying thicknesses of several centimeters whereas the cutting veins are relatively thin, showing maximum thicknesses of few tens of millimeters. The younger, cutting veins display no folding and are oriented in a uniform manner with a strike ranging between 132 to 160 degrees with steep dips.

Shearing within Domain IV was observed in six different localities. Two localities have lithological, shearing-associated contacts. First of these observations have a mylonitic contact between a granodioritic unit and a supracrustal paragneiss unit. The intensity of the foliation in the granodioritic unit increases towards the contact. The second tectonic contact is situated between a supracrustal paragneiss and a mafic volcanic rock. The alteration in the paragneiss increases towards the contact, displaying rusty, strongly foliated texture with very little amounts of partial melts (Figure 21, B). A strongly silicified, tens of centimeters thick unit is also present in the proximal parts of the contact (Figure 21, A) consisting of mobilized quartz and very fine-grained texture. The rusty parts are likely to represent the pelitic composition of the host rock with weathered biotite causing the rusty appearance whereas the strongly silicified sections are more likely to be of psammitic composition.

Four smaller scale shearing observations display sinistral shearing of diverse character. A small, 2–3 cm thick quartz lens is situated parallel with the dominant foliation with pressure tails indicating sinistral shearing, matching the dextral setting required to form the shearband boudins (Figure 20, C). Two observations with granodioritic host rocks host small-scale sinistral shearing with displacement averaging at five centimeters. First of these two observations have shearing in various orientations and the second hosts sinistral shearing striking roughly at N-S -orientation, conforming with the antithetic sinistral shearing at the shearband boudins (Figure 20, C).

Figure 21: Characteristic structures for Domain IV. **A)** Strongly silicified psammitic section of a paragneiss unit in the proximal part of a tectonic contact to the mafic metavolcanics rock and associated N-S -striking fracture sets. JUMA-2018-119. N: 6827315, E: 249435. **B)** A rusty paragneiss with pelitic composition, in the vicinity of a tectonic contact between a supracrustal paragneiss and mafic metavolcanite. JUMA-2018-119, N: 6827315, E: 249435. **C)** Two generations of quartz veining, thicker vein parallel with the foliation representing the older generation and younger veins cutting it at an oblique angle. JUMA-2018-31, N: 6826925, E: 247623. **D)** Quartz-sulphide -mineralization at the pressure minimums of the folded sequence of pinch-and-swell -boudins in an intermediate metavolcanite. View towards NW. JUMA-2018-39, N: 6827070, E: 247830. **E)** Massive molybdenite mineralization in the contact between the pegmatitic dike and intermediate metavolcanite. JUMA-2018-29, N: 6827061, E: 247490. **F)** Coarse-grained pegmatitic dike intruded into the intermediate metavolcanic host rock displaying deflection of the foliation towards the dike. JUMA-2018-29, N: 6827061, E: 247490.

Systematic fracturing was observed in four localities within Domain IV. Four fracture measurements were made from the same outcrop where shearband boudins are situated, hosting roughly N-S striking 1 mm wide mineral-filled fractures with moderate dip degrees ranging from 39 to 52 degrees. Three fracture measurements were made from the tectonic contact between the supracrustal paragneiss and mafic metavolcanite, hosting conjugate fracture sets in orientations 079/80 and 227/82 (Figure 21, A) with one more gently dipping fracture set in an orientation of 278/40. The 079/80 oriented fracture set is 1 mm wide and open whereas the two latter ones have mineral filling and display 0.5 cm wide alteration zones. A second conjugate fracture set was observed with orientations 154/88 and 193/83.

4.2.1.5 Domain V

Domain V, hosting the Välimäki, Saarijärvi and Silmusuo gold targets, is characterized as the most homogenous structural domain with respect to foliation, as almost all of the foliation measurements strike in an NE-SW -orientation, similar to Domain IV (Figure 16). The dip is towards SE, dip degree showing only moderate variation with respect to Domain IV, ranging between 27 to 90 degrees, averaging at 64 degrees, defining the statistical β-axis of 039/02 for the fold patterns in Domain V. The vertical structures are sited at the Välimäki prospect and its vicinity, and the rest of the Domain V hosts structural features with gentler dips. The linear features within Domain V display much greater scattering with respect to Domains I-IV (Figure 16), as the measurements are dominantly oriented towards ESE-NNE. Only four linear measurements plunge towards SSW, sited southwards from the Välimäki target. Within Domains I, II and IV the transition from NE to SW in linear features takes place in the central parts of Pomarkku block, clearly distinguishable from measurements taken within Domain V. Foliation patterns within Domain V are tightly stacked with vertical to subvertical dips towards SE whereas the linear features, tightly clustered in northern domains, display distinct scattering. The linear features averaging towards ENE-plunges of lineations range between 15 to 50 degrees. Linear features plunging towards SSW have a plunge ranging between 22 to 42 degrees. A total of 43 foliation and 24 linear measurements were taken from this subarea.

Domain V hosts rocks that are dominantly S>L- to S-tectonites that is visible in the relatively low amounts of linear features observed from Domain V. The dominant lithological unit within Domain V is supracrustal paragneiss, and the dominant pelitic composition is prone to display planar features. Crenulation folding (Figure 22, A; Figure 32. B) was observed in three localities within Domain V, most likely associated with the open folding also present within Domain V. The open folding was observed to represent dextral asymmetries in three localities. Axial planes of the open folding remained ambiguous. The leucosomes within Domain V displays commonly tight folding with axial plane parallel to the main foliation, including both sinistral and dextral asymmetries associated with larger scale folding and limb-related S- and Z-folds.

The migmatization within Domain V is generally strong due to the substantial amounts of supracrustal units with pelitic composition. The plutonic rocks display also strong partial melting, associated with more intense foliation. Partial melts occur most commonly parallel with the dominant foliation as a layer-bound feature, reflecting the compositional variation of the host rock. Partial melts also occur in the pressure minimums of pinch-and-swell boudins, characteristic for Domain V, similar to Domain IV. Garnet porphyroblasts are a very common feature within Domain V and appear in all lithological units, most commonly in leucosomes. Garnets display foliation deflecting around them, representing a syntectonic formation with respect to main foliation forming event.

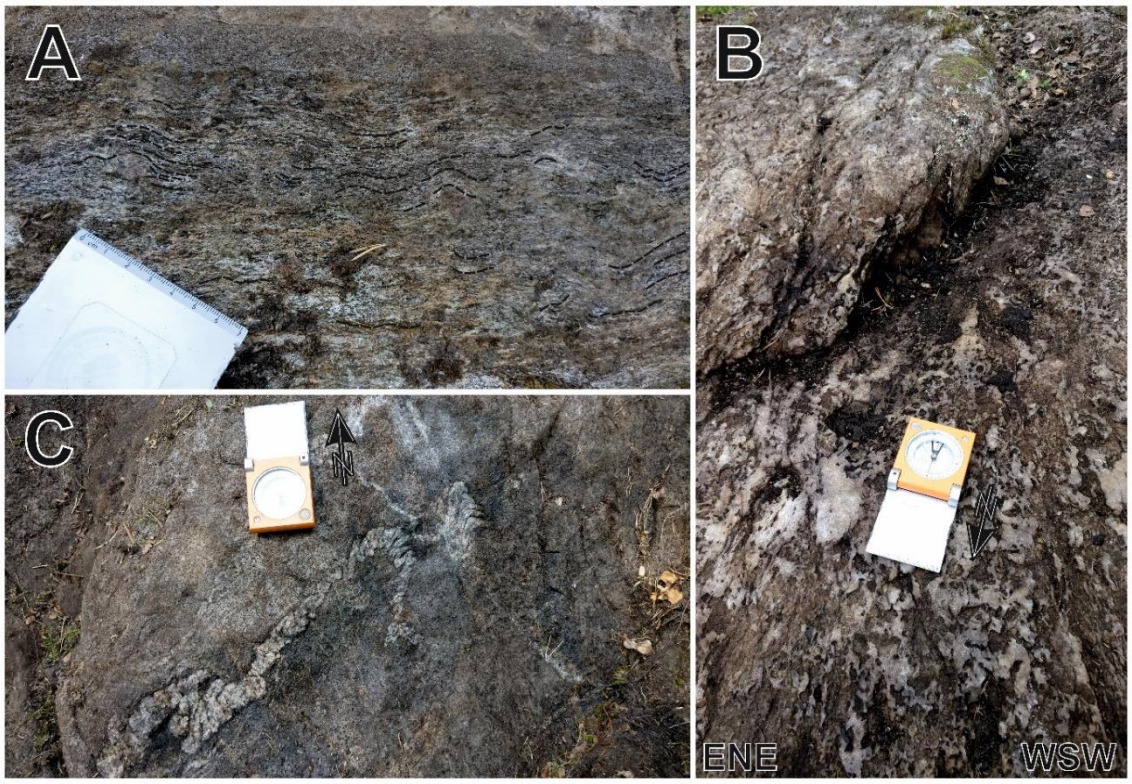

Figure 22: Characteristic structures for Domain V. **A)** Crenulation folding on the biotite grains in a supracrustal paragneiss host rock. JUMA-2018-81, N: 6823540, E: 247945. **B)** Mobilized quartz in a sheared rock with protomylonitic to mesomylonitic composition with strongly weathered surface, plutonic protolith displays strong foliation in the same outcrop. JUMA-2018-89, N: 6824598, E: 248500. **C)** Ptygmatic folding in a leucosome vein in a supracrustal paragneiss host rock. JUMA-2018-111, N: 6823618, E: 247778.

Veining within Domain V is more absent with respect to Domain IV. Pegmatitic veins parallel with the foliation and as a cutting feature, displaying similar deflection of foliation as in Domain IV, are common, but represent partial melts of the host rock. Quartz veining was observed in three localities, including veining parallel to the foliation and veins that have been tightly folded with axial plane parallel with the foliation, pre- to syntectonic formation with the dominant foliation. An N-S -trending, younger cutting quartz-feldspar veins were observed. Quartz lenses were observed, co-occurring with

quartz veins (Figure 15, B). Some quartz veins and lenses have rusty shade, indicating possible sulphide mineralization or weathering of biotite in the proximal parts of the vein. Sulphide mineralization and associated presence of quartz was observed as an axial planar feature, intruded into biotite with king banding (Figure 23).

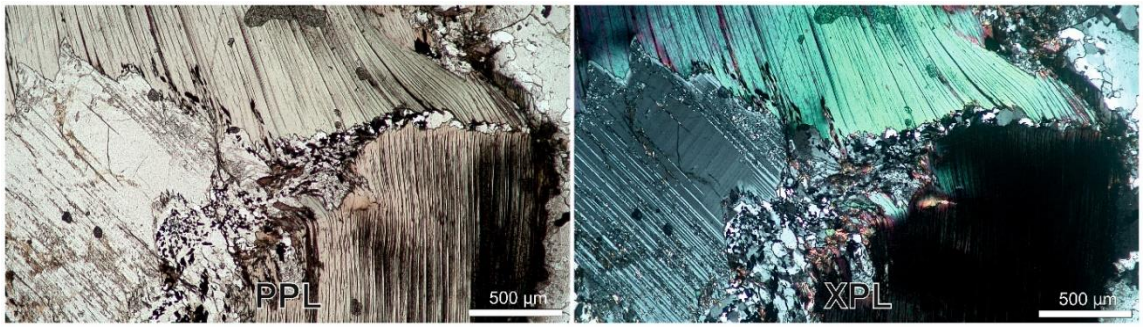

Figure 23: Kink banding in a biotite grain with quartz-sulphide veining as an axial planar feature. Plane- (PPL) and cross-polarized (XPL) images. JUMA-2018-88, N: 6824436, E: 248153.

Shearing was observed in five localities within Domain V, displaying both layer-parallel and -cutting geometries. Layer-parallel shearing was observed in three localities. A contact between a diorite and paragneiss (Figure 24, A) displays reduction in grains size and absence of hornblende in the diorite towards the contact. A large-scale dextral folding was observed, indicating right-lateral (dextral) kinematics for the shearing. A second layer-parallel shearing observation was of small-scale, dextral shearing in a supracrustal paragneiss host rock. Third, allegedly layer-parallel shearing observation is sited in the Välimäki target with very strong silicification together with sulphide mineralization present in the host rock (Figure 24, C), acting as an indicator of shearing and associated fluid flow and alteration of the host rock. The host rock, a supracrustal paragneiss oriented at 147/72, hosts garnet porphyroblasts as a pervasive feature together with boudinage formations with melts in the pressure minimums. Two layer-cutting shearing observations were made. An observation of a protomylonite oriented at 083/73 displaying strong mobilization of quartz with no visible porphyroclasts (Figure 22, B) in a strongly migmatized and foliated plutonic host rock oriented at 138/45. The second, layer cutting observation of shearing within Domain V is a left-lateral (sinistral) shear zone with a displacement of roughly 15 cm in the horizontal surface (Figure 13, A). Leucosome from the host rock has intruded into the NNW-SSW -striking shear zone.

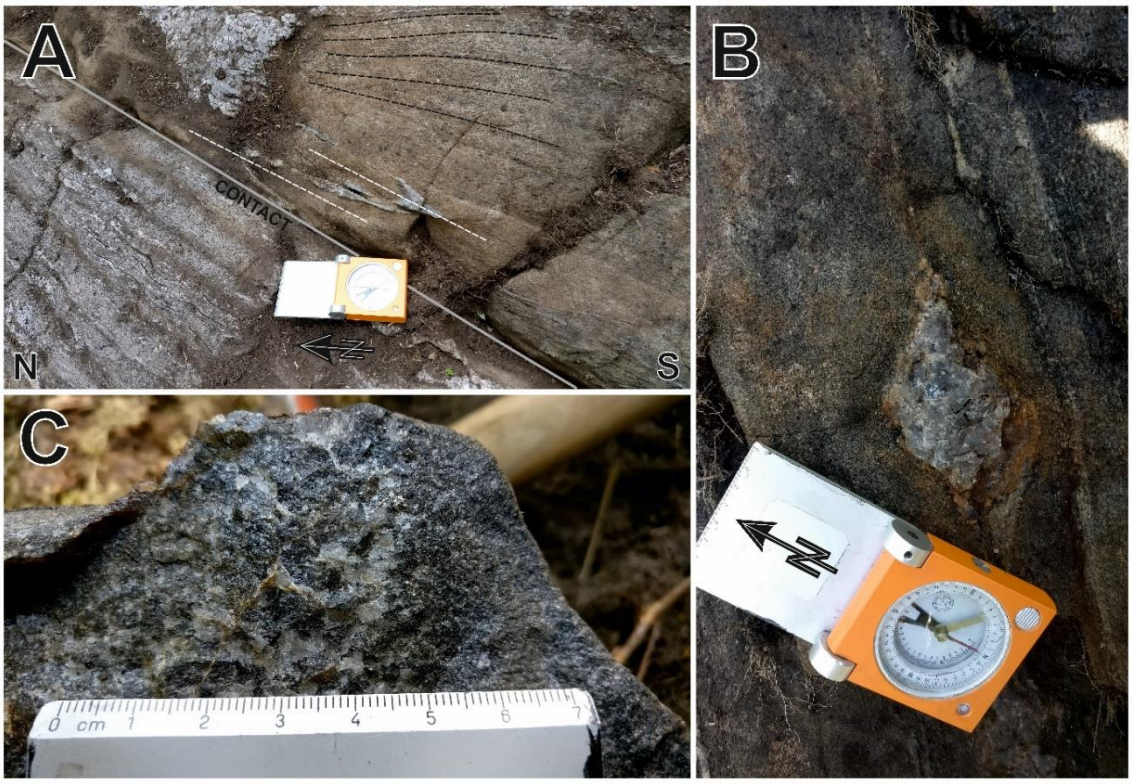

Figure 24: Characteristic structures for Domain V. **A)** A contact between a diorite and paragneiss. Folded quartz vein with axial plane parallel to foliation. Crenulation folding on the supracrustal unit and pinch-and-swell type boudinage on the diorite with quartz-feldspar melts on the pressure minimums. JUMA-2018-12, N: 6825066, E: 248787. **B)** A rusty quartz lens hosted by a pelitic paragneiss, in the vicinity of Välimäki deposit. JUMA-2018-80, N: 6823507, E: 247508. **C)** Strongly silicified supracrustal paragneiss from the Välimäki prospect, visible sulphides. JUMA-2018-110, N: 6823682, E: 247738.

4.2.1.6 Domain VI

Domain VI represents the second large-scale fold structure within the study area, forming an antiform structure plunging very gently towards NE (Figure 16). Foliation data collected from Domain VI is sited mostly at the fold hinge and the data displays clearly visible smaller scale, parasitic folding. Foliation dips within Domain VI range between 8 to 72 degrees and but the amount of observations is too sparse for the definition of a statistical β-axis. Linear features within Domain VI are oriented towards NNE, plunge ranging from 5 to 29 degrees, averaging at 24 degrees. Both supracrustal paragneisses and plutonic units were observed within Domain VI and a total of 7 foliation and 6 linear measurements were taken from this subarea.

Open folding, characteristic for other domains, was observed in three localities within Domain VI with unclear asymmetries. Migmatization within Domain VI is present on the supracrustal units and partial melts in the plutonic units appears as pegmatitic veins. Veining was observed in five localities within Domain VI. Pegmatitic veins appear commonly as features parallel to foliation and display boudinage formations in one

outcrop (Figure 25, B). The foliation in this outcrop is oriented at 209/72, representing parasitic foliation at the fold hinge of the large-scale structure. The pegmatitic vein is oriented NE-SW, parallel with the axial plane of the large-scale folding. Cutting quartz veins within the same outcrop have a strike of 070. Parallel with these veins, cutting quartz-feldspar veins were also observed from a 072/25 oriented granodiorite in a perpendicular manner to the foliation.

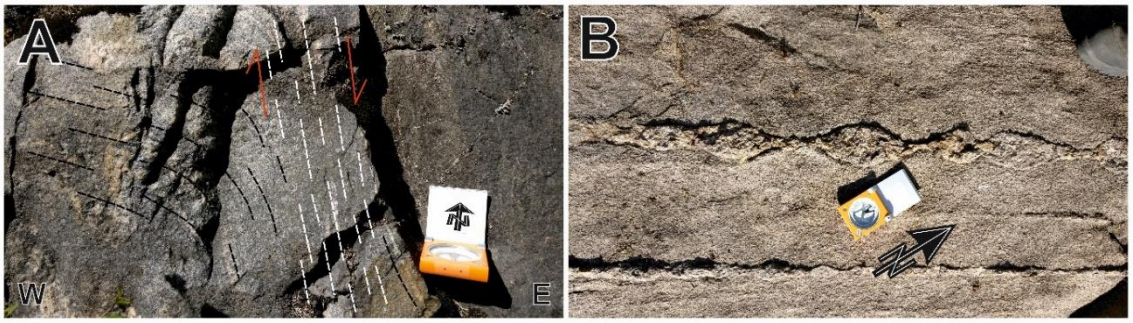

Figure 25: Characteristic structures for Domain VI. **A)** A 072/83 oriented normal fault with W-side up -kinematics. Flat lying, 002/08 oriented foliation of the tonalitic protolith transposes towards the ductile shear zone. View towards N. JUMA-2018-17, N: 6823721, E: 251122. **B)** Pinch-and-swell boudinages in a pegmatitic leucosome cutting the 209/72 oriented foliation parallel with the axial plane in a psammitic paragneiss, syntectonic formation. JUMA-2018-19, N: 6824017, E: 253853.

Shearing was observed in one locality within Domain VI. A roadcut displays multiple shear zones with a width of few centimeters. On the western end of the roadcut the outcrop displays flat-lying foliation in an orientation of 002/08. Moving towards east, the texture turns into more massive and the mylonitic shear zone transposes the dominant foliation into a subvertical 072/83 orientation. The deflection of the main foliation indicates dip-slip normal faulting with W-side up -kinematics in a ductile deformation regime (Figure 26, A and C; Figure 25, A). The quartz in the thin sections displays static recrystallization with 120-degree junctions between individual quartz grains (Figure 26, B).

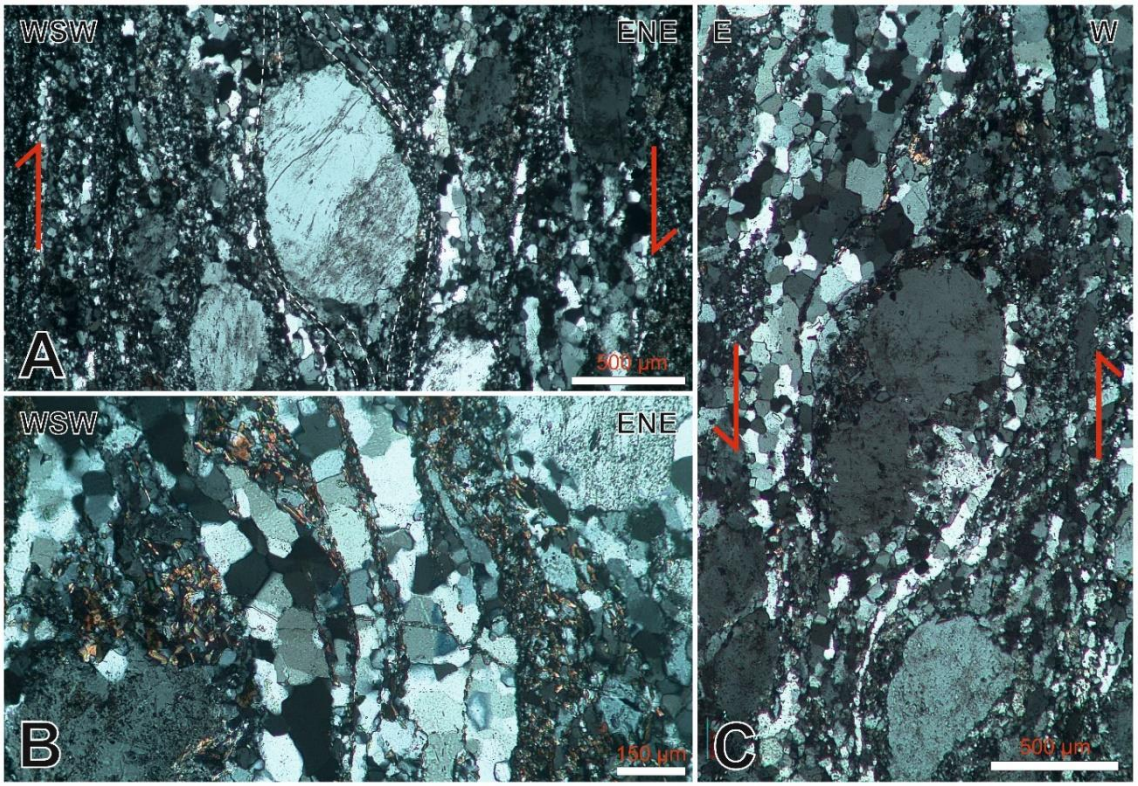

Figure 26: Thin section images from the outcrop displaying flat-lying foliation and vertical mylonitic shear zones. **A)** A sigma-clast indicating W-side up -kinematics, view towards NNW. Observation JUMA-2018-17, N: 6823721, E: 251122, sample PMSK-2018-1.1 from the same locality. **B)** Static recrystallization in quartz bands with multiple 120° junctions. Observation JUMA-2018-17, N: 6823721, E: 251122, sample PMSK-2018-1.1. **C)** Sinistral sigma-clast indicating W-side up -kinematics, view towards S. JUMA-2018-17. N: 6823721, E: 251122.

4.2.1.7 Domain VII

The structural data for Domain VII consist mostly of old observations made by the Geological Survey of Finland and Outokumpu Oy and as a result, the detailed description is more limited as in Domains I-VI. Domain VII consist of two dominant foliation orientations: NE-SW -trends, parallel with Domain V, and roughly E-W -trends affected by transposition in the vicinity of the crustal-scale Kankaanpää shear zone. The structural data displays transitional shifting from NE-SW -orientations to E-W -orientation, reflecting the gradual transpositioning towards Kankaanpää shear zone. A total of 76 foliation measurements and 52 linear measurements are displayed in Figure 16 in which three foliation and four planar measurements were collected during this study.

From the three observations made in Domain VII, two observations display clear foliation and the third observation is a L>S -tectonite with very weak planar features (Figure 27, B). Folding was observed in one location, displaying tight sinistral asymmetries. Veining was observed in two localities in which quartz veining occurs as a parallel feature with the foliation. The third locality hosts granitic veins parallel to foliation with both

pegmatitic and aplitic textures. Garnet porphyroblasts appeared as an abundant, pervasive feature in two localities (Figure 27, A). Conjugate fracture sets with alkali feldspar filling and associated sericite alteration of feldspars were observed in one locality, fractures oriented at 053/80 and 204/84 (Figure 27, B).

Figure 27: Characteristic structures for Domain VII. **A)** Garnet porphyroblasts in a highly deformed orthogneiss with granodioritic protolith. JUMA-2018-65, N: 6827266, E: 256121. **B)** An L-tectonite with tonalitic composition displaying later conjugate fracture sets with sericite alteration zones. JUMA-2018-123, N: 6828516, E: 255545.

4.2.2. Detailed form line map

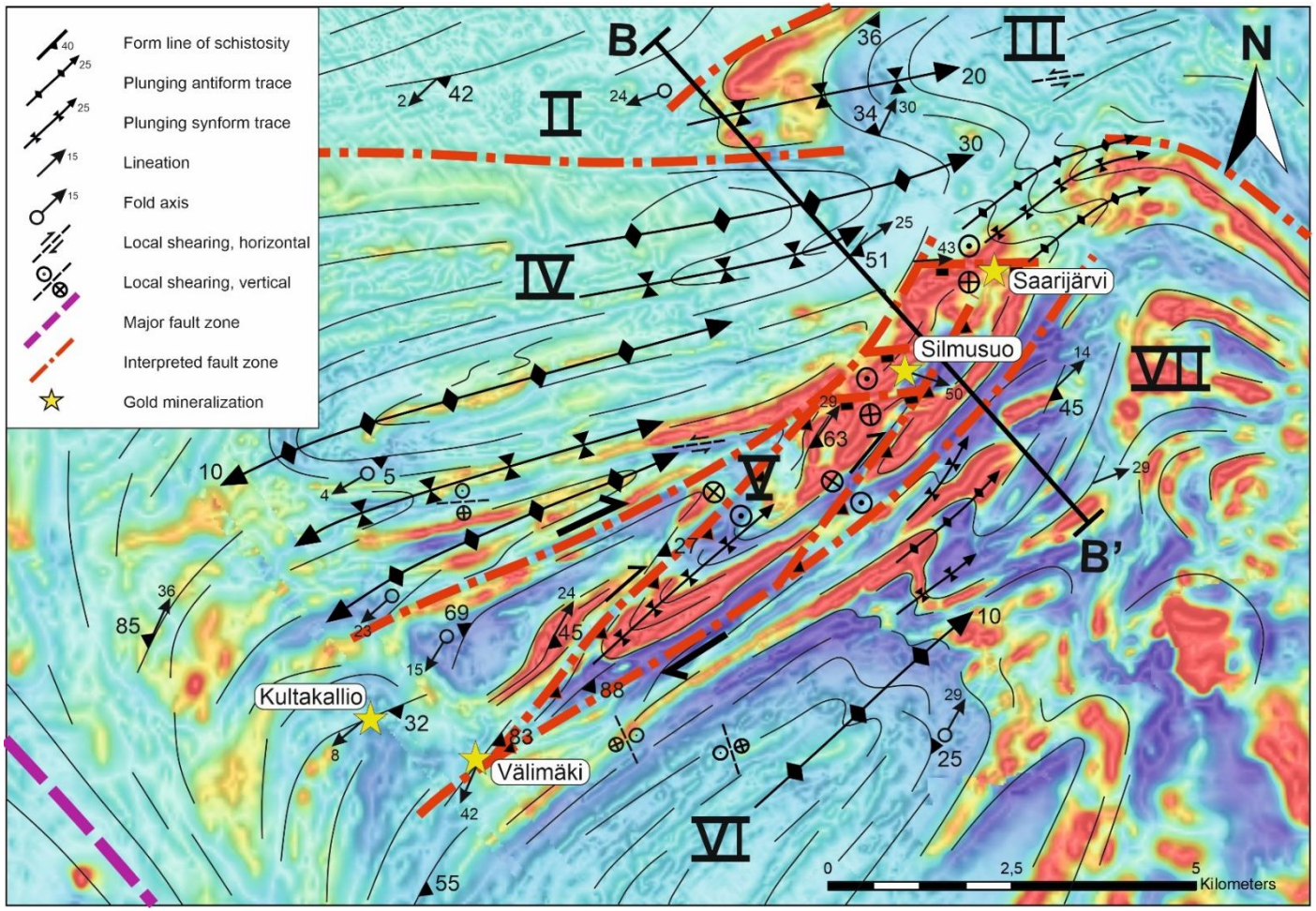

Figure 28: A detailed form line map of the study area with aeromagnetic map ©Geological Survey of Finland. Black line indicates the positioning of cross section B-B' from the study area (Figure 30).

4.2.3. Cross sections

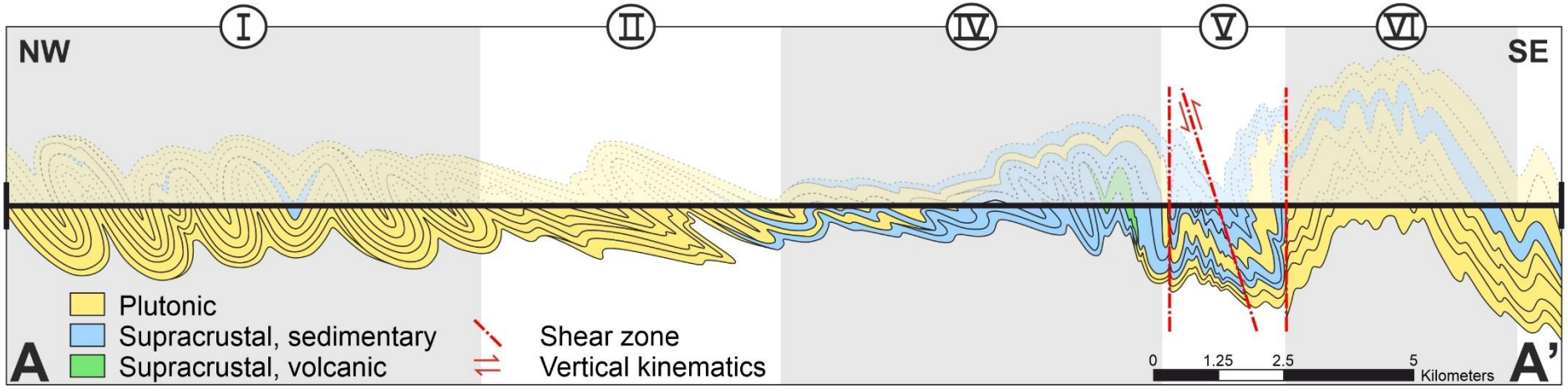

Figure 29: Cross section A-A'.

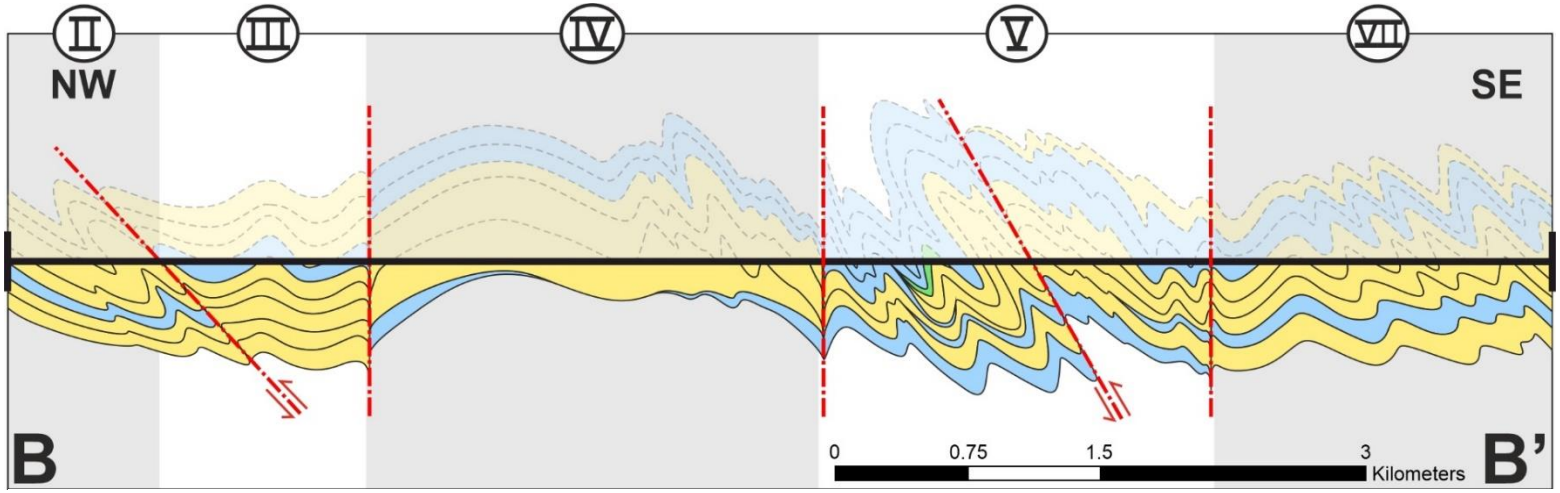

Figure 30: Cross section B-B'.

4.2.4. Gold target structures

The four known gold prospects within Pomarkku block display structural differences both in planar and linear features. The Välimäki, Silmusuo and Saarijärvi prospects are clearly spatially associated with shear zones while the Kultakallio mineralization displays no distinct association with shear zones. The Välimäki prospect displays vertical structures with gently plunging linear features. The Kultakallio target hosts moderately dipping planar structures and very gently plunging linear features. Silmusuo prospect hosts moderately dipping structures and steeply plunging linear features, hence differing from the Välimäki and Kultakallio prospects. The Saarijärvi target is sited within the vicinity of the same interpreted fault zone as the Silmusuo prospect and the previous studies in the Saarijärvi target display ENE-trending foliation with 60–70 NW dips. No data of the Saarijärvi prospect was available in this study. Välimäki, Saarijärvi and Silmusuo are sited in Domain V whereas the Kultakallio prospect is sited in Domain IV (Figure 16).

4.2.4.1. Välimäki

The Välimäki prospect hosts the largest number of outcrops in the vicinity of the known gold mineralization, providing a good starting point for the structural interpretation. The vertical planar structures trending NE-SW (Figure 31), associated with silicification (Figure 24, C) indicate strike-slip type shearing and associated fluid flow. Gently plunging linear features are conforming to the strike-slip kinematics. The geometrical shapes visible in the aeromagnetic map indicate dextral sense of shear for the shear zone (Figure 28). The Välimäki prospect is sited in the vicinity of the convergence between the strike-slip and interpreted reverse-type shear zones.

The lithology within Välimäki prospect and its vicinity consists of supracrustal paragneisses with both pelitic and psammitic compositions and stromatic textures as a common feature. Crenulation of the main foliation (Figure 32, B) is present in the pelitic sequences and tight folding of leucosome with axial plane parallel to main foliation is also present. Veining is present as parallel to foliation and as a cutting feature in which the veins are folded with axial plane parallel to main foliation. A 50 cm wide aplitic granite vein was observed, cutting the main foliation at an oblique angle. Garnet porphyroblasts are a very common layer-bound or pervasive feature in the Välimäki prospect, indicating alteration in the area.

The foliation in the host rock most likely forms a weakness zone, controlling the siting of the veins. These smaller, gold-critical shear zones likely represent third-order structures and the interpreted NE-SW -trending dextral shear zone (Figure 28) represents a second-order structure, controlling the fluid flow in the Välimäki prospect.

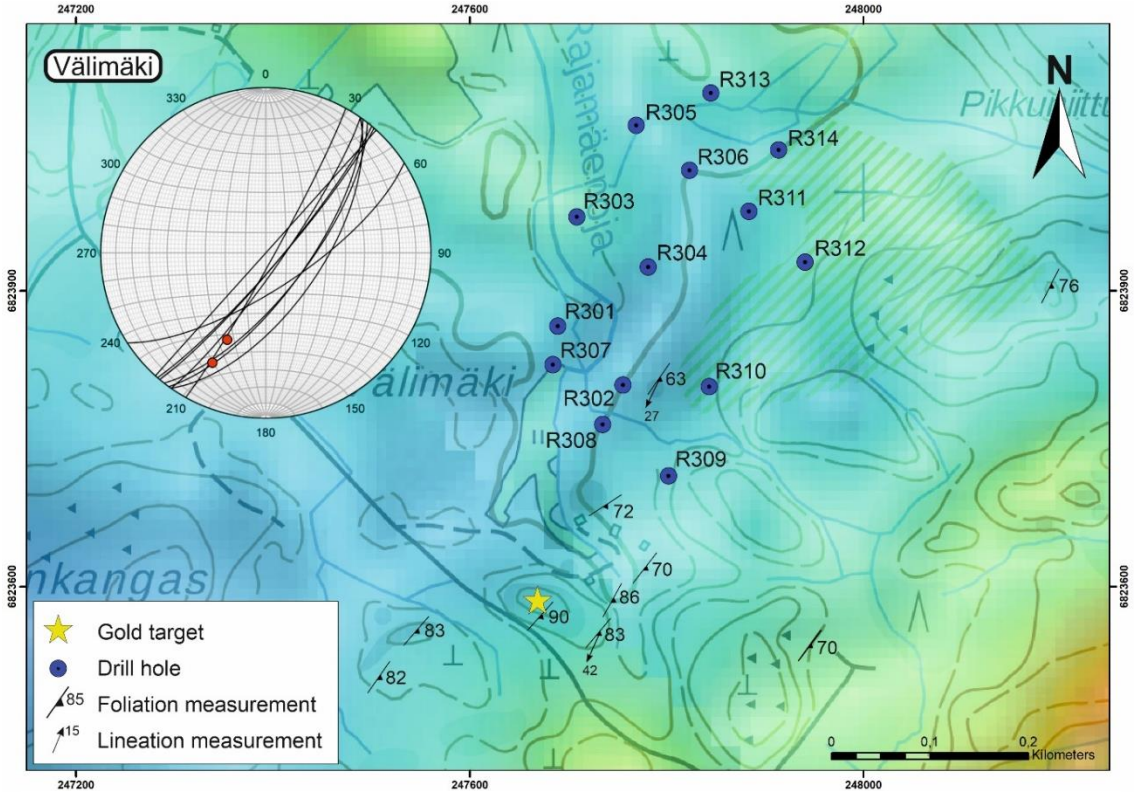

Figure 31: Positioning of the structural measurements of the Välimäki prospect with lower hemisphere stereographic projection displaying foliation (great circles) and lineation (red dots) measurements. Drill hole locations indicated. Aeromagnetic map ©Geological Survey of Finland.

Shearing was not observed in the outcrops of Välimäki and therefore no kinematic indicators are present. All of the thin sections from the Välimäki prospect and its vicinity display recrystallization of quartz which display no visible kinematics and are therefore interpreted to be formed during static recrystallization (Fossen, 2016). According to Otani & Wallis (2006), straight grain boundaries and lack of undulose extinction are characteristic for static recrystallization (Figure 32, A and B) and this type of recrystallization of quartz is typical for high-grade gneissic terranes indicating that the shear deformation occurred prior to or synchronously with high-T conditions.

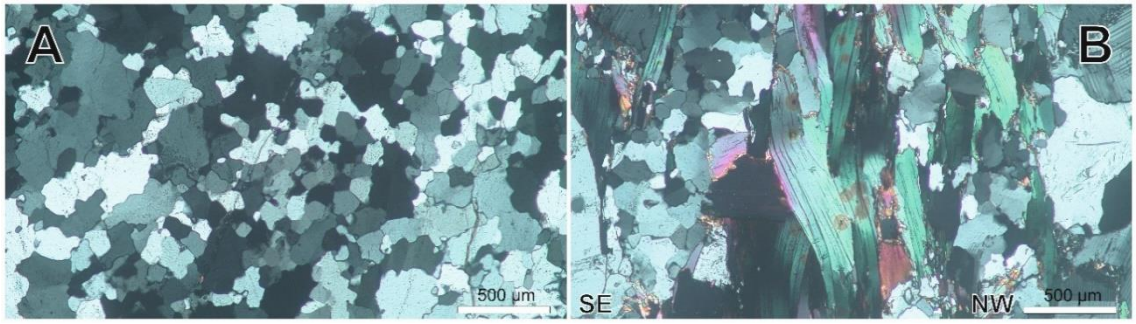

Figure 32: A) Static recrystallization of quartz. JUMA-2018-5, N: 6823569, E: 247642. Sample JUMA-2018-5.1. **B)** Crenulation folding visible in the biotite grains, quartz grains display static recrystallization. View towards SW. JUMA-2018-80, N: 6823507, E: 247508. Sample JUMA-2018-80.1.

4.2.4.2. Kultakallio

The Kultakallio prospect is sited 1.5 km to WNW from the Välimäki target and is significantly more restricted in the number of outcrops with respect to Välimäki. The previously studied large outcrop consists of quartz diorite whereas the newly discovered outcrop ESE from the quartz diorite consists of paragneiss. The contact between these lithological units remained ambiguous. Two nearly parallel foliation measurements were acquired with one lineation measurement from the plutonic quartz-diorite in the WNW, plunging very gently towards SW (Figure 33). Paragneiss within the ESE part of the target did not display linear structures. Shearing in these two outcrops is absent, both in micro- and macro-scale both outcrops display strong foliation suitable for pure shear -environment. Quartz in the thin sections displays recrystallization, similar to Välimäki prospect's static recrystallization but undulating extinction is also present in some grains, representing small dislocations in the crystal lattice (Fossen, 2016), indicating the presence on simple shear component in addition to pure shear. The contact between these two lithological units remained ambiguous.

The very gentle plunge of the lineation indicates a strike-slip type kinematics and the lack of structural continuities in the aeromagnetic data in the area displays no evidence of a larger-scale shearing in the vicinity of Kultakallio prospect. The geophysical data displays a weak signature of a fold-pattern with the Kultakallio prospect sited in the vicinity of the fold hinge. This associated with the near presence of the crustal-scale Kynsikangas shear zone has most likely contributed to the formation of weakness zones and placement of gold-critical sulphide mineralizations in the Kultakallio prospect.

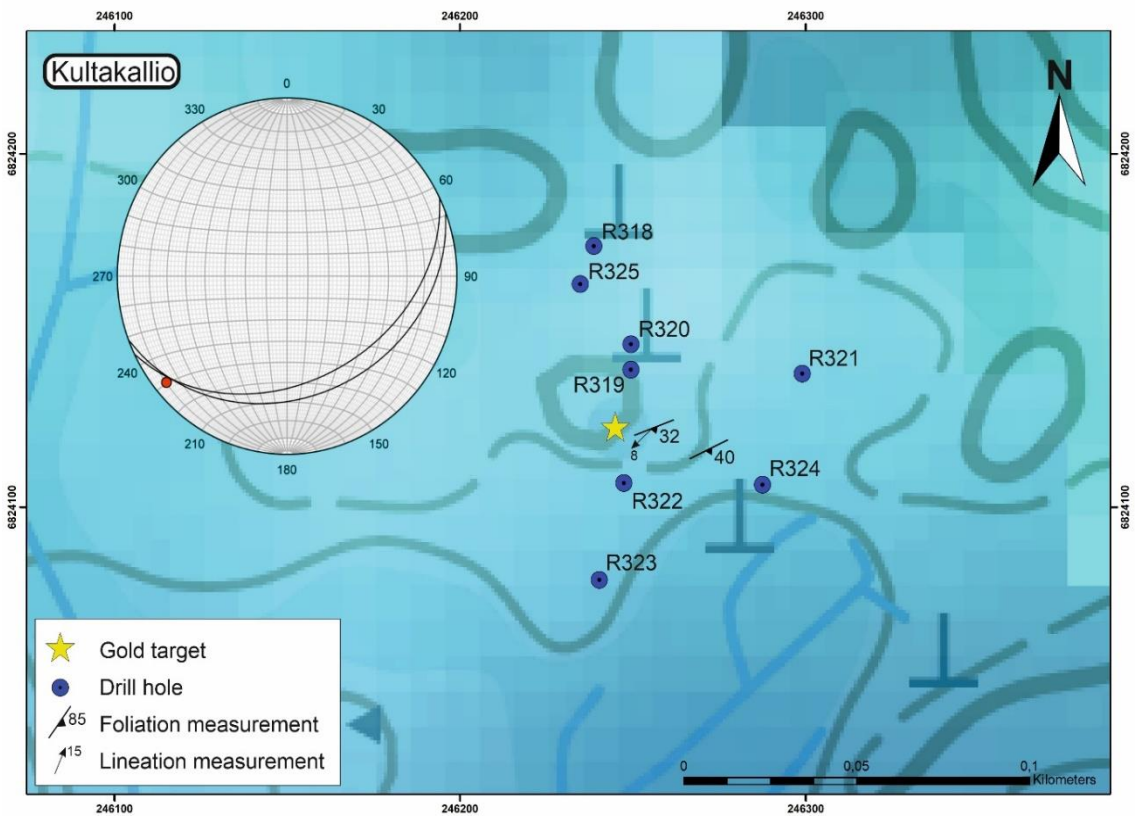

Figure 33: Positioning of the structural measurements of the Kultakallio prospect with lower hemisphere stereographic projection displaying foliation (great circles) and lineation (red dots) measurements. Drillhole locations indicated. Aeromagnetic map ©Geological Survey of Finland.

Garnets are present in both outcrops in large amounts, indicating strong alteration in the area. Felsic pressure shadows are present in the psammitic sections of the supracrustal paragneisses and display no kinematics (Figure 34). Veining of two generations is present in the quartz-diorite. The older generation of veining is 5–10 mm thick, sited parallel with the foliation and is locally folded. The younger generation of veining is 10–150 mm thick and oriented at 047/75. Sulphides are present in both host rocks as a disseminated feature and the sample with highest gold grades (JUMA-2018-26.3) was located on the Kultakallio prospect.

A large arsenopyrite-rich boulder was found during previous studies by the GTK and was analyzed for the presence of gold and associated minerals in this study (Figure 41, Table 1). Sulphide mineralization was observed in two other localities within Domain IV, both hosted by an intermediate volcanic rock only few hundred meters apart from each other. First of these two observations displays quartz-sulphide mineralization in the necks of pinch-and-swell -boudins (Figure 21, D) together with later quartz veining with a strike of 132 degrees and steep dip. The second mineralization was observed in the upper contact between intermediate volcanic rock and coarse-grained pegmatitic vein. The

sulphide was interpreted as molybdenite (MoS_2) on the field and it appeared as a massive continuous layer along the length of the contact (Figure 21, E).

Figure 34: Felsic pressure shadows in the garnet porphyroblasts sited in the paragneiss with psammitic composition. JUMA-2018-99. N: 6824111, E: 246265.

4.2.4.3. Silmusuo

A total of five observations were collected from the the Silmusuo prospect in which one is the gold-critical boulder observation (JUMA-2018-37). Three paragneiss outcrops are clustered and display homogenous structural orientations (Figure 35). One observation of a plutonic rock is sited roughly 150 m SSE from these observations and displays a slightly different orientation with respect to foliation. The linear measurements are clustered in this area and display steeper plunges. The plutonic rock is also classified as an L-tectonite, hosting very strong linear features, common in plutonic rocks within the study area. The paragneiss outcrops in the Silmusuo prospect host both pelitic and psammitic compositions. Partial melts are also present in the tonalitic outcrop, parallel with the foliation. Garnet porphyroblasts are present in the paragneiss outcrop, both in the leucosome and host rock. The porphyroblasts in the leucosome display larger grains sine compared to the ones in the host rock, reaching sizes of several centimetres in width.

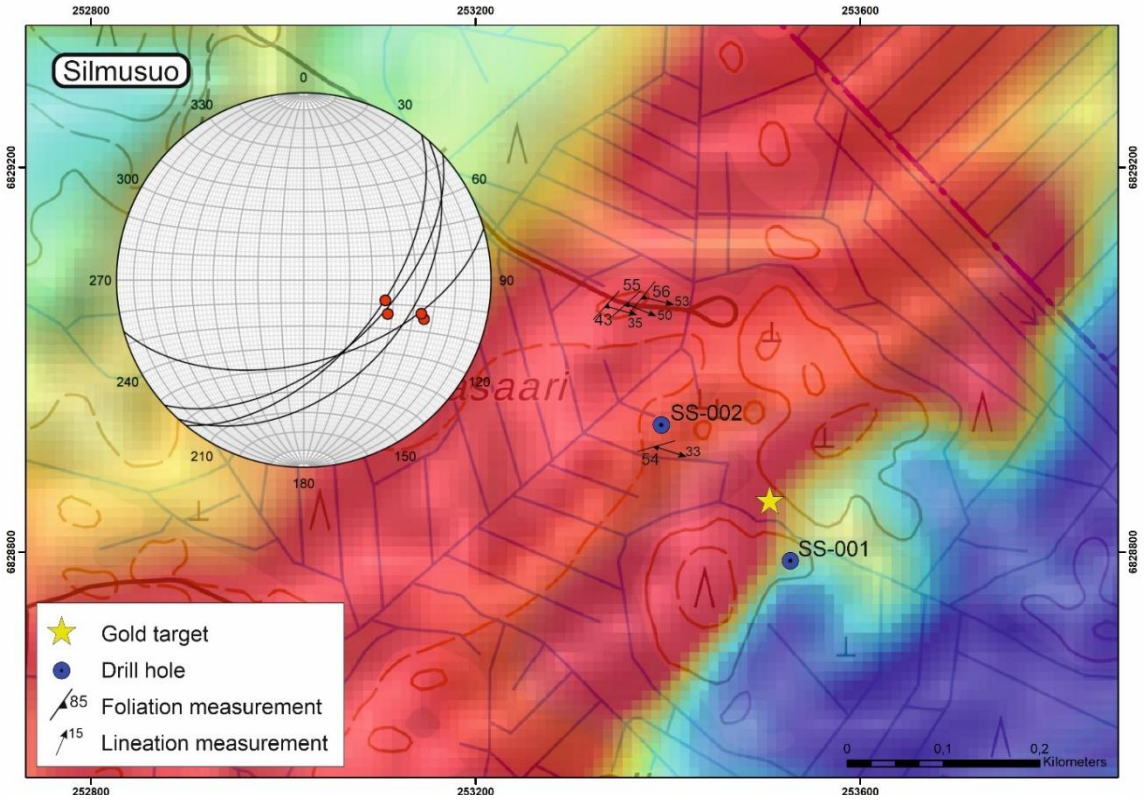

Figure 35: Positioning of the structural measurements of the Silmusuo prospect with lower hemisphere stereographic projection displaying foliation (great circles) and lineation (red dots) measurements. Drillhole locations indicated. Aeromagnetic map ©Geological Survey of Finland.

The relatively steeply plunging lineations within the outcrops in the Silmusuo prospect indicate dip-slip dominated deformation, differing from the Välimäki and Kultakallio targets. The magnetic anomalies in the vicinity of the Silmusuo prospect are cut by roughly E-W -trending non-magnetic continuations forming visible jogs in the magnetic sections (Figure 35). These are interpreted as shear zones and in an overall NE-SW -oriented dextral setting within the gold-critical Domain V (Figure 28), E-W trending structures are most likely normal faults with S-side down -kinematics or antithetic left-lateral strike-slip systems. The gold-critical boulders within the Silmusuo prospect have been interpreted as a strongly silicified metasedimentary rock. The required fluid flow indicates a presence of a fault structure and therefore the mineralization in the Silmusuo prospect is likely hosted by third-order normal faults related to NE-SW dextral strike-slip faults (Figure 28).

4.2.4.4. Saarijärvi

The Saarijärvi prospect hosts only one outcrop, observed in the previous studies (Kärkkäinen et al., 2016). The main foliation strikes NE and dips 60–70 degrees, similar to the Silmusuo prospect, but the dip direction is opposite, NW. The opposite dip direction indicates folding as the Silmusuo and Saarijärvi prospects are sited in the same continuous

aeromagnetic anomaly. Narrow quartz veins appear as a parallel feature with respect to the dominant foliation. The outcrop is cut by a shear zone oriented at 150/80.

Similar E-W -trending continuities in the geophysical maps with respect to Silmusuo prospect are also present in the Saarijärvi target, although not as distinct as in the Silmusuo prospect. The Saarijärvi is also sited in the vicinity of fold structures in NE which can also have an impact on the formation of gold-critical structures. With the restricted amount of data, it can be assumed that Saarijärvi prospect is controlled by similar structures as the Silmusuo prospect.

4.3. Geochemistry

4.3.1. Major elements

Fourteen plutonic rocks were analysed within the study area (Figure 3) from which eleven are classified as granodiorites and diorites in the Total Alkali vs. Silica (TAS)-diagram due to their intermediate SiO_2 content and relatively low contents of Na_2O and K_2O (Figure 36, A). Sample JUMA-2018-22.1 plots into the monzodiorite -field and samples JUMA-2018-26.2 (Kultakallio prospect) and TALE-2018-31.1 (heterogenic, locally strongly sheared) are located in the gabbroic diorite field. All the samples form a continuous series with alkali contents slightly increasing with increasing silica contents.

In the Zr/Ti vs. Nb/Y -diagram (Figure 36, B) majority of the samples plot in the andesite and basaltic andesite and trachyandesite fields with the sample JUMA-2018-22.1 (blue triangle) in the same cluster. This indicates that the sample has undergone a slight alteration, likely related to the two sets of quartz-feldspar veins in the outcrop. The two

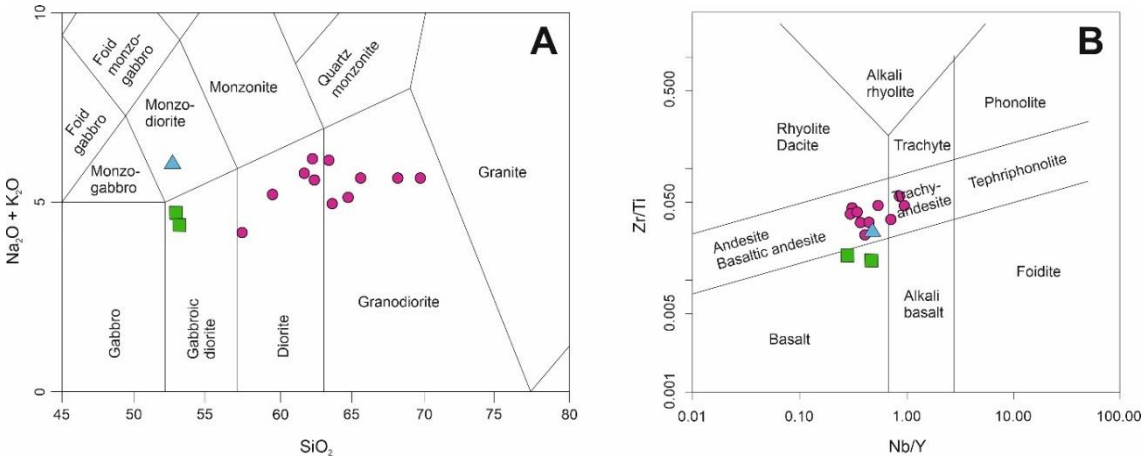

Figure 36: Geochemical classification of the plutonic rocks in the study area. **A)** TAS-diagram (Middlemost, 1994) of the plutonic rocks. Granodioritic and dioritic samples: purple circles; gabbroic diorites: green squares; monzodiorite: blue triangle. **B)** Immobile element diagram (Pearce, 1996) of plutonic rocks.

gabbroic diorites (green squares) plot in the basaltic field but are still somewhat in the same cluster with the other samples.

The SiO_2-content in the plutonic rocks varies between 51.92 and 68.94 wt-% (Figure 36). In the Harker diagrams the dioritic and granodioritic samples form continuous trends with no remarkable deviation (Figure 37). The gabbroic diorite (TALE-2018-31.1) and the monzodioritic (JUMA-2018-22.1) samples display a variation in the Harker diagrams (Figure 37; A, B, D). The Al_2O_3-content ranges between 14.64–19.39 wt-% and the gabbroic diorite sample TALE-2018-31.1 plots outside the general trend, displaying relatively low ratios between Al_2O_3 and SiO_2. In thirteen samples, MgO-content ranges between 1.14–4.94 wt-% and sample TALE-2018-31.1 has MgO-content of 7.57 wt-%. The CaO-content ranges between 3.01–8.18 wt-%. The Na_2O-content ranges between 2.43–3.87 wt-% and the monzodioritic sample JUMA-2018-22.1 has relatively high ratios

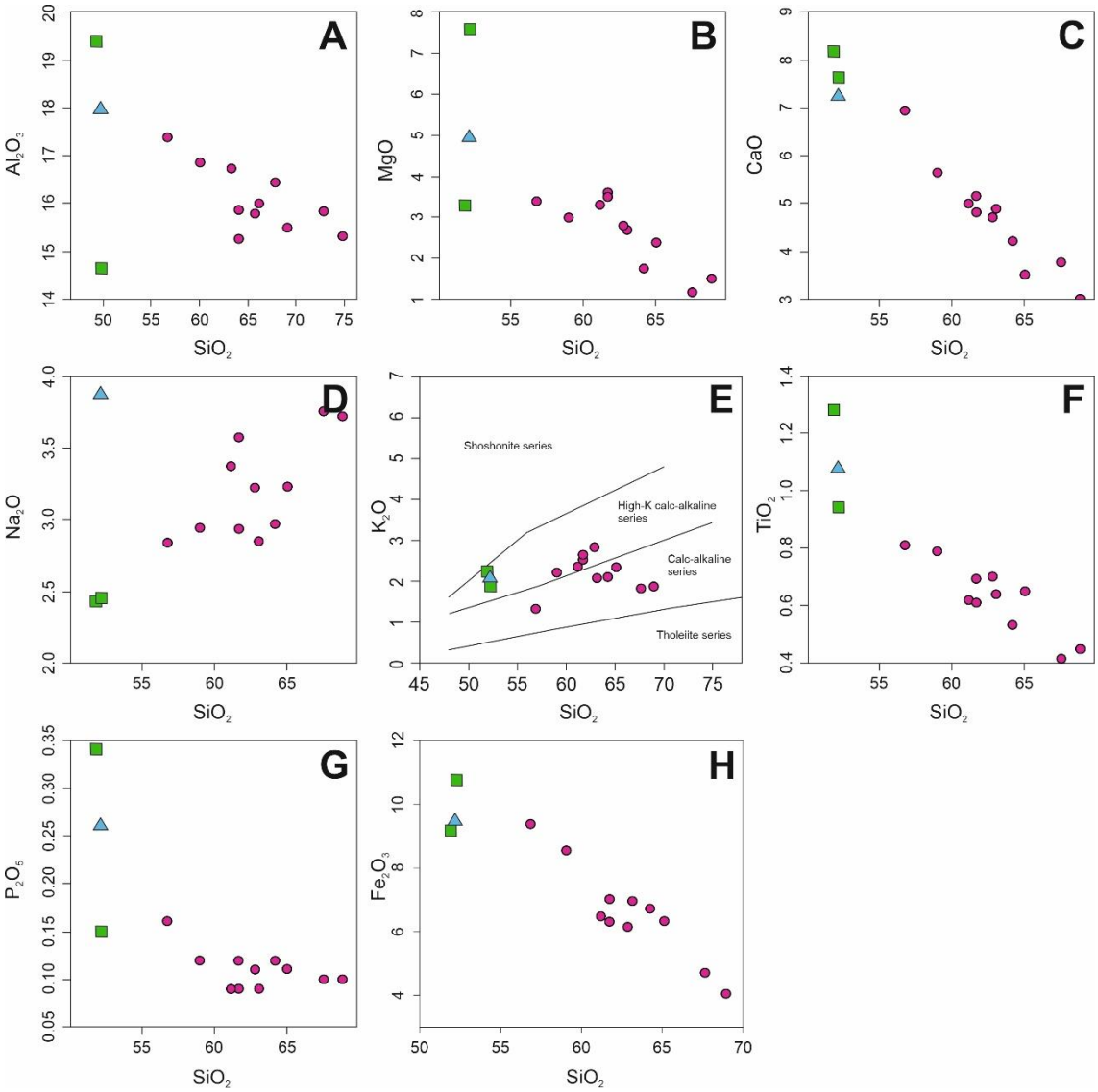

Figure 37: Bivariate SiO_2 versus major element Harker diagrams of the plutonic rocks, symbols as in Figure 36. **E)** SiO_2 vs. K_2O after Peccerillo & Taylor (1976).

of Na_2O and SiO_2. The K_2O-content ranges between 1.32–2.83 wt-% and all samples plot either into the calc-alkaline or high-K calc-alkaline series (Peccerillo & Taylor, 1976), indicating a subduction-related environment. The TiO_2-content ranges between 0.41–1.28 wt-%. The P_2O_5-content ranges between 0.09–0.34 wt-%. The Fe_2O_3-content ranges between 4.05–10.76 wt-%.

4.3.2. Trace elements

The REE-patterns in the chondrite normalized REE Spider-diagram are negative and gently sloping (Figure 38). The plutonic rocks are enriched in LREE (La_N/Yb_N = 3.44–12.66), (La_N/Sm_N = 1.13–5.39), (Gd_N/Yb_N = 1.16–2.15). Two anomalous samples were counted out from the REE calculations: JUMA-2018-17.1, depleted in HREE (La_N/Yb_N = 46.37), (La_N/Sm_N = 8.00), (Gd_N/Yb_N = 3.28) and JUMA-2018-115.1, very slightly enriched in HREE and depleted in LREE (La_N/Yb_N =1.49), (La_N/Sm_N = 3.29), (Gd_N/Yb_N = 0.53) (Figure 38). The europium anomaly varies from moderately negative to non-existent or weakly positive (Eu/Eu* = 0.54–1.17). The two anomalous samples (JUMA-2018-17.1, JUMA-2018-115.1) represent the two highest Eu/Eu*-values (1.15 and 1.17) but are not anomalously high and have not been counted out for the Eu/Eu*-calculations. The total REE-content varies in the range of 78.89–201.54, sample JUMA-2018-115.1 representing the lowest REE_{tot}.

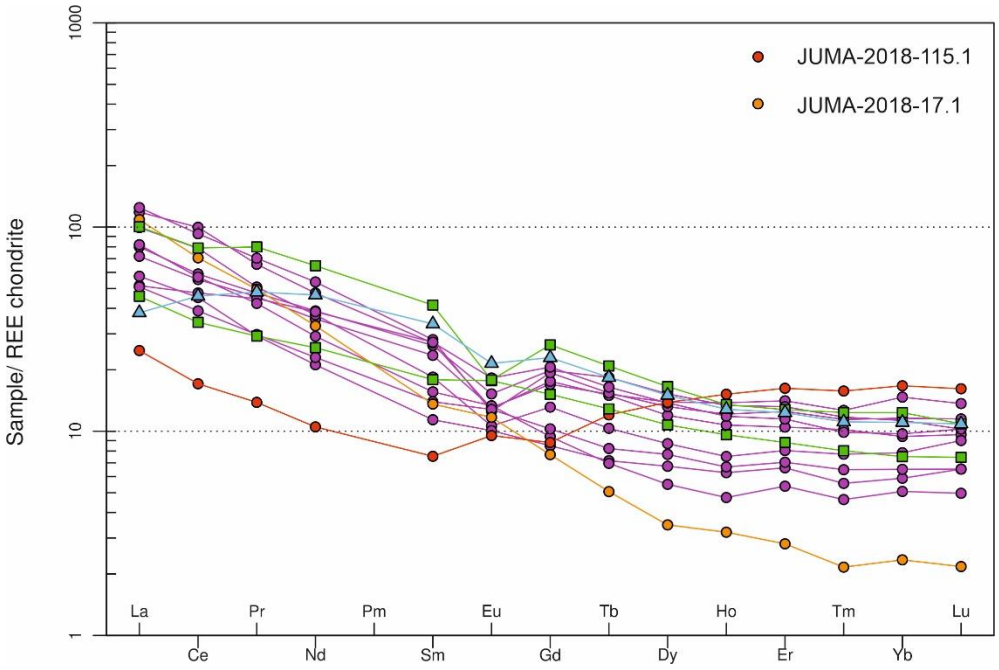

Figure 38: Chondrite-normalized REE- Spider diagram (Boynton, 1984) of the plutonic rocks, symbols as in Figure 36. REE-anomalous samples indicated.

The multielement diagram of trace elements (Pearce, 1983) displays a fairly uniform subduction-type trend (Figure 39). A negative Nb-Ta -anomaly with respect to Th and

Ce together with negative Ti-anomaly are typical for subduction-related rocks (Pearce, 1996). High amounts of Rb, Ba and Th and low concentrations of Y and Yb indicate a subduction component (Hawkesworth et al., 1991) (Figure 39). The fluid-mobile elements (Sr, K, Rb, Ba) form uniform clusters with remarkable deviation only in Ba. In the tectonic classification Y+Nb/Rb -diagram by Pearce et al. (1984), all the plutonic rocks plot into the volcanic arc granitoid (VAG) -field (Figure 40).

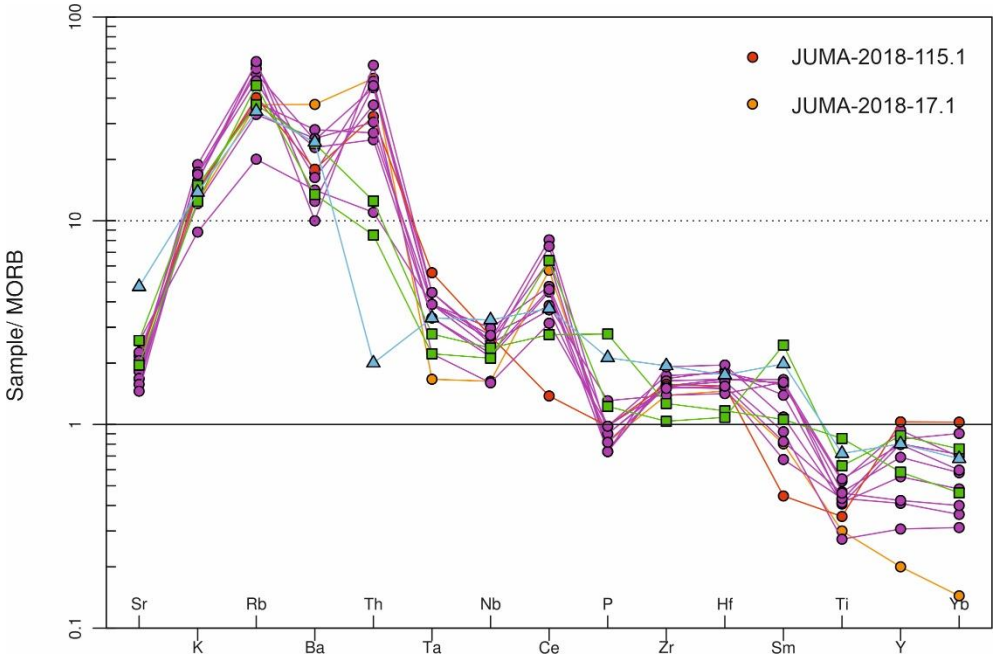

Figure 39: MORB-normalized multielement diagram (Pearce, 1983) of the plutonic rocks, symbols as in Figure 36. REE-anomalous samples as in Figure 38.

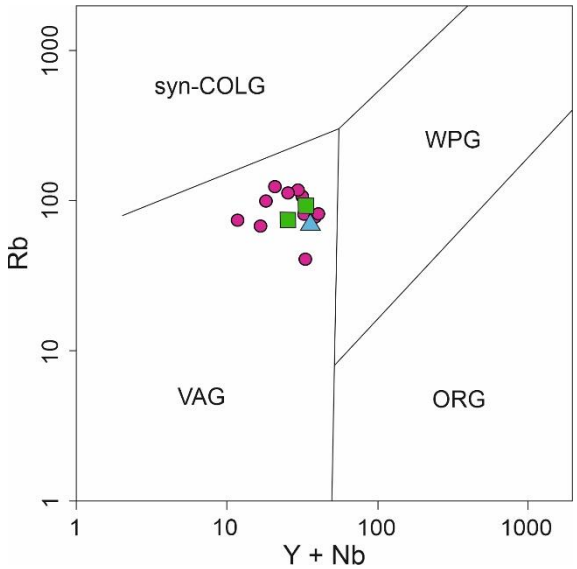

Figure 40: Tectonic classification diagram for plutonic rocks by Pearce et al. (1984). Symbols as in Figure 36.

4.3.3. Gold-critical samples

Three gold-critical samples were identified from the whole-rock analysis (Figure 41, Table 1). Sample JUMA-2018-107.1 (368.3 ppb Au) is from a paragneiss outcrop from the Välimäki prospect with visible silicification. Sample JUMA-2018-26.3 (46570.6 ppb Au) is from a boulder at the Kultakallio prospect, very rich in arsenic sulphide and is also enriched in Ag, Cu, Sb, Bi and Te. Sample JUMA-2018-37.1 (78.6 ppb Au) is from a boulder from the Silmusuo prospect, most likely silicified supracrustal rock enriched in As and Cu. The full list of the analysis results can be seen in Appendix 1.

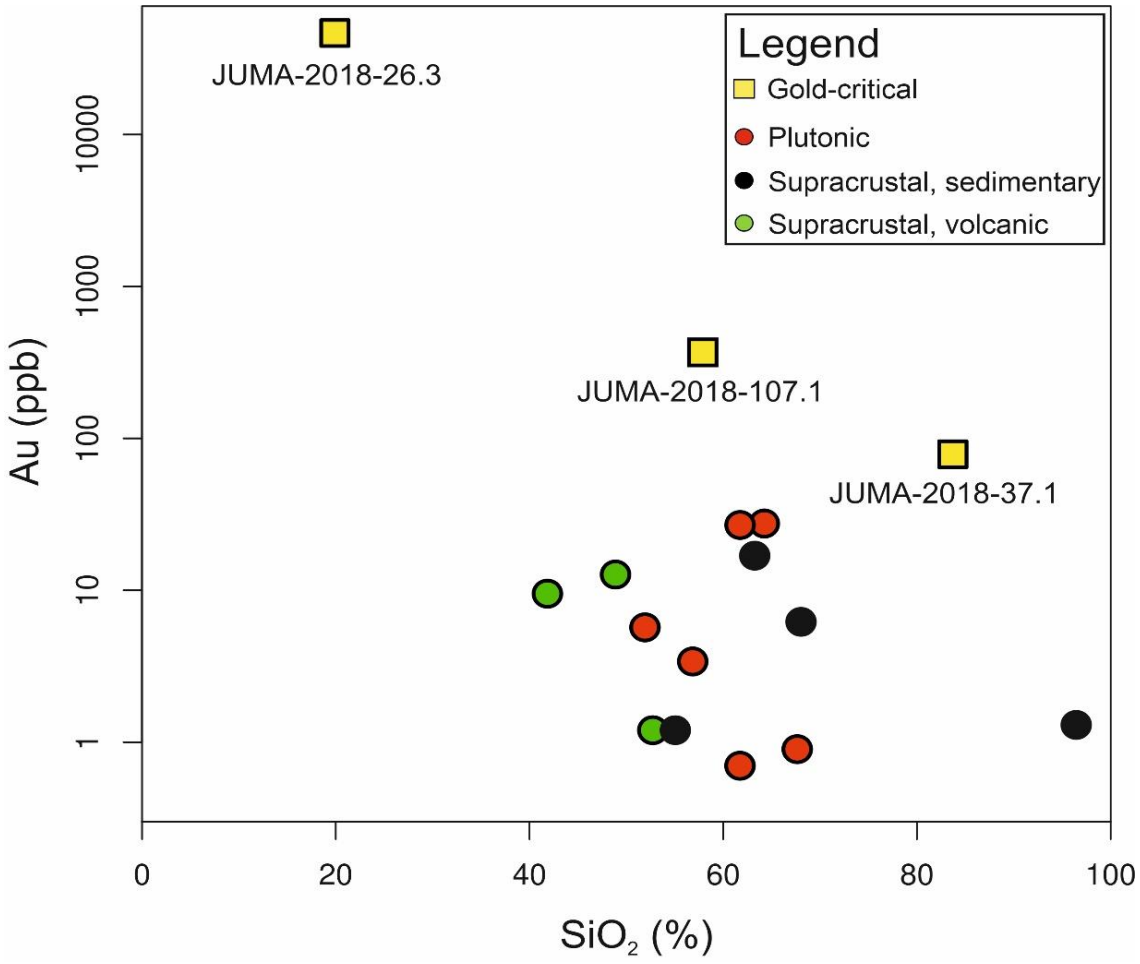

Figure 41: SiO_2 (%) vs. Au (ppb) binary plot. Note that two of the gold-critical samples (JUMA-2018-26.3, JUMA-2018-37.1) are from boulders.

Table 1: Gold-critical samples and associated elements.

Sample	Au (ppb)	SiO_2 (%)	S (%)	As (ppm)	Ag (ppm)	Cu (ppm)	Sb (ppm)	Bi (ppm)	B (ppm)	W (ppm)	Hg (ppm)	Te (ppm)
JUMA-2018-107.1	368.3	57.89	0.62	43.5	0.2	90.7	<0.1	0.6	21	2.7	<0.01	<0.2
JUMA-2018-26.3	46570.6	19.91	>10.00	>10000.0	5.3	586.4	47.5	58.6	<20	3.9	0.01	19.6
JUMA-2018-37.1	78.6	83.70	6.82	3707.5	1.2	615.3	5.7	0.6	<20	0.3	<0.01	0.6

4.4. U-Pb age determination

4.4.1. U-Pb zircon analyses

The terminology used for describing the zircon grains is adapted from the "Atlas of Zircon Textures" by Corfu *et al.* (2003).

The shape of the zircon grains separated from the leucosome sample varies (Figure 42), displaying both elongated, doubly-terminated crystals (Figure 42) and stubby, equant shapes indicating heterogeneous composition of the parental melt from the supracrustal paragneiss protolith. Many of the grains are subrounded, typical for metamorphically grown grains. The length of the grains is mostly 100–200 µm with few grains exceeding

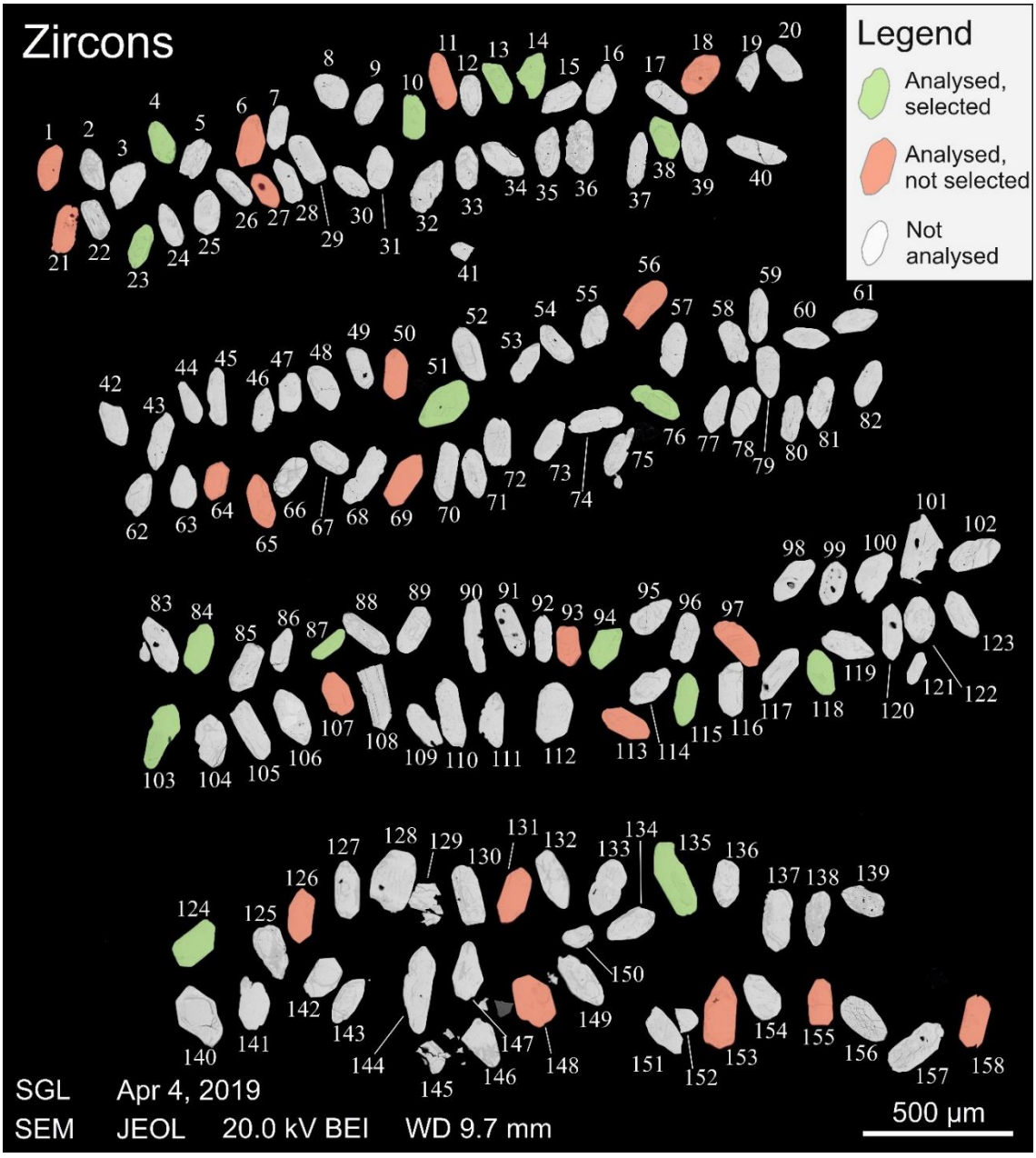

Figure 42: BSE-image of the zircons separated from the Välimäki leucosome sample. Zircons analyzed and used for the age termination displayed green and zircons analyzed but not used for age determination displayed pink. Zircons not analyzed displayed white.

lengths of 250 µm and width ranges between 50–100 µm. Most of the grains are metamict at some degree and this alongside with fracturing was the dominant decisive factor for selecting the suitable grains for U-Pb analysis. Detrital cores are present in multiple grains alongside with inclusions and zonal growth which also are present in few grains. The aim was to analyse grains as homogeneous as possible. Detrital cores alongside with outer zones from the same grain were also analysed.

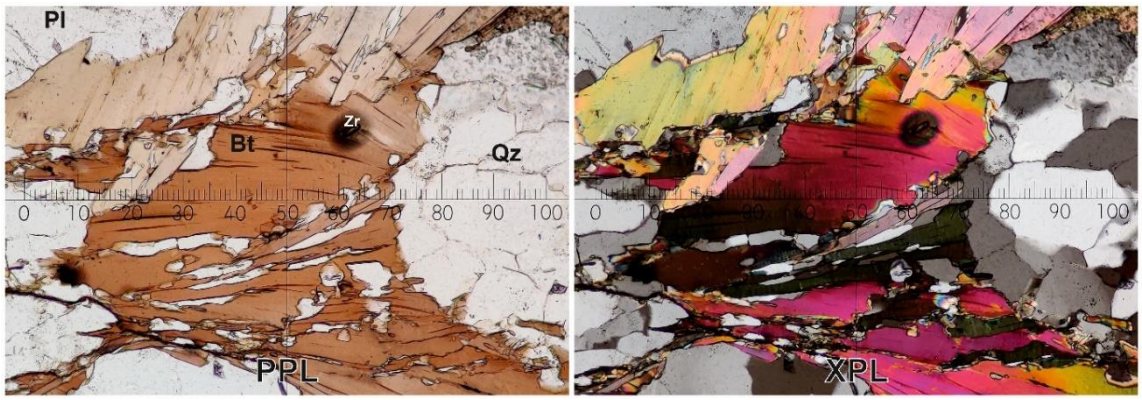

Figure 43: Microphotographs of the leucosome sample JUMA-2018-5.1 collected for age dating. Plane- (PPL) and cross-polarized (XPL) images displaying zircon grains within biotite, radioactive decay halo visible in the biotite. Images not to scale.

From the received age data, 25 of the oldest grains were ruled out. Three oldest analyse results display Archean ages (Figure 44, B), two which display concordant ages and one discordant (Figure 44, A). The concordant ages are from a core (Figure 42, 11) and from very homogenous zircon (Figure 42, 56). The discordant age is derived also from a core with metamict zone around it. From the older Paleoproterozoic grains, 22 were omitted with ages ranging between 1899–2185 Ma. The youngest, discordant age result was also omitted (Figure 44, A).

Out of the selected zircons, 43 analyses were performed on 37 grains. Seventeen analyse results were used determining the age of the peak metamorphism in the study area. The youngest analyse result and 25 of the oldest analyse results were ruled out. The concordia age of the selected samples yields an age of 1886.8 ± 6.9 Ma (Figure 45, A). The upper intercept age for the same samples yields an age of 1884.8 ± 6.8 Ma (Figure 45, B) and the $^{207}Pb/^{206}Pb$ weighted average age for the samples yields an age of 1885.1 ± 6.9 Ma (Figure 45, C). The full list of the analysis results can be seen in Appendix 2.

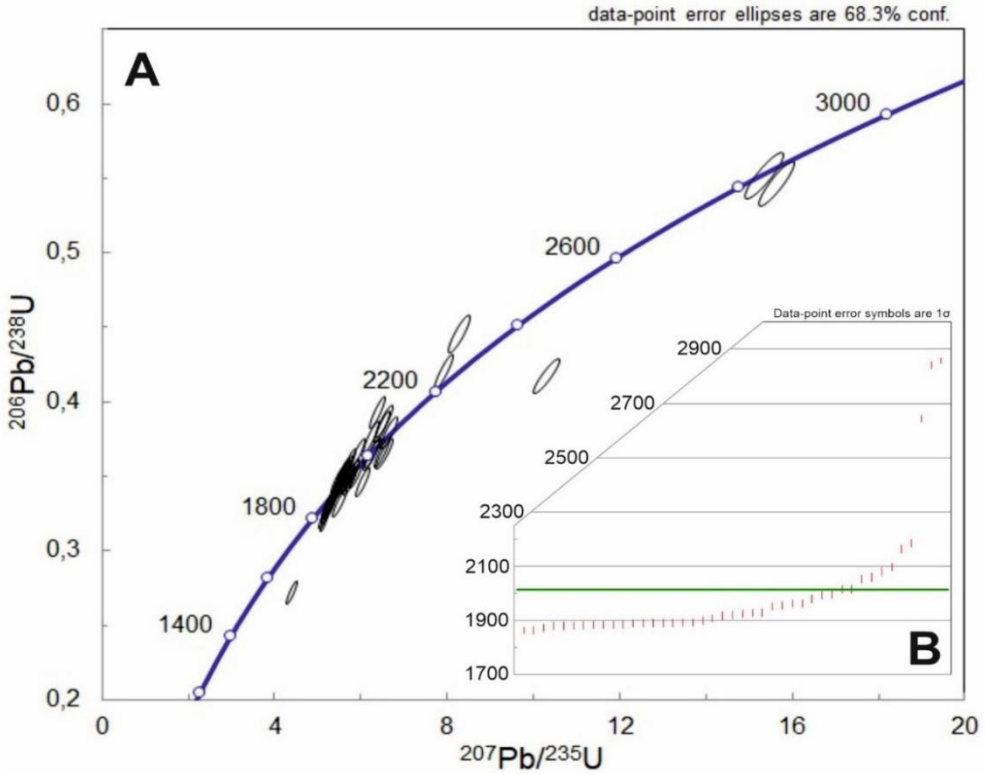

Figure 44: A) Concordia ages for all the analyzed zircons. **B)** $^{207}Pb/^{206}Pb$ weighted average ages for all the age data from Välimäki leucosome. Green line represents the weighted average of all analyses.

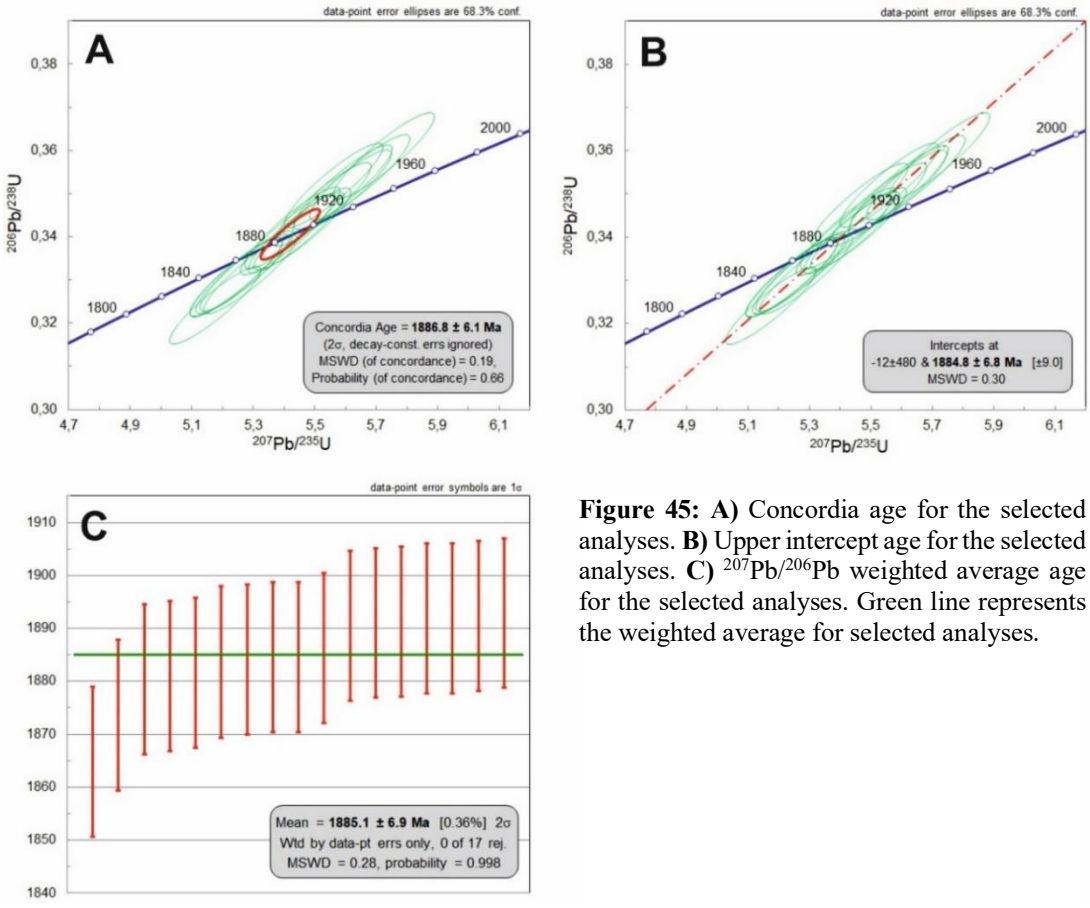

Figure 45: A) Concordia age for the selected analyses. **B)** Upper intercept age for the selected analyses. **C)** $^{207}Pb/^{206}Pb$ weighted average age for the selected analyses. Green line represents the weighted average for selected analyses.

4.4.2. U-Pb monazite analyses

The monazite grains separated from the same leucosome sample as the zircon grains display very homogenous, rounded shapes (Figure 46; Figure 47) with individual flat crystal faces in some grains (Figure 46, e.g. 87 and 105). The diameter of the monazite grains ranges between 100–250 µm. The internal texture of monazites displays no metamictism, zonation or detrital cores, differing significantly from the zircon grains. Fracturing is present but more absent than in zircon grains. Inclusions can be found in several grains, but on average the monazite grains are very homogenous with very little or no fracturing.

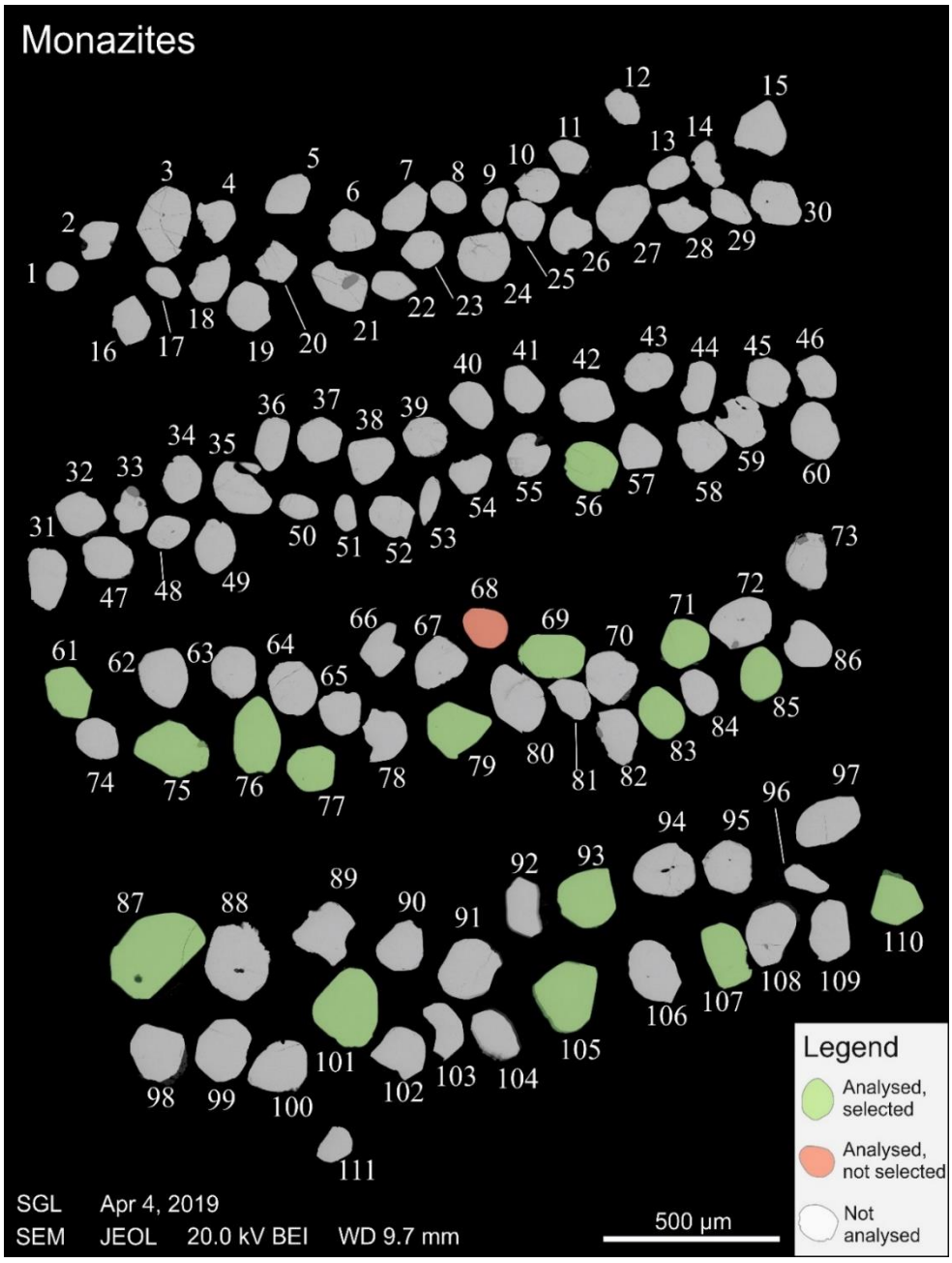

Figure 46: BSE-image of the monazites separated from the Välimäki leucosome sample. Monazites analyzed and used for the age termination displayed green and monazites analyzed but not used for age determination displayed red. Monazites not analyzed displayed

Out of the selected grains, 23 analysis were done on 17 grains with one analysis failing due to tripping. The remaining 22 analyses present uniform monazite age data. The concordia age for the selected analyses yields an age of 1799.2 ± 3.8 Ma (Figure 48, A). The Tera-Wasserburg concordia age for the selected analyses yields an age of 1799.4 ± 3.8 Ma (Figure 48, B) and the $^{207}Pb/^{206}Pb$ weighted average age yields an age of 1802.7 ± 4.2 Ma (Figure 48, C). Consequently, the monazite age data display roughly 85 Ma younger ages than the zircon data from the same sample. The full list of the analysis results can be seen in Appendix 3.

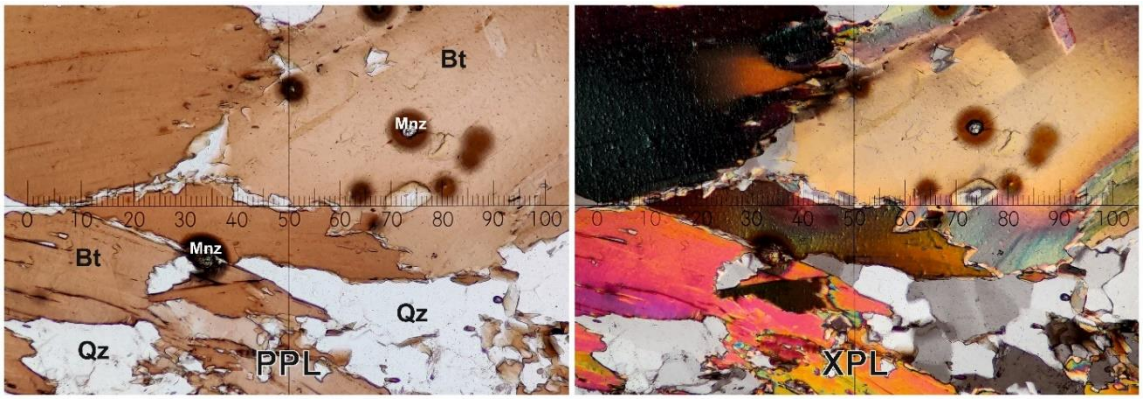

Figure 47: Microphotographs of the leucosome sample JUMA-2018-5.1 collected for age dating. Plane- (PPL) and cross-polarized (XPL) images displaying monazite grains within biotite, radioactive decay halo visible in the biotite. Grid not to scale.

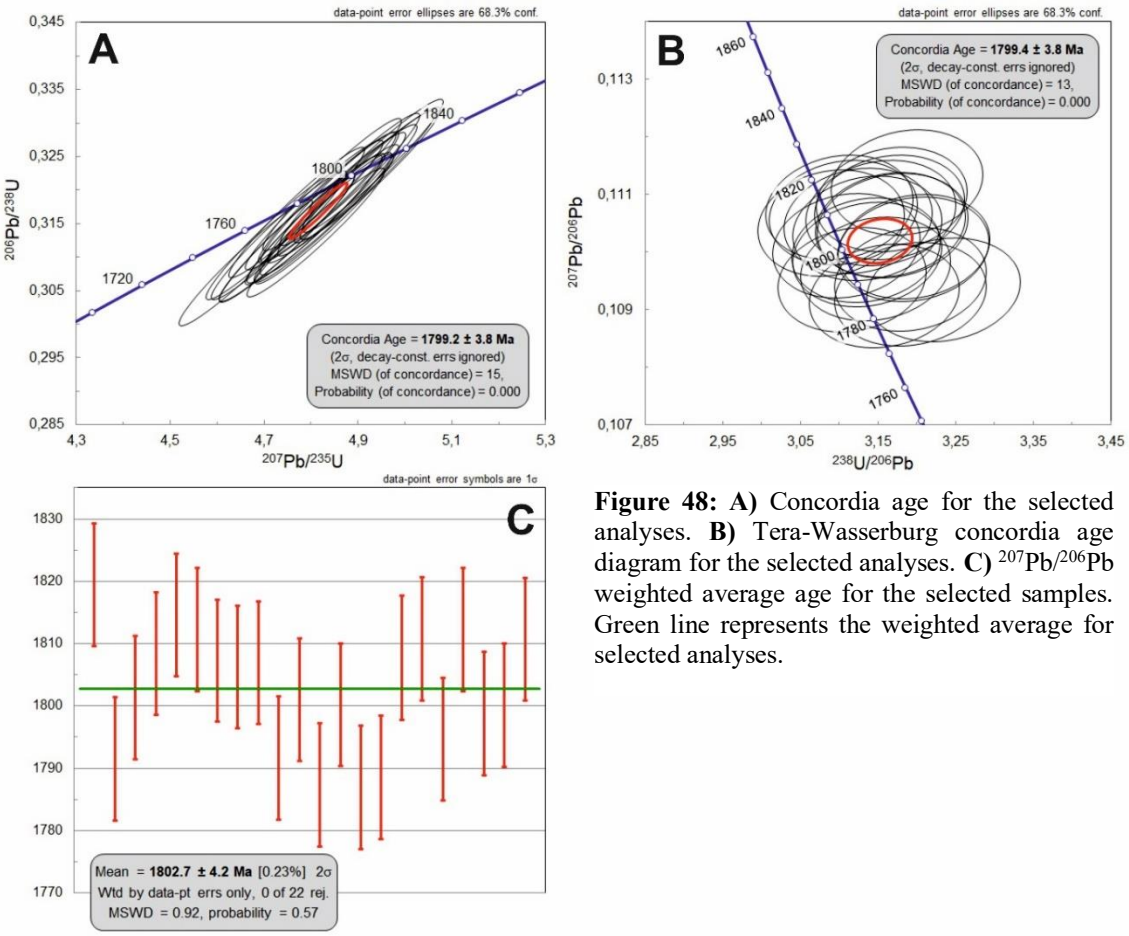

Figure 48: A) Concordia age for the selected analyses. **B)** Tera-Wasserburg concordia age diagram for the selected analyses. **C)** $^{207}Pb/^{206}Pb$ weighted average age for the selected samples. Green line represents the weighted average for selected analyses.

5. Discussion

5.1. Strain partitioning within the study area

The subdivision of the study area into structural domains is based on the heterogenous strain partitioning. With respect to the structures hosting the mineralizations, Domains I and II represent the background structures characterized by ENE-WSW -trending asymmetric folds with vergence towards NNW (Figures 29 and 30). Domain IV represents transitional zone from the moderately dipping fold structures in the north to the shear-controlled, NE-SW -trending vertical to subvertical structures within Domain V, hosting three of the known gold deposits and displaying the highest structural complexity and internal strain partitioning within the study area. Domains III and VI represent large-scale fold structures with fold hinges appearing on the map surface, differing from the fold patterns in the Domains I and II where no fold closures are present due to the horizontal attitude of the fold axes. Domain VII represents the transpositioning of dominant foliation towards the Kankaanpää shear zone in the west.

Deformation in Domain I is homogenous and pervasive in nature and the dominant plutonic units display strong flat-lying ENE-WSW -oriented linear features, dominantly classified as L- and LS-tectonites. This together with a low amount and highly constricted shearing, Domain I is a strong substantiation of a coaxial strain within Domain I with NNW-SSE -oriented compressional setting forming the ENE-WSW -oriented foliation. Rheological heterogeneities are often considered to form the most important internal control in strain partitioning (Lister & Williams, 1983). Lithological features form a controlling factor in the formation of different tectonic textures and strain partitioning throughout the current study area. The supracrustal paragneisses observed in Domain I host strong planar features indicating flattening strain in close spatial association to the L-tectonites observed in plutonic rocks. Similar lithological control was observed by Sullivan (2006) with comparable lithological units with respect to the current study area. According to Sullivan (2006), L-tectonites were preferentially formed in the homogenous units whereas more heterogenous units, such as banded gneisses, tend to deform by progressive folding with fold axes parallel with the maximum elongation orientation.

The lower hemisphere stereographic projections (Figure 16) display both lineation and fold axis measurements in tight cluster. Relative hinge-zone thickening of folds caused by near-coaxial strain is in this case liable for the formation of L-tectonites with lineation occurring parallel to the fold axes (Ramsay, 1967). Sullivan (2013) also pointed out that

L-tectonites can also form in hinge lines under non-coaxial deformation, as long as the hinge lines are parallel with the maximum elongation direction. Domains I and II also have no direct constraining borders, a factor favouring coaxial strain partitioning, pointed out by Lister & Williams (1986). Domain II hosts the most uniform rheology, comprising almost completely of plutonic units. The presence of planar features in plutonic units is increasingly present within Domain II though L>S-tectonites are still dominant. The flattening strain, liable for the formation of planar features, most likely concentrated on the banded gneisses when present, and in Domain II where these rocks are absent, formed the L>S-tectonites in plutonic units. Shear stresses, partitioned on more ductile banded gneisses in Domain I, are forced to be localized also on the plutonic units within Domain II, indicated by the increasing number of small-scale shearing observations. Lithological boundary zones display features indicating a presence of non-coaxial deformation broadly in the study area (e.g. Figure 24, A). Lister & Williams (1983) pointed out that boundary zones, whether or not they are capable of maintaining shear stresses, can dictate if a rock acts in a competent manner.

The field observations indicate that the relative amount of partial melts increases towards the southern parts of the study area, also an explanatory factor in the increasing number of shearing observations in Domain II with respect to Domain I. An experimental study by Rosenberg & Handy (2005) indicates that when the melt fraction exceeds 7 %, forming a connected network, the mechanical properties of the rock weaken significantly. Partial melting increases the lithological heterogeneities, an important factor on strain partitioning on all scales (Fossen & Cavalcante, 2017). Partial melts localize strain and especially simple shear in various localities in the study area (e.g. Figures 13, A; 18, D). The melt-interconnectivity of the study area is also affected by the lithology as the compositional variations in the supracrustal paragneisses interfere with the melt connectivity whereas plutonic units have better connectivity considering the more homogenous composition. The lack of mylonitic rocks in the study area is therefore explicable with the partitioning of strain, especially simple shear, into these more ductile units hosting partial melts, preventing strain localization into narrow zones.

Domain IV and V, hosting the known gold targets, display the most complex structures of the study area. As the structures in the northern part of the study area are ENE-WSW -trending, the Domain V and southern parts of Domain IV host NE-SW -trending structures (Figure 16) associated with more vertical fold axial planes, differing from the northern domains with asymmetric fold vergences towards NNW (Figure 29). Domain V

is interpreted to be bordered by two vertical strike-slip zones with apparent right lateral kinematics. These shear zones are displayed in the geophysical data as negative continuous zones cross-cutting magnetic anomalies (Figure 28). Linear features from Domain V display greatest scattering and generally steeper plunges than other domains, indicating complex internal structures and vertical flow of material.

With the assumption that the map-scale structures in the study area represent relatively synchronous formation, the NE-SW -oriented structures were formed in a NW-SE transpressional setting followed rapidly after NNW-SSE -oriented principal stress regime, eligible for the ENE-WSW -trending structures in the northern part of the study area. Crude main shortening direction of (W)NW-(E)SE (Reimers et al., 2018) is identified as a later deformation event, reactivating the pre-existing NE-SW oriented structures. A zone with dominant right-lateral flow of material (Figure 49) is formed in the NE-SW -oriented structures during the NW-SE transpressional setting. The differing mechanical behaviour of this zone is most likely the consequence of the high proportion of the supracrustal units (Figures 29 and 39) and their more ductile flow with respect to the more rigid plutonic units, abundant in the northern parts of the study area, or a pre-existing deeper structure.

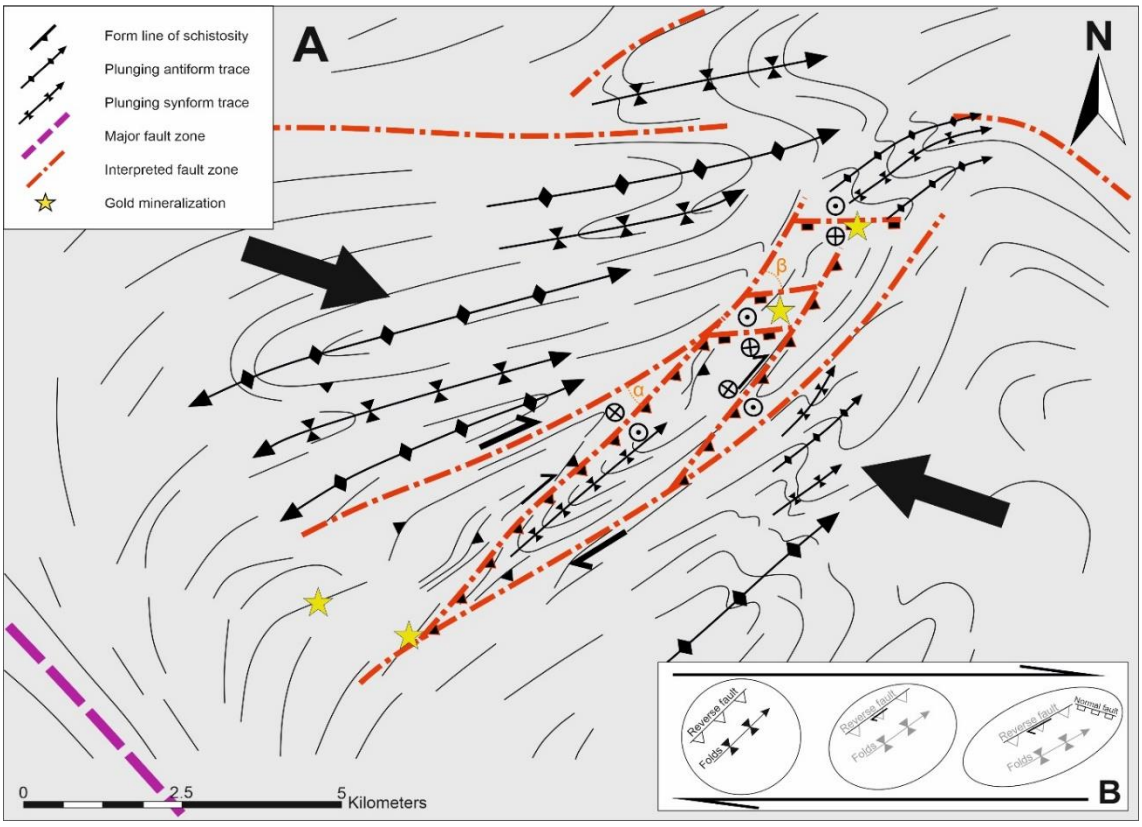

Figure 49: A) A simplified form line map of the study area hosting the high-strain structures. Arrows denote (W)NW-(E)SE shortening direction at 1.80 Ga. **B)** Strain ellipse depicting the progressive deformation and formation of structures.

Strain partitioning within Domain V is interpreted to have formed both compressional and extensional structures. The apparent right-lateral vertical strike-slip zones form the borders for the high-strain zone. Two NE-SW -oriented oblique slip zones, traversing through the high-strain zone (Domain V) between the right-lateral strike-slip zones, are interpreted based on the plunge of the lineations and continuations on the geophysical data (Figure 28) as well as the fluctuations in the strike of the foliation. The oblique slip is interpreted to be right-lateral, reverse (top to NW), suitable for the prevailed stress regime, forming contractional duplexes (Woodcock & Fischer, 1986). Given the fairly tight angle between the main strike-slip zones and the traversing oblique zones (Figure 49, A, angle α), it is likely that the angle between these high-strain zones has been more open in the early stages, during which thrust has dominated (Figure 49, B). As the progressive deformation continued, the relative amount of horizontal slip has increased with respect to vertical slip, further tightening the angle α between the strike-slip and oblique-slip zones. The two traversing oblique slip zones and associated fold patterns in between (Figure 49, A) are interpreted to form a flower structure, a characteristic feature formed by bends in the strike-slip domains (Woodcock & Fischer, 1986).

Geophysical data displays E-W -trending discontinuities in the magnetic layers in the vicinity of Silmusuo and Saarijärvi prospects (Figure 28). These discontinuities may represent normal faulting, localised along releasing linkage structures between subparallel strike-slip and oblique-slip zones (Figure 49, A), suitable for the same stress regime. The angle between these interpreted normal faults and strike-slip zones (Figure 49, A, angle β) is roughly 45 degrees, indicating no transpositioning of these structures and therefore formation in the later stages of progressive deformation. However, it should be noted that these structures are derived from geophysical data only and highly open to interpretation. An alternate interpretation for the E-W -oriented structures is an antithetic strike-slip dominated setting, congruent for the WNW-ESE compressional regime.

Reimers et al. (2018) address that the NW-SE striking Kynsikangas shear zone displays overprinting brittle deformation in an E-W compressional setting with east-block-up -kinematics in the Kynsikangas shear zone. Several observations of conjugate fracture sets suitable for this E-W compressional regime were made, congruent with the study by Reimers et al. (2018). These structures represent the latest notable deformation event within the study area. Motion along these brittle structures was not recognized and these fractures are dominantly vacant of mineral fillings, an indicator of absence of volatiles during this event. The NW-SE oriented planar structures in the Kynsikangas shear zone

have most likely hosted the movement due to their more favourable orientation with respect to the E-W oriented compressional regime.

5.2. Gold-critical structures

Quartz veining is identified to be sited in three distinguishable settings: i) foliation-parallel, ii) younger, foliation-intersecting and iii) shear-related veining. The foliation-parallel veining is interpreted to represent the oldest generation of veining, representing syn- to late-tectonic emplacement during peak metamorphism. Folding of these veins with axial planes parallel to the main foliation supports the syntectonic formation environment. Quartz veins intersecting the dominant foliation but folded with axial planes parallel to main foliation are also present, indicating pre- to early-tectonic emplacement. The 1886.8 ± 6.1 Ma concordia age obtained from the zircons in the Välimäki prospect defines the peak metamorphism and the maximum age for the gold mineralization in the Välimäki prospect. As the mineralizations are sited within the same structural domain, the maximum age for the mineralization event in the Kultakallio, Silmusuo and Saarijärvi prospects is most likely same as the Välimäki mineralization. In the Jokisivu gold prospect (Figure 2, B), Saalmann et al. (2010) received an age of 1884 ± 4 Ma and 1881 ± 3 Ma ages for the host rock, coeval within error with the age obtained in this study. This c. 1.88 Ga D_3 event in the Jokisivu site (Saalmann et al., 2010) is also correlated with the migmatization event, indicating similar ages of peak metamorphism. The presence of foliation- and fold-parallel quartz veins indicates that the oldest generation of quartz veining is coeval with the peak metamorphism at 1.88 Ga.

The monazite U/Pb age displays a concordia age of 1799.2 ± 3.8 Ma, approximately 80–90 Ma younger than the age of the zircon grains. This late-Svecofennian event is also recognized in the Jokisivu prospect (Saalmann et al., 2010), correlated to the gold mineralization event in Jokisivu and in other localities in Finland, e.g. in the Kolari area (Niiranen et al., 2007). Saalmann et al. (2010) correlates the 1.82–1.78 Ga event to WNW-ESE dextral transpressional event. The younger generation of quartz veins are striking systematically at NW-SE -orientation with steep dips, displaying no folding patterns and intersecting the older, folded set of quartz veins. These veins are not hosted by shear zones and display linear shapes and are generally thinner than the older vein generation. The geometries of this vein array support the formation above or in the brittle-ductile -transition zone at an WNW-ESE transpressional event, coherent with the main mineralization event in the Jokisivu prospect (Saalmann et al., 2010). This WNW-ESE

compressional stress regime is also compatible with the paleostress orientation during the formation of the Kynsikangas shear zone (Reimers et al., 2018).

The third setting for veining, shear-related, is most likely related to the same event as the younger generation of veining. During the peak metamorphism, strain distributed more evenly throughout the study area but in the younger deformation event, strain localized into narrower shear zones. Shear zones host quartz veins in multiple orientations, e.g. N-S- (Figure 20, C) and E-W -oriented antithetic sinistral veins, suitable for the WNW-ESE compressional setting and the predominant dextral internal structures in the gold-critical zone. The first-order structure, controlling the fluid flow in the study area, is the NW-SE -striking Kynsikangas shear zone. The relevance of NW-SE -oriented shear zones is identified also in the Jokisivu (Saalmann et al., 2010), Satulinmäki & Riukka (Saalmann, 2007) and in areas north of the Uusimaa Belt in general (Saalmann et al., 2009). The NE-SW oriented strike- and oblique-slip structures (Figure 49, A) represent the second- and third-order structures, hosting the gold mineralizations in the study area.

Given the tectonic framework for the main mineralizing event discussed above, the correlation of individual mineralizations in the study area to the framework is of relevance. The Välimäki prospect, characterized by vertical NE-SW -striking foliation trajectories and subhorizontal lineations, is in the sphere of influence of the dextral second-order strike-slip structures. The drill-core data states the presence of gold-critical vein arrays in narrow shear zones and as a foliation-parallel feature. The shear-related veining most likely branches from the strike-slip zone, most likely hosting both antithetic and synthetic kinematics and related orientations. The Kultakallio prospect hosts also the foliation parallel vein setting and NW-SE -oriented younger set. The foliation is dipping moderately towards SSE with flat-lying linear features. The weak fold pattern visible in the geophysical data suggest that the Kultakallio prospect is sited at the fold hinge. Drill hole data indicated parallel shearing, both mylonitic and breccia-type to be parallel with the foliation. These structures indicate reactivation of pre-existing structures in the later c. 1.80 Ga WNW-ESE compressional regime and provided fluid conduits for the mineralization event. The more mafic composition of the Kultakallio plutonic host rock with respect to the adjacent lithologies indicates a contrast in the mechanical behavior, displaying more rigid properties. The competence differences between the rigid unit and adjacent paragneiss units is interpreted to be liable for the formation of gold-bearing structures even though larger scale structures, present in other prospects, are absent. The Silmusuo prospect is most likely associated to the oblique slip environment due to steeply

plunging lineations with respect to the foliation trajectories. The pervasive silicification of observed gold-critical boulders requires the presence of tectonic fluids, an indication of large structure in the vicinity acting as the fluid conduit. The most ambiguous Saarijärvi prospect hosts foliation-parallel and folded arrays of quartz veining, lacking the younger main mineralization event features, and is therefore of least interest with respect to prospectivity taking account the very limited amount of data available.

5.3. Tectono-thermal evolution

5.3.1. Tectonic framework

The obtained structural, U/Pb and geochemical data provides a solid premise for the interpretation of tectono-thermal evolution and association of the study area to the Svecofennian domain and its multi-event formation. The ENE-WSW trending fold patterns in the northern part of the study area are analogous to E-W fold patterns in the Pirkanmaa Belt (Kilpeläinen, 1998). The N-S -oriented compressional setting is unfit regarding the formation of NE-SW -oriented structures and Lahtinen et al. (2014) suggest an orthogonal switch in the principal stress orientation to NW-SE, initiating the buckling and the formation of coupled Bothnian oroclines (Figure 6). This NW-SE -oriented principal stress regime would be suitable not only to the formation of the NE-SW -oriented structures, but also the formation of the Kynsikangas shear zone during this event. The buckling is also liable for the flow of CFGC towards SW (Figure 6), a plausible interpretation for the thrust-type kinematics for the Kankaanpää shear zone.

Pajunen et al. (2008) suggest that the Pomarkku block underwent clockwise rotation during NW-SE transpressional event, supported by the left-lateral kinematics of the Kynsikangas shear zone and oblique dextral kinematics of the Kankaanpää shear zone. A more recent study by Lahtinen et al. (2014) suggest flow of CFGC towards SW in a NW-SE -oriented principal stress regime (Figure 6). The main shortening direction in the Kynsikangas shear zone according to Reimers (2018) is NW-SE, analogous with Lahtinen et al. (2014). The clockwise rotation of Pomarkku block is a viable explanation for the formation of semi-crustal-scale apparent right-lateral features in the gold critical zone (Figure 49), acting as a hinge-zone between more rigid plutonic units to the north NW and SE. This NW-SE -oriented transpressional setting has therefore formed the NE-SW -oriented structures in the gold-critical zone, which were later reactivated in the 1.80 Ga WNW-ESE compressional setting along with the Kynsikangas shear zone but in a more localized manner, providing the conduits for the auriferous fluids. It should be noted that

Reimers (2018) disagreed with the clockwise rotation of the Pomarkku block, based on the opposite sense of rotation in the predominant sense of rotation in the microkinematic indicators as shown by Passchier & Simpson (1986). Whether the use of kinematic indicators and their suitability in a crustal-scale structural interpretation is a reliable method is beyond the scope of this study.

5.3.2. Lithology

The lithology in the study area is prominent in migmatites, characteristic for the Pirkanmaa Belt and a feature typically lacking in the Häme and Tampere belts (Lahtinen et al. 2017 and references therein). Granodiorites and their gradual transition to quartz diorites is a characteristic plutonic feature in the Pirkanmaa Belt (Lahtinen et al., 2017), a conforming feature also recognized in the study area (Figure 36, A). Lahtinen et al. (2017) correlated the major 1885–1875 Ma metamorphic event to the emplacement of syn- to late-tectonic plutonic units. The 1885 Ma metamorphic peak is recognized in multiple locations in the Pirkanmaa Belt and geochemical analyses from samples dated at 1885 and 1881 Ma (Lahtinen et al., 2017) display similar features in the Pirkanmaa Belt and the current study area (Figure 50). Negative Ba and Nb-Ta -anomalies are also present in the plutonic units dated with maximum ages of 1885 Ma in the study by Lahtinen et al. (2017), analogous with this study (Figure 50). Negative Ti anomaly is present in both the samples included in this study and in the plutonic units aged at 1881 Ma. According to Briqueu et al. (1984), the negative Ti-anomaly is formed by progressive fractionation of the parental magma, indicating that the samples in this study and the 1881 Ma samples are more fractionated with respect to Ti in the 1885 Ma samples in Lahtinen et al. (2017). It can be concluded that the plutonic units display similar characteristics as other plutonic units in the Pirkanmaa Belt and therefore belong in the same lithological unit.

Mäkitie & Lahti (2001) dated a granitoid in the northern part of the Pomarkku block at 1872 ± 2 Ma, indicating the emplacement of the unit in the late stages of the major 1885-1875 Ma event. The tectonomagmatic diagrams of the Luopa fayalite-augite quartz monzonite (see Figure 11 in Mäkitie & Lahti, 2001) classify this unit as a within-plate granitoid and is associated with the CFGC and is not therefore geochemically comparable with the plutonic units, classified as volcanic arc granitoids (Figure 40), in the study area. The overall arched shape of the intrusion (see Appendix-Figure 7.1c in Pajunen et al., 2008) and the overall only slightly deformed structure and presence of narrow ductile shear zones (Mäkitie & Lahti, 2001) is a strong evidence of late-tectonic emplacement.

The plutonic units in the study area are more strongly deformed and together with the geochemical similarities with the plutonic units of Pirkanmaa Belt, the emplacement in the earlier stages of the major 1885–1875 Ma event is suggested.

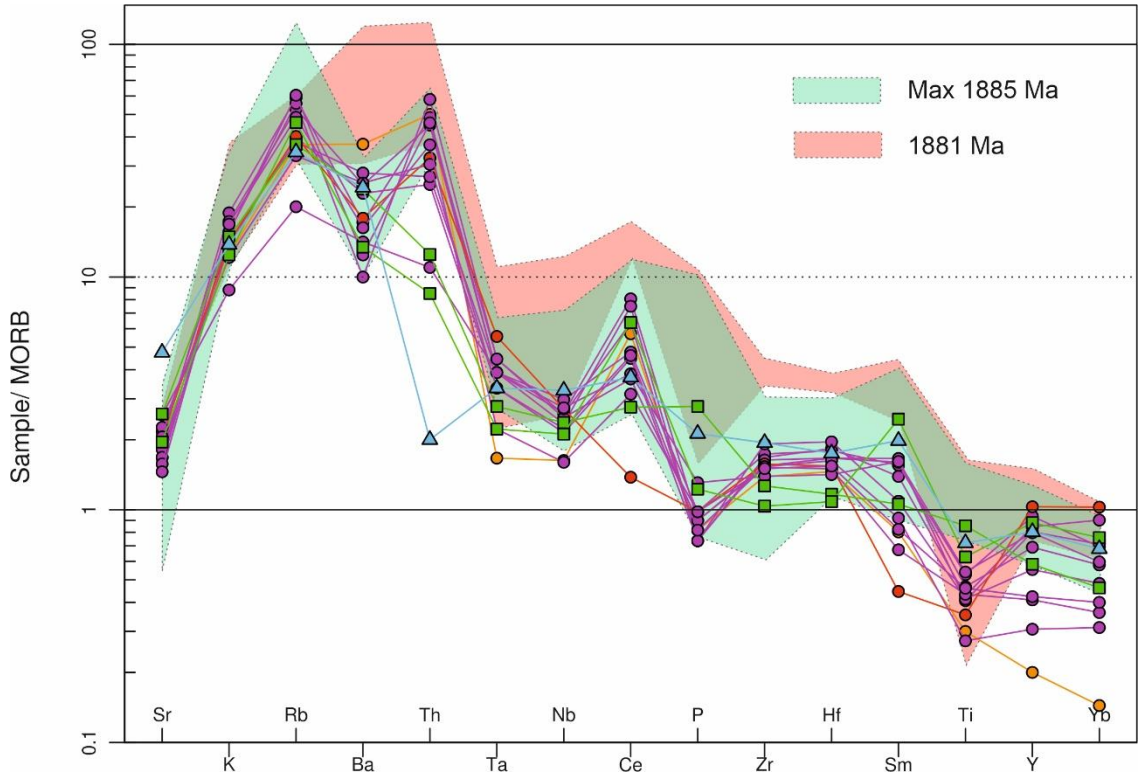

Figure 50: MORB-normalized multielement diagram (Pearce, 1983) of the plutonic rocks in the study area along with two sets of 1885 and 1881 Ma aged plutonic units from Pirkanmaa Belt (Lahtinen et al., 2017) illustrated for comparison.

5.3.3. Geochronology

The U/Pb age data from the zircon grains display the 1.88 Ga age which represents the age of peak metamorphism, analogous with other studies dating the peak metamorphism of the Pirkanmaa Belt at 1.88–1.87 Ga (Mouri et al., 1999; Lahtinen et al., 2009a; Rutland et al., 2004). This age defines the maximum age for the gold mineralization. Three hypotheses can be made for the formation of 1.80 Ga monazite grains: i) monazites were overprinted in the later 1.80 Ga event, resulting into a complete reset of the U/Pb ages, ii) monazites were formed during the 1.80 Ga event or iii) the U/Pb system stayed open for a long period of time from 1.88 to 1.80 Ga until the temperature dropped and sealed the system. The internal structures of monazite grains display no zonal textures or cores (Figure 46) in the BSE images, very likely ruling out inherited origin and the prolonged heat source from 1.88 to 1.80 Ga. The homogeneity of the monazite grains with respect to their internal textures leads to a conclusion that the dated monazites were most likely

crystallized during this 1.80 Ga event instead of only overprinting as the zonal texture is absent.

The zircon grains display no 1.80 Ga ages (Figure 44, B), indicating that the metamorphic event at 1.80 Ga was capable to form or reset the monazites but not strong enough to overprint the zircon grains. The closure temperature T_c for the U-Pb system in monazite grains has been estimated in empirical experiments to range from 675 to 730 ˚C (Parrish, 1990). This temperature range overlaps with the titanite T_c, a geochronometer used in the Jokisivu prospect by Saalmann et al. (2010). Rubatto et al. (2001) noted new crystallization of monazite at temperatures <650 ˚C whereas the zircon does not react to metamorphism below 700 ˚C and during partial melting, zircon grew on detrital cores which were preserved up to the temperatures of 750–800 ˚C. The 1.88 Ga zircons are therefore formed during partial melting, a feature absent in the 1.80 Ga event in the study area. Saalmann et al. (2010) correlated the 1.80 Ga event to hydrothermal activity and emplacement of gold mineralizations. Conforming results with respect to the behaviour of monazite during subsequent metamorphism has also been recognized in the Ljusdal Domain in west-central Svecofennian domain, central Sweden by Högdahl et al. (2012) in which zircon ages yielded 1.87–1.86 Ga ages whereas monazites displayed double peaks at 1.87–1.86 and 1.82–1.80 Ga. The formation of the monazite is the Ljusdal Domain was also correlated to subsolidus conditions and late-orogenic, shear zone - controlled, hydrothermal metamorphism (Högdahl et al., 2012).

The formation of hydrothermal monazite is identified by multiple authors (e.g. Schandl & Gorton, 2004; Gervais & Hynes, 2013) and the monazite observed in the thin sections from the Välimäki prospect (Figure 47) appears as clusters which is a strong evidence of hydrothermal origin (Schandl & Gorton, 2004). The rounded shapes of monazite grains indicate Th-rich composition according to Catlos (2013) which conflicts with the study by Schandl & Gorton (2004), stating a strong correlation of low-Th content with hydrothermal monazites. The rounded shapes of the monazite grains could also be due to detrital origin and related abrasion in a sedimentary environment (Williams, 2001), indicating complete overprinting during the 1.80 Ga event, but the formation of new monazite grains is preferred.

6. Conclusions

- The gold-critical area comprises dominantly right-lateral features. The NW-SE -oriented Kynsikangas shear zone represents the first-order structure in the area. NE-SW oriented strike-slip zones represent the second order structures from which third order, smaller shear zones splay from.
- Strain is partitioned in a heterogenous manner in the study area. Plutonic units host L- and L>S-tectonites formed under coaxial strain. Non-coaxial strain is partitioned in the supracrustal units and lithological boundary zones throughout the study area.
- Northern part of the study area has acted as a single block and displays ENE-WSW -oriented structures formed in the early stages of the 1885–1875 Ma event. Later tectonic overprinting is of little significance in the northern parts of the study area.
- The gold-critical zone has undergone four principal stress regimes: i) NNW-SSE (ductile), ii) NW-SE (ductile), iii) ESE-WNW (brittle-ductile) and iv) E-W (brittle). The NE-SW-oriented structures were reactivated and localized strain in the ENE-WSW principal stress regime.
- The Pomarkku block represents the western continuation for the Pirkanmaa Belt. Geochemistry of the plutonic units displays subduction-type signatures and the geochemical features are analogous with the plutonic units of the Pirkanmaa Belt.
- Two thermal peaks are identified from the obtained age data. These events are correlated to the emplacement of mineralized quartz veins in the study area and are analogous with other gold mineralizations in Southern Finland.
- Zircon grains dated at 1886.8 ± 6.1 Ma are formed during peak metamorphism and associated migmatization in the study area. This is in agreement with the peak metamorphism in the Pirkanmaa Belt. Older generation of foliation-parallel quartz veining is correlated with this event.
- Monazite grains dated at 1799.2 ± 3.8 Ma represent the later metamorphic event. This is correlated with the emplacement of younger cross-cutting quartz veins. The formation of monazite grains is interpreted to be of hydrothermal origin.

Acknowledgements

To begin with, I would like to give the biggest compliments to the Geological Survey of Finland for funding this project and for providing the essential equipment for the field work. I would like to thank geologists Markku Tiainen and Hanna Leväniemi for supervision and guidance in the initiation of the project and for providing the fundamental geophysical and GIS-data. I would like to thank MSc Jaakko Kara for his contribution to this study during field work, supervision and guidance in the Finnish Geosciences Laboratory during the U-Pb analysis and data reduction for the U/Pb geochronological data and for assistance in the early stages of the writing process. Special thanks go to professor Pietari Skyttä and university lecturer Markku Väisänen. Their guidance throughout the whole study played a key role during the field work and the writing process and fruitful conversations are highly appreciated. Laboratory technician Arto Peltola is thanked for his guidance in the in the thin section preparation process and for his efforts in the preparation of the zircon mount for the BSE images. Student Anssi Arminen is also thanked for his efforts during the zircon separation process. Finally, I would like to express my thanks to MSc Tuomas Leskelä for his contribution during field work.

References

Bierlein, F. P., & Maher, S. (2001). Orogenic disseminated gold in Phanerozoic fold belts—examples from Victoria, Australia and elsewhere. *Ore Geology Reviews*, *18*(1-2), 113-148.

Bogdanova, S. V., Bingen, B., Gorbatschev, R., Kheraskova, T. N., Kozlov, V. I., Puchkov, V. N., & Volozh, Y. A. (2008). The East European Craton (Baltica) before and during the assembly of Rodinia. *Precambrian Research*, *160*(1-2), 23-45.

Boynton, W. V. (1984). Cosmochemistry of the rare earth elements: meteorite studies. In *Developments in geochemistry* (Vol. 2, pp. 63-114). Elsevier.

Briqueu, L., Bougault, H., & Joron, J. L. (1984). Quantification of Nb, Ta, Ti and V anomalies in magmas associated with subduction zones: petrogenetic implications. *Earth and Planetary Science Letters*, *68*(2), 297-308.

Catlos, E. J. (2013). Generalizations about monazite: Implications for geochronologic studies. *American Mineralogist*, *98*(5-6), 819-832.

Corfu, F., Hanchar, J. M., Hoskin, P. W., & Kinny, P. (2003). Atlas of zircon textures. *Reviews in mineralogy and geochemistry*, *53*(1), 469-500.

Daly, J. S., Balagansky, V. V., Timmerman, M. J., & Whitehouse, M. J. (2006). The Lapland-Kola orogen: Palaeoproterozoic collision and accretion of the northern Fennoscandian lithosphere. *Geological Society, London, Memoirs*, *32*(1), 579-598.

Dragon Mining 2020. Available at: http://www.dragonmining.com/

Eilu, P., & Groves, D. I. (2001). Primary alteration and geochemical dispersion haloes of Archaean orogenic gold deposits in the Yilgarn Craton: the pre-weathering scenario. *Geochemistry: Exploration, Environment, Analysis*, *1*(3), 183-200.

Eilu, P., Sorjonen-Ward, P., Nurmi, P., & Niiranen, T. (2003). A review of gold mineralization styles in Finland. *Economic Geology*, *98*(7), 1329-1353.

Fossen, H. (2016). *Structural geology*. Cambridge University Press.

Fossen, H., & Cavalcante, G. C. G. (2017). Shear zones–A review. *Earth-Science Reviews*, *171*, 434-455.

Gervais, F., & Hynes, A. (2013). Linking metamorphic textures to U–Pb monazite in-situ geochronology to determine the age and nature of aluminosilicate-forming reactions in the northern Monashee Mountains, British Columbia. *Lithos*, *160*, 250-267.

Goldfarb, R., Baker, T., Dube, B., Groves, D. I., Hart, C. J., & Gosselin, P. (2005). Distribution, character and genesis of gold deposits in metamorphic terranes. Society of Economic Geologists.

Goldfarb, R. J., & Groves, D. I. (2015). Orogenic gold: Common or evolving fluid and metal sources through time. *Lithos*, *233*, 2-26.

Goldfarb, R. J., Groves, D. I., & Gardoll, S. (2000). Orogenic gold and geologic time: a global synthesis. *Ore geology reviews*, *18*(1-2), 1-75.

Gorbatschev, R., & Bogdanova, S. (1993). Frontiers in the Baltic shield. *Precambrian Research*, *64*(1-4), 3-21.

Goscombe, B. D., Passchier, C. W., & Hand, M. (2004). Boudinage classification: end-member boudin types and modified boudin structures. *Journal of structural Geology*, *26*(4), 739-763.

Groves, D. I., Goldfarb, R. J., Gebre-Mariam, M., Hagemann, S. G., & Robert, F. (1998a). Orogenic gold deposits: a proposed classification in the context of their crustal distribution and relationship to other gold deposit types. *Ore geology reviews*, *13*(1-5), 7-27.

Groves, D. I., Goldfarb, R. J., Knox-Robinson, C. M., Ojala, J., Gardoll, S., Yun, G. Y., & Holyland, P. (2000). Late-kinematic timing of orogenic gold deposits and significance for computer-based exploration techniques with emphasis on the Yilgarn Block, Western Australia. *Ore Geology Reviews*, *17*(1-2), 1-38.

Groves, D. I., & Santosh, M. (2016). The giant Jiaodong gold province: the key to a unified model for orogenic gold deposits? *Geoscience Frontiers*, *7*(3), 409-417.

Groves, D. I., Santosh, M., Goldfarb, R. J., & Zhang, L. (2018). Structural geometry of orogenic gold deposits: Implications for exploration of world-class and giant deposits. *Geoscience Frontiers*, *9*(4), 1163-1177.

Grönholm, S., & Voipio, T. (2012). The Palokallio gold occurrence at Huittinen, southern Finland. *Geological Survey of Finland, Special Paper*, *52,* 91-99.

Hawkesworth, C. J., Hergt, J. M., McDermott, F., & Ellam, R. M. (1991). Destructive margin magmatism and the contributions from the mantle wedge and subducted crust. *Australian Journal of Earth Sciences*, *38*(5), 577-594.

Hermansson, T., Stephens, M. B., Corfu, F., Page, L. M., & Andersson, J. (2008). Migratory tectonic switching, western Svecofennian orogen, central Sweden: Constraints from U/Pb zircon and titanite geochronology. *Precambrian Research*, *161*(3-4), 250-278.

Hronsky, J. M., & Groves, D. I. (2008). Science of targeting: definition, strategies, targeting and performance measurement. *Australian Journal of Earth Sciences*, *55*(1), 3-12.

Högdahl, K., Majka, J., Sjöström, H., Nilsson, K. P., Claesson, S., & Konečný, P. (2012). Reactive monazite and robust zircon growth in diatexites and leucogranites from a hot, slowly cooled orogen: implications for the Palaeoproterozoic tectonic evolution of the central Fennoscandian Shield, Sweden. *Contributions to Mineralogy and Petrology*, *163*(1), 167-188.

Hölttä, P., & Heilimo, E. (2017). Metamorphic map of Finland. *Geological Survey of Finland, Special Paper*, *60*, 77-128.

Kalliomäki, H., Wagner, T., Fusswinkel, T., & Schultze, D. (2019). Textural evolution and trace element chemistry of hydrothermal calcites from Archean gold deposits in the Hattu schist belt, eastern Finland: indicators of the ore-forming environment. *Ore Geology Reviews*, *112*, 103006.

Kara, J., Manninen, J., Leskelä, T., Skyttä, P., Väisänen, M., Tiainen, M., & Leväniemi, H. (2018). Characterisation of the structural evolution and structural control of the gold mineralisations in the Kullaa area, SW Finland. In *Tenth symposium on structure, composition and evolution of litosphere,* Institute of Seismology, University of Helsinki, Report S-67, 37-40.

Kilpeläinen, T. (1998). Evolution and 3D modelling of structural and metamorphic patterns of the Palaeoproterozoic crust in the Tampere-Vammala area, southern Finland. Geological Survey of Finland, Bulletin 397, 124 pp.

Korsman, K., Koistinen, T., Kohonen, J., Wennerström, M., Ekdahl, E., Honkamo, M., ... & Pekkala, Y. (1997). Suomen kallioperäkartta–Berggrundskarta över Finland–Bedrock map of Finland. *Espoo, Finland, Geological Survey of Finland, scale*, *1*(1), 000.

Kähkönen, Y. (1987). Geochemistry and tectonomagmatic affinities of the metavolcanic rocks of the early Proterozoic Tampere Schist Belt, southern Finland. *Precambrian Research*, *35*, 295-311.

Kähkönen, Y. (2005). Svecofennian supracrustal rocks. In *Developments in Precambrian Geology, 14*, 343-405.

Kärkkäinen, N., Huhta, P., & Leväniemi, H. (2016). Kullaan vyöhykkeen malmipotentiaali, Saarijärven ja Kultakallion Au-mineralisaatiot. *Geological Survey of Finland, Archive report*, 75/2016, 42p.

Lahtinen, R., Huhma, H., Kähkönen, Y., & Mänttäri, I. (2009a). Paleoproterozoic sediment recycling during multiphase orogenic evolution in Fennoscandia, the Tampere and Pirkanmaa belts, Finland. *Precambrian Research*, *174*(3-4), 310-336.

Lahtinen, R., Huhma, H., Sipilä, P., & Vaarma, M. (2017). Geochemistry, U-Pb geochronology and Sm-Nd data from the Paleoproterozoic Western Finland supersuite–A key component in the coupled Bothnian oroclines. *Precambrian Research, 299*, 264-281.

Lahtinen, R., Hölttä, P., Kontinen, A., Niiranen, T., Nironen, M., Saalmann, K., & Sorjonen-Ward, P. (2011). Tectonic and metallogenic evolution of the Fennoscandian Shield: Key questions with emphasis on Finland. *Geological Survey of Finland Special Paper*, *49*, 23-33.

Lahtinen, R., Johnston, S. T., & Nironen, M. (2014). The Bothnian coupled oroclines of the Svecofennian Orogen: a Palaeoproterozoic terrane wreck. *Terra Nova*, *26*(4), 330-335.

Lahtinen, R., Korja, A., & Nironen, M. (2005). Paleoproterozoic tectonic evolution. In *Developments in Precambrian Geology* (Vol. 14, pp. 481-531). Elsevier.

Lahtinen, R., Korja, A., Nironen, M., & Heikkinen, P. (2009b). Palaeoproterozoic accretionary processes in Fennoscandia. *Geological Society, London, Special Publications*, *318*(1), 237-256.

Lehto, T., & Kärkkäinen, N. (2006). Tutkimustyöselostus Kullaan kunnassa valtausalueella Välimäki, kaivosrekisterinumero 7101/1, suoritetuista malmitutkimuksista. *Geological Survey of Finland, Claim report*, 12p.

Lister, G. S., & Williams, P. F. (1983). The partitioning of deformation in flowing rock masses. *Tectonophysics*, *92*(1-3), 1-33.

Lohva, J., & Jokinen, T. (2012). New data for gold exploration in southern Finland-detailed airborne geophysical measurements. *Geological Survey of Finland, Special Paper 52*, 55-72.

McCuaig, T. C., & Kerrich, R. (1998). P—T—t—deformation—fluid characteristics of lode gold deposits: evidence from alteration systematics. *Ore Geology Reviews*, *12*(6), 381-453.

Middlemost, E. A. (1994). Naming materials in the magma/igneous rock system. *Earth-Science Reviews*, *37*(3-4), 215-224.

Mikucki, E. J., & Groves, D. I. (1990). Gold transport and depositional models. *Gold deposits of the Archaean Yilgarn Block, Western Australia: nature, genesis and exploration guides. Publication*, *20*, 278-284.

Miller, L. D., Goldfarb, R. J., Gehrels, G. E., & Snee, L. W. (1994). Genetic links among fluid cycling, vein formation, regional deformation, and plutonism in the Juneau gold belt, southeastern Alaska. *Geology*, *22*(3), 203-206.

Molnár, F., Mänttäri, I., O'Brien, H., Lahaye, Y., Pakkanen, L., Johanson, B., ... & Sakellaris, G. (2016). Boron, sulphur and copper isotope systematics in the orogenic gold deposits of the Archaean Hattu schist belt, eastern Finland. *Ore Geology Reviews*, *77*, 133-162.

Mouri, H., Korsman, K., & Huhma, H. (1999). Tectono-metamorphic evolution and timing of the melting processes in the Svecofennian Tonalite-Trondhjemite Migmatite Belt: an example from Luopioinen, Tampere area, southern Finland. *Bulletin of the Geological Society of Finland, 71*(1), 31-56.

Mäkitie, H., & Lahti, S. I. (2001). The fayalite-augite quartz monzonite (1.87 Ga) of Luopa, western Finland, and its contact aureole. *Special paper 30, Geological Survey of Finland*, 61-98.

Neumayr, P., Walshe, J., Hagemann, S., Petersen, K., Roache, A., Frikken, P., ... & Halley, S. (2008). Oxidized and reduced mineral assemblages in greenstone belt rocks of the St. Ives gold camp, Western Australia: vectors to high-grade ore bodies in Archaean gold deposits?. *Mineralium Deposita*, *43*(3), 363-371.

Niiranen, T., Poutiainen, M., & Mänttäri, I. (2007). Geology, geochemistry, fluid inclusion characteristics, and U–Pb age studies on iron oxide–Cu–Au deposits in the Kolari region, northern Finland. *Ore Geology Reviews*, *30*(2), 75-105.

Nironen, M. (1989). The Tampere Schist Belt: structural style within an early Proterozoic volcanic arc system in southern Finland. *Precambrian Research*, *43*(1-2), 23-40.

Nironen, M. (1997). The Svecofennian Orogen: a tectonic model. *Precambrian Research*, *86*(1-2), 21-44.

Nironen, M., Kousa, J., Luukas, J. & Lahtinen, R. (2016). Geological Map of Finland. 1:1 000 000. *Espoo, Finland. Geological Survey of Finland.*

Nurmi, P. & Sorjonen-Ward, P. (1993). Geological development, gold mineralization, and exploration methods in the late Archaean Hattu schist belt, Ilomantsi, eastern Finland: *Geological Survey of Finland, Special Paper*, 17, 386 p.

Ojala, V. J., Ridley, J. R., Groves, D. I., & Hall, G. C. (1993). The Granny Smith gold deposit: the role of heterogeneous stress distribution at an irregular granitoid contact in a greenschist facies terrane. *Mineralium Deposita*, *28*(6), 409-419.

Otani, M., & Wallis, S. (2006). Quartz lattice preferred orientation patterns and static recrystallization: Natural examples from the Ryoke belt, Japan. *Geology*, *34*(7), 561-564.

Pajunen, M., Airo, M. L., Elminen, T., Mänttäri, I., Niemelä, R., Vaarma, M., ... & Wennerström, M. (2008). Tectonic evolution of the Svecofennian crust in southern Finland. *Geological Survey of Finland, Special Paper*, *47*, 15-160.

Pajunen, M., Airo, M. L., Wennerström, M., Niemelä, R., & Wasenius, P. (1987). The "Shear zone research and rock engineering" project, Pori area, south-western Finland. *Geological Survey of Finland, Special Paper*, (31-32), 7.

Parrish, R. R. (1990). U–Pb dating of monazite and its application to geological problems. *Canadian Journal of Earth Sciences*, *27*(11), 1431-1450.

Passchier, C. W., & Simpson, C. (1986). Porphyroclast systems as kinematic indicators. *Journal of Structural Geology*, *8*(8), 831-843.

Pearce, J. A. (1983): Role of the sub-continental lithosphere in magma genesis at active continental margins. *Continental Basalts and Mantle Xenoliths*, 230-249.

Pearce, J. A. (1996). A user's guide to basalt discrimination diagrams. *Trace element geochemistry of volcanic rocks: applications for massive sulphide exploration. Geological Association of Canada, Short Course Notes*, *12*, 79-113.

Pearce, J. A., Harris, N. B., & Tindle, A. G. (1984). Trace element discrimination diagrams for the tectonic interpretation of granitic rocks. *Journal of petrology*, *25*(4), 956-983.

Peccerillo, A., & Taylor, S. R. (1976). Geochemistry of Eocene calc-alkaline volcanic rocks from the Kastamonu area, northern Turkey. *Contributions to mineralogy and petrology*, *58*(1), 63-81.

Pietikäinen, K. (1994). The geology of the Paleoproterozoic Pori Shear Zone. *Michigan Tech, PhD thesis*. 129p.

Ramsay, J. G. (1967). Folding and fracturing of rocks. *Mc Graw Hill Book Company*, *568*.

Reimers, S. (2018). Kinematic Evolution of the Paleoproterozoic Kynsikangas Ductile Shear Zone, SW Finland. *University of Hamburg, MSc thesis.* 36 p.

Reimers, S., Engström, J., & Riller, U. (2018). The Kynsikangas shear zone, Southwest Finland: Importance for understanding deformation kinematics and rheology of lower crustal shear zones. In *Tenth symposium on structure, composition and evolution of the litosphere*. 95-98.

Rosenberg, C. L., & Handy, M. R. (2005). Experimental deformation of partially melted granite revisited: implications for the continental crust. *Journal of Metamorphic Geology*, *23*(1), 19-28.

Rubatto, D., Williams, I. S., & Buick, I. S. (2001). Zircon and monazite response to prograde metamorphism in the Reynolds Range, central Australia. *Contributions to Mineralogy and Petrology*, *140*(4), 458-468.

Rutland, R. R., Williams, I. S., & Korsman, K. (2004). Pre-1.91 Ga deformation and metamorphism in the Palaeoproterozoic Vammala Migmatite Belt, southern Finland, and implications for Svecofennian tectonics. *Bulletin of the Geological Society of Finland*, *76*(1-2), 93-140.

Saalmann, K. (2007). Structural control on gold mineralization in the Satulinmaki and Riukka prospects, Hame Schist Belt, southern Finland. *Bulletin of the Geological Survey of Finland*, *79*(1), 69.

Saalmann, K., Mänttäri, I., Peltonen, P., Whitehouse, M. J., Grönholm, P., & Talikka, M. (2010). Geochronology and structural relationships of mesothermal gold

mineralization in the Palaeoproterozoic Jokisivu prospect, southern Finland. *Geological Magazine*, *147*(4), 551-569.

Saalmann, K., Mänttäri, I., Ruffet, G., & Whitehouse, M. J. (2009). Age and tectonic framework of structurally controlled Palaeoproterozoic gold mineralization in the Häme belt of southern Finland. *Precambrian Research*, *174*(1-2), 53-77.

Saltikoff, B., Puustinen, K., & Tontti, M. (2006). Metallogenic zones and metallic mineral deposits in Finland. *Explanation to the Metallogenic Map of Finland. Geological Survey of Finland Special Paper*, (35), 66.

Schandl, E. S., & Gorton, M. P. (2004). A textural and geochemical guide to the identification of hydrothermal monazite: criteria for selection of samples for dating epigenetic hydrothermal ore deposits. *Economic Geology*, *99*(5), 1027-1035.

Shchipansky, A. A., & Bogdanova, S. V. (1996). The Sarmatian crustal segment: Precambrian correlation between the Voronezh massif and the Ukrainian Shield across the Dniepr-Donets aulacogen. *Tectonophysics*, *268*(1-4), 109-125.

Sibson, R. H. (1987). Earthquake rupturing as a mineralizing agent in hydrothermal systems. *Geology*, *15*(8), 701-704.

Sibson, R. H., Robert, F., & Poulsen, K. H. (1988). High-angle reverse faults, fluid-pressure cycling, and mesothermal gold-quartz deposits. *Geology*, *16*(6), 551-555.

Sotkamo Silver 2020. Available at: http://www.silver.fi/sivu/en/

Sullivan, W. A. (2006). Structural significance of L tectonites in the eastern-central Laramie Mountains, Wyoming. *The Journal of geology*, *114*(5), 513-531.

Sullivan, W. A. (2013). L tectonites. *Journal of Structural Geology*, *50*, 161-175.

Sundblad, K. (2003). Metallogeny of gold in the Precambrian of northern Europe. *Economic geology*, *98*(7), 1271-1290.

Van Achterbergh, E., Ryan, C. G., & Griffin, W. L. (1999). GLITTER: On-line interactive data reduction for the laser ablation inductively coupled plasma mass spectrometry microprobe. In *Ninth Annual VM Goldschmidt Conference*.

Vormisto, K. (1956). Lavian y.m. Porin ympäristöalueiden tutkimuksista v:na 1954-1956. *Outokumpu Oy, report 001/1143, 1144/RV, RH/54-56*. 22 p.

Walshe, J. L., Halley, S. W., Hall, G. A., & Kitto, P. (2003). Contrasting fluid systems, chemical gradients and controls on large-tonnage, high-grade Au deposits, Eastern Goldfields Province, Yilgarn Craton, Western Australia. In *Biennial SGA Meeting*. Vol. 7, 827-830.

Williams, I. S. (2001). Response of detrital zircon and monazite, and their U–Pb isotopic systems, to regional metamorphism and host-rock partial melting, Cooma Complex, southeastern Australia. *Australian Journal of Earth Sciences*, *48*(4), 557-580.

Woodcock, N. H., & Fischer, M. (1986). Strike-slip duplexes. *Journal of structural geology*, *8*(7), 725-735.

Wyche, N. L., Eilu, P., Koppström, K., Kortelainen, V. J., Niiranen, T., & Välimaa, J. (2015). The Suurikuusikko gold deposit (Kittilä mine), northern Finland. In *Mineral Deposits of Finland*. Elsevier, 411-433.

Appendix 1: Geochemical analysis results used for identifying gold-critical samples. Plutonic samples used for geochemical classification displayed green.

Sample	SiO2	Al2O3	Fe2O3	MgO	CaO	Na2O	K2O	TiO2	P2O5	MnO	Cr2O3	Ba	Sc	LOI	Be	Co	Cs	Ga	Hf	Nb	Rb	Sn	Sr	Ta	Th	U	V	W	Zr	Y	As	Au (ppb)
JUMA-2018-107.1	57.89	16.90	8.38	3.33	6.28	2.84	1.98	1.02	0.21	0.08	0.005	423	17	0.8	2	15.1	3.3	20.3	3.5	12.6	68.1	3	300.7	0.8	3.3	2.4	148	7.1	148.3	17.7	43.5	368.3
JUMA-2018-108.1	48.88	13.60	12.68	7.30	10.75	2.23	0.47	2.37	0.18	0.16	0.008	87	30	1.1	<1	37.6	0.1	20.7	3.6	20.7	4.1	7	275.3	1.1	4.9	1.6	404	3.0	140.8	22.3	12.7	12.7
JUMA-2018-109.1	68.03	14.55	5.20	2.57	2.39	3.17	2.43	0.61	0.13	0.04	0.014	389	14	0.6	3	13.2	6.1	15.8	4.1	8.4	96.0	1	191.9	0.7	9.6	4.2	114	3.7	151.0	17.0	27.6	6.2
JUMA-2018-110.1	63.25	15.41	5.04	1.89	12.68	0.20	0.02	0.60	0.15	0.30	0.012	17	13	0.3	<1	12.1	<0.1	17.6	5.5	9.9	0.5	3	126.1	0.8	11.1	3.5	89	1.3	202.2	27.8	15.1	16.9
JUMA-2018-115.1	64.24	16.43	6.72	1.73	4.20	2.97	2.11	0.53	0.12	0.27	0.004	358	10	0.5	3	6.2	14.0	17.4	3.7	9.5	80.4	7	246.3	1.0	6.5	6.2	61	2.4	141.6	30.9	274.9	27.5
JUMA-2018-119.2	96.44	0.30	2.12	0.09	0.06	0.04	<0.01	0.01	0.02	0.01	0.003	1	<1	0.9	<1	3.0	<0.1	<0.5	<0.1	0.3	0.3	<1	1.2	<0.1	<0.2	2.7	65	<0.5	1.6	0.3	16.2	1.3
JUMA-2018-12.1	51.07	15.74	11.92	6.88	8.44	1.82	1.42	1.18	0.13	0.19	0.020	249	32	0.9	<1	36.5	4.3	16.4	2.6	6.8	46.1	4	162.8	0.5	0.8	0.8	261	0.7	91.9	19.8	22.4	<0.5
JUMA-2018-123.1	56.85	17.38	9.38	3.38	6.93	2.84	1.32	0.81	0.16	0.12	0.005	283	18	0.6	<1	23.0	2.2	19.0	3.4	9.6	40.1	1	306.2	0.7	2.2	1.2	138	<0.5	125.2	23.9	2.1	3.4
JUMA-2018-125.1	69.09	13.86	5.40	2.34	2.44	2.60	2.47	0.59	0.12	0.06	0.012	343	12	0.8	2	12.4	3.5	15.3	5.1	8.1	93.6	<1	197.9	0.8	10.2	2.0	102	1.1	185.8	15.0	5.4	<0.5
JUMA-2018-13.1	63.15	15.98	6.96	2.67	4.88	2.85	2.07	0.64	0.09	0.10	0.008	458	15	0.4	<1	16.2	3.2	17.1	4.4	7.5	79.8	1	200.9	0.6	5.0	2.3	107	<0.5	151.0	25.4	0.8	<0.5
JUMA-2018-17.1	68.94	15.31	4.05	1.48	3.01	3.72	1.87	0.45	0.10	0.05	0.009	745	7	0.8	1	7.9	2.2	17.2	3.5	5.7	74.2	<1	259.9	0.3	10.0	0.9	38	<0.5	125.0	6.0	<0.5	<0.5
JUMA-2018-22.1	52.18	17.96	9.44	4.94	7.24	3.87	2.07	1.08	0.26	0.13	0.016	486	25	0.5	2	25.9	2.2	24.3	4.2	11.4	68.9	2	569.0	0.6	0.4	1.2	136	<0.5	174.6	24.1	<0.5	<0.5
JUMA-2018-25.1	59.06	16.85	8.55	2.97	5.65	2.94	2.21	0.79	0.12	0.13	0.005	560	18	0.5	<1	18.5	5.7	19.1	4.3	10.4	76.2	3	218.5	0.7	5.4	1.4	124	0.6	156.2	28.1	0.7	<0.5
JUMA-2018-26.2	51.92	19.39	9.17	3.27	8.18	2.43	2.23	1.28	0.34	0.13	0.002	478	19	1.4	<1	25.1	7.9	20.3	2.8	8.3	74.2	<1	309.8	0.5	2.5	1.4	168	0.9	114.0	17.5	24.7	5.7
JUMA-2018-26.3	19.91	2.78	36.32	0.26	0.89	0.40	0.19	0.09	<0.01	0.02	0.003	50	2	28.0	<1	899.1	1.5	1.3	0.9	10.5	6.1	<1	34.0	0.2	0.3	<0.1	15	4.4	30.1	4.1	>10000.0	46570.6
JUMA-2018-34.1	62.86	15.77	6.15	2.78	4.69	3.22	2.83	0.70	0.11	0.09	0.012	344	16	0.6	5	14.5	6.1	18.4	4.0	9.1	117.8	3	234.4	0.7	9.7	2.3	69	<0.5	139.0	20.7	14.2	<0.5
JUMA-2018-35.1	61.74	15.25	7.02	3.58	5.14	2.93	2.60	0.61	0.09	0.10	0.024	498	19	0.7	2	19.4	3.8	16.6	4.0	8.2	105.4	5	201.7	0.7	9.0	1.8	116	<0.5	147.3	24.1	416.5	26.9
JUMA-2018-36.1	61.20	16.71	6.48	3.28	4.99	3.37	2.35	0.62	0.09	0.10	0.019	200	16	0.6	7	17.0	5.9	18.5	4.7	9.0	111.5	6	188.9	0.8	11.6	3.3	111	<0.5	172.7	16.6	3.9	<0.5
JUMA-2018-37.1	83.70	0.08	10.32	0.02	0.02	<0.01	<0.01	<0.01	<0.01	<0.01	<0.002	2	<1	5.7	<1	148.2	<0.1	<0.5	0.1	0.9	0.5	<1	0.6	<0.1	<0.2	9.8	16	<0.5	5.1	1.0	3707.5	78.6
JUMA-2018-40.1	41.85	13.92	17.27	8.47	11.36	2.22	0.57	2.63	0.23	0.22	0.026	67	32	0.9	2	68.9	0.3	23.2	4.1	23.2	4.4	3	278.3	1.3	1.7	0.3	407	0.7	165.3	25.7	7.3	9.5
JUMA-2018-46.1	57.20	17.13	9.15	3.72	5.08	2.77	2.38	0.85	0.13	0.11	0.025	319	25	1.2	<1	24.9	3.8	18.0	3.6	6.8	113.6	1	258.8	0.5	7.4	2.7	145	0.7	131.0	23.9	1.4	<0.5
JUMA-2018-5.1	76.55	13.22	1.82	0.37	2.84	3.54	0.87	0.05	0.06	0.09	0.003	159	7	0.5	2	2.2	0.9	9.2	0.6	1.1	16.2	<1	215.9	0.2	1.4	1.6	13	<0.5	19.2	27.5	9.2	<0.5
JUMA-2018-54.1	65.12	15.50	6.33	2.36	3.50	3.23	2.34	0.65	0.11	0.09	0.009	249	14	0.6	2	15.2	9.9	17.6	3.6	8.7	120.9	3	174.8	0.8	9.2	3.1	91	1.0	137.0	12.3	21.2	<0.5
JUMA-2018-7.1	52.73	20.23	10.04	3.17	6.90	3.61	1.19	1.09	0.15	0.18	0.007	155	30	0.5	<1	26.9	1.7	20.9	3.1	5.6	41.3	<1	264.5	0.4	3.5	1.9	208	0.8	109.6	27.3	16.5	1.2
JUMA-2018-76.1	59.01	15.92	8.45	4.36	6.00	2.56	1.55	0.76	0.11	0.11	0.046	343	25	0.9	<1	21.0	2.5	17.1	3.6	7.1	56.0	2	232.9	0.7	7.5	1.9	147	<0.5	136.3	22.5	2.1	<0.5
JUMA-2018-80.1	53.29	17.89	11.21	5.31	1.58	2.15	5.40	1.20	0.07	0.07	0.029	727	26	1.5	2	26.2	12.5	26.6	5.2	16.3	222.6	5	163.2	1.7	15.0	4.1	205	2.3	174.7	27.0	8.1	<0.5
TALE-2018-2.1	55.05	18.83	10.41	4.04	1.09	1.49	4.59	0.95	0.07	0.15	0.007	1017	29	3.0	7	21.4	5.2	23.2	6.3	18.5	194.0	<1	131.4	1.4	19.5	4.0	105	0.5	227.7	41.8	<0.5	1.2
TALE-2018-22.1	67.64	15.84	4.71	1.14	3.77	3.75	1.82	0.41	0.10	0.07	0.003	507	5	0.6	1	7.6	1.7	18.2	3.9	7.8	66.5	<1	271.3	0.6	6.1	0.8	28	<0.5	137.9	9.2	<0.5	0.9
TALE-2018-31.1	52.28	14.64	10.76	7.57	7.63	2.45	1.87	0.94	0.15	0.19	0.067	269	27	1.2	<1	35.1	3.0	17.7	2.6	7.4	92.3	5	234.7	0.4	1.7	1.3	176	<0.5	93.3	26.4	1.7	<0.5
TALE-2018-36.1	61.73	15.86	6.31	3.49	4.80	3.57	2.53	0.69	0.12	0.09	0.019	326	14	0.6	<1	17.7	4.8	16.1	3.7	5.6	97.2	3	246.9	0.4	7.4	1.7	97	<0.5	135.3	12.7	0.6	0.7

Sample	La	Ce	Pr	Nd	Sm	Eu	Gd	Tb	Dy	Ho	Er	Tm	Yb	Lu	F	Mo	Cu	Pb	Zn	Ag	Ni	Cd	Sb	Bi	Cr	B	Na	Hg	Tl	S	Se	Te
JUMA-2018-107.1	22.9	44.4	5.15	20.8	3.88	1.25	3.80	0.58	3.34	0.66	1.90	0.27	1.85	0.27	637	31.8	90.7	2.5	70	0.2	14.2	<0.1	<0.1	0.6	26	21	0.340	<0.01	0.6	0.62	1.0	<0.2
JUMA-2018-108.1	26.0	58.7	7.37	29.3	6.09	3.18	6.01	0.85	4.70	0.93	2.60	0.33	2.14	0.32	436	1.1	171.0	1.4	23	0.1	30.0	<0.1	0.4	0.1	15	<20	0.267	<0.01	<0.1	0.30	0.6	<0.2
JUMA-2018-109.1	34.8	64.2	7.79	29.2	5.24	1.25	4.39	0.66	3.40	0.71	2.02	0.26	1.74	0.28	487	3.5	152.1	2.4	120	<0.1	25.1	0.1	<0.1	0.1	91	<20	0.069	<0.01	0.5	0.17	1.6	<0.2
JUMA-2018-110.1	39.0	74.6	8.90	33.9	6.14	1.42	5.38	0.79	4.79	0.92	2.90	0.43	2.75	0.42	160	1.1	147.7	2.8	3	0.1	27.8	0.1	<0.1	0.5	18	<20	0.152	<0.01	<0.1	0.72	1.1	<0.2
JUMA-2018-115.1	7.7	13.8	1.69	6.3	1.47	0.70	2.28	0.57	4.46	1.09	3.41	0.51	3.49	0.52	325	3.9	9.8	2.1	64	<0.1	6.3	<0.1	0.1	0.1	20	<20	0.175	<0.01	0.5	<0.05	<0.5	<0.2
JUMA-2018-119.2	0.6	0.6	0.07	<0.3	0.06	<0.02	<0.05	<0.01	0.09	<0.02	<0.03	<0.01	<0.05	<0.01	26	22.6	27.4	1.5	10	<0.1	60.2	0.1	0.4	0.1	15	<20	0.004	<0.01	<0.1	0.29	1.7	<0.2
JUMA-2018-12.1	10.6	24.3	3.57	15.9	3.58	1.01	3.94	0.65	3.71	0.82	2.19	0.33	2.05	0.33	339	2.1	28.9	2.2	50	<0.1	25.2	<0.1	<0.1	<0.1	54	<20	0.504	<0.01	0.3	<0.05	<0.5	<0.2
JUMA-2018-123.1	16.0	38.4	5.45	23.1	5.32	1.34	5.34	0.78	4.43	0.85	2.41	0.32	2.03	0.33	436	1.8	82.2	1.7	56	<0.1	13.6	<0.1	<0.1	<0.1	18	<20	0.332	<0.01	0.2	0.11	<0.5	<0.2
JUMA-2018-125.1	31.2	64.8	7.14	27.0	4.87	1.15	4.17	0.60	2.93	0.56	1.45	0.20	1.43	0.22	462	1.8	9.0	2.8	80	<0.1	31.2	<0.1	<0.1	0.1	90	<20	0.093	<0.01	0.5	<0.05	<0.5	<0.2
JUMA-2018-13.1	22.3	44.7	5.56	21.3	4.59	0.96	4.40	0.72	4.47	0.99	2.96	0.41	3.07	0.44	419	1.5	18.3	4.5	70	<0.1	15.6	<0.1	<0.1	<0.1	39	<20	0.258	<0.01	0.6	<0.05	<0.5	<0.2
JUMA-2018-17.1	33.7	57.1	6.05	19.7	2.65	0.86	1.99	0.24	1.12	0.23	0.59	0.07	0.49	0.07	278	1.0	3.1	2.1	71	<0.1	11.0	<0.1	<0.1	<0.1	37	<20	0.118	<0.01	0.4	<0.05	<0.5	<0.2
JUMA-2018-22.1	11.8	37.1	5.86	27.9	6.54	1.58	5.94	0.87	4.83	0.92	2.59	0.36	2.31	0.35	721	1.4	25.5	1.1	85	<0.1	29.3	<0.1	<0.1	<0.1	57	<20	0.117	<0.01	0.5	<0.05	<0.5	<0.2
JUMA-2018-25.1	24.8	47.6	5.80	23.3	5.13	1.12	5.14	0.87	4.91	0.96	2.77	0.38	2.36	0.33	523	2.2	5.6	1.8	77	<0.1	10.9	<0.1	<0.1	<0.1	23	<20	0.287	<0.01	0.5	<0.05	<0.5	<0.2
JUMA-2018-26.2	14.2	27.6	3.57	15.4	3.49	1.30	3.93	0.61	3.46	0.69	1.85	0.26	1.57	0.24	297	1.4	80.2	2.0	51	0.1	8.6	<0.1	<0.1	0.1	7	<20	0.357	<0.01	<0.1	0.42	<0.5	<0.2
JUMA-2018-26.3	3.7	7.7	0.87	4.2	0.66	0.14	0.95	0.12	0.75	0.13	0.45	0.05	0.38	0.05	62	10.3	586.4	5.1	10	5.3	240.4	<0.1	47.5	58.6	3	<20	0.047	0.01	0.2	>10.00	20.7	19.6
JUMA-2018-34.1	36.7	80.6	8.02	28.5	5.28	0.95	4.55	0.71	3.85	0.77	2.20	0.33	1.97	0.31	538	2.4	8.3	3.0	79	<0.1	12.2	<0.1	<0.1	<0.1	71	<20	0.155	<0.01	0.7	<0.05	<0.5	<0.2
JUMA-2018-35.1	38.6	74.9	8.59	32.3	5.48	0.92	5.01	0.73	4.25	0.87	2.63	0.37	2.42	0.37	522	1.8	5.3	3.1	69	<0.1	21.6	<0.1	<0.1	0.3	131	<20	0.283	<0.01	0.7	<0.05	<0.5	<0.2
JUMA-2018-36.1	30.8	63.6	6.20	22.3	3.59	0.78	3.40	0.49	2.80	0.54	1.69	0.25	1.64	0.29	455	1.6	18.3	5.8	81	<0.1	17.8	<0.1	<0.1	<0.1	117	<20	0.207	<0.01	0.8	<0.05	<0.5	<0.2
JUMA-2018-37.1	2.7	4.3	0.46	1.4	0.20	<0.02	0.22	0.03	0.23	0.04	0.14	0.01	0.06	0.02	20	37.3	615.3	3.2	9	1.2	173.6	0.8	5.7	0.6	8	<20	0.004	<0.01	<0.1	6.82	12.4	0.6
JUMA-2018-40.1	24.2	57.9	8.01	34.7	6.98	2.38	7.12	1.00	5.58	1.00	2.66	0.35	2.05	0.30	643	0.8	4.0	1.0	42	<0.1	34.6	<0.1	0.4	<0.1	48	<20	0.375	<0.01	<0.1	<0.05	<0.5	<0.2
JUMA-2018-46.1	22.7	44.8	5.18	19.9	3.99	1.00	3.95	0.62	4.13	0.89	2.74	0.40	2.57	0.40	534	0.9	25.0	2.6	80	<0.1	20.6	<0.1	<0.1	<0.1	143	<20	0.290	<0.01	0.6	<0.05	<0.5	<0.2
JUMA-2018-5.1	8.0	13.6	1.48	5.1	1.07	1.19	1.49	0.34	3.41	1.02	3.68	0.61	4.03	0.62	75	2.1	5.3	2.1	20	<0.1	5.9	<0.1	<0.1	<0.1	14	<20	0.157	<0.01	<0.1	<0.05	<0.5	<0.2
JUMA-2018-54.1	17.8	36.5	3.58	12.7	2.22	0.74	2.20	0.34	2.17	0.45	1.39	0.18	1.23	0.21	453	2.3	7.3	3.5	78	<0.1	13.6	<0.1	<0.1	0.1	55	<20	0.175	<0.01	0.7	<0.05	<0.5	<0.2
JUMA-2018-7.1	20.8	40.6	5.48	21.8	4.95	1.41	5.20	0.82	4.85	1.01	3.13	0.44	2.77	0.46	244	1.2	42.7	2.8	59	0.1	8.9	<0.1	0.1	<0.1	31	<20	0.499	<0.01	0.2	<0.05	<0.5	<0.2
JUMA-2018-76.1	24.7	50.5	6.20	25.1	5.07	1.09	4.80	0.72	4.09	0.81	2.43	0.33	2.26	0.36	365	1.2	30.2	3.5	56	<0.1	21.5	<0.1	<0.1	<0.1	182	<20	0.356	<0.01	0.4	<0.05	<0.5	<0.2
JUMA-2018-80.1	48.0	92.2	10.83	40.4	7.27	1.00	6.28	0.92	5.02	1.02	3.01	0.39	2.56	0.37	1087	1.2	19.0	4.2	181	<0.1	69.3	<0.1	<0.1	0.3	199	<20	0.079	<0.01	1.3	<0.05	<0.5	<0.2
TALE-2018-2.1	51.2	101.6	12.26	45.5	9.08	1.13	8.49	1.27	7.21	1.52	5.01	0.77	5.12	0.82	906	1.3	16.8	4.6	91	<0.1	38.8	<0.1	<0.1	<0.1	47	<20	0.045	<0.01	1.1	<0.05	<0.5	<0.2
TALE-2018-22.1	25.4	46.0	5.16	17.5	3.04	0.98	2.44	0.33	1.77	0.34	1.13	0.15	1.06	0.16	330	1.2	10.4	1.1	74	<0.1	4.0	<0.1	<0.1	<0.1	13	<20	0.107	<0.01	0.4	<0.05	<0.5	<0.2
TALE-2018-31.1	31.1	63.8	9.75	38.8	8.09	1.31	6.86	0.99	5.33	0.97	2.68	0.40	2.58	0.35	905	1.8	5.6	2.0	93	<0.1	47.1	0.2	<0.1	0.2	229	<20	0.182	<0.01	0.6	<0.05	<0.5	<0.2
TALE-2018-36.1	15.8	31.4	3.63	13.8	2.72	0.94	2.66	0.39	2.48	0.48	1.48	0.21	1.36	0.21	430	1.6	20.4	2.8	62	<0.1	35.7	<0.1	<0.1	<0.1	117	<20	0.116	<0.01	0.8	<0.05	<0.5	<0.2

Appendix 2: Zircon U-Pb analysis results

file	sample	comment	Pb^{206}/Pb^{204}	Pb	Th	U	Th/U	207Pb/206Pb	1s	207Pb/235U	1s	206Pb/238U	1s	r	% Concordance	207Pb/206Pb	1s	207Pb/235U	1s	206Pb/238U	1s
~~66637_TRA_Data~~	~~66637~~	~~64~~	~~715~~	~~338~~	~~4~~	~~1004~~	~~0.004~~	~~0.1140~~	~~0.0007~~	~~5.166~~	~~0.080~~	~~0.322~~	~~0.006~~	~~0.90~~	~~97~~	~~1864~~	~~12~~	~~1847~~	~~13~~	~~1798~~	~~29~~
~~66635_TRA_Data~~	~~66635~~	~~84b~~	~~1399587~~	~~295~~	~~4~~	~~830~~	~~0.005~~	~~0.1140~~	~~0.0009~~	~~5.464~~	~~0.103~~	~~0.348~~	~~0.006~~	~~0.91~~	~~101~~	~~1865~~	~~14~~	~~1895~~	~~16~~	~~1923~~	~~30~~
66664_TRA_Data	66664	4	1199120	253	2	710	0.003	0.1146	0.0009	5.561	0.105	0.352	0.006	0.91	102	1874	14	1910	16	1944	31
66660_TRA_Data	66660	23	1651312	349	6	1039	0.006	0.1150	0.0009	5.245	0.099	0.331	0.006	0.91	99	1880	14	1860	16	1842	29
66652_TRA_Data	66652	38	1988564	421	11	1248	0.009	0.1151	0.0009	5.244	0.099	0.331	0.006	0.91	99	1881	14	1860	16	1841	29
66603_TRA_Data	66603	124b	1937475	409	4	1152	0.003	0.1151	0.0009	5.427	0.103	0.342	0.006	0.91	100	1882	14	1889	16	1896	30
66657_TRA_Data	66657	10	1344103	285	10	843	0.012	0.1152	0.0009	5.265	0.100	0.331	0.006	0.91	99	1884	14	1863	16	1845	29
66633_TRA_Data	66633	103	1302059	275	3	807	0.003	0.1153	0.0009	5.277	0.100	0.332	0.006	0.91	99	1884	14	1865	16	1848	29
66607_TRA_Data	66607	135b	1449421	306	4	867	0.005	0.1153	0.0009	5.413	0.102	0.341	0.006	0.91	100	1885	14	1887	16	1889	30
66634_TRA_Data	66634	84a	1488525	314	3	882	0.003	0.1153	0.0009	5.524	0.105	0.348	0.006	0.91	101	1885	14	1904	16	1923	30
66643_TRA_Data	66643	76b	1512841	320	4	890	0.004	0.1154	0.0009	5.593	0.106	0.352	0.006	0.91	101	1886	14	1915	16	1942	31
66640_TRA_Data	66640	51	1400196	297	8	825	0.010	0.1157	0.0009	5.588	0.106	0.350	0.006	0.91	101	1891	14	1914	16	1937	31
66617_TRA_Data	66617	118	1579055	334	3	947	0.003	0.1157	0.0009	5.439	0.103	0.341	0.006	0.91	100	1891	14	1891	16	1891	30
66655_TRA_Data	66655	13b	1603568	339	3	928	0.003	0.1157	0.0009	5.724	0.108	0.359	0.007	0.91	102	1891	14	1935	16	1976	31
66625_TRA_Data	66625	87	1395409	296	15	809	0.018	0.1158	0.0009	5.646	0.107	0.354	0.006	0.91	102	1892	14	1923	16	1953	31
66653_TRA_Data	66653	14	2049826	433	3	1284	0.002	0.1158	0.0009	5.289	0.100	0.331	0.006	0.91	99	1892	14	1867	16	1845	29
66620_TRA_Data	66620	115	1631360	345	3	1030	0.003	0.1158	0.0009	5.176	0.098	0.324	0.006	0.91	98	1892	14	1849	16	1810	29
66621_TRA_Data	66621	94	1784268	377	4	1069	0.004	0.1158	0.0009	5.460	0.103	0.342	0.006	0.91	100	1893	14	1894	16	1896	30
~~66624_TRA_Data~~	~~66624~~	~~107~~	~~1843505~~	~~390~~	~~4~~	~~1153~~	~~0.004~~	~~0.1162~~	~~0.0009~~	~~5.257~~	~~0.100~~	~~0.328~~	~~0.006~~	~~0.91~~	~~98~~	~~1899~~	~~14~~	~~1862~~	~~16~~	~~1829~~	~~29~~
~~66604_TRA_Data~~	~~66604~~	~~126b~~	~~2113994~~	~~447~~	~~4~~	~~1249~~	~~0.004~~	~~0.1168~~	~~0.0009~~	~~5.546~~	~~0.105~~	~~0.344~~	~~0.006~~	~~0.91~~	~~100~~	~~1908~~	~~14~~	~~1908~~	~~16~~	~~1908~~	~~30~~
~~66619_TRA_Data~~	~~66619~~	~~97b~~	~~1537585~~	~~329~~	~~62~~	~~1157~~	~~0.053~~	~~0.1175~~	~~0.0009~~	~~4.405~~	~~0.084~~	~~0.272~~	~~0.005~~	~~0.91~~	~~91~~	~~1918~~	~~14~~	~~1713~~	~~16~~	~~1551~~	~~25~~
~~66623_TRA_Data~~	~~66623~~	~~113~~	~~966451~~	~~208~~	~~19~~	~~542~~	~~0.035~~	~~0.1176~~	~~0.0009~~	~~5.923~~	~~0.112~~	~~0.365~~	~~0.007~~	~~0.91~~	~~102~~	~~1921~~	~~14~~	~~1965~~	~~16~~	~~2007~~	~~32~~
~~66662_TRA_Data~~	~~66662~~	~~1a~~	~~1306901~~	~~277~~	~~8~~	~~693~~	~~0.011~~	~~0.1179~~	~~0.0009~~	~~6.388~~	~~0.121~~	~~0.393~~	~~0.007~~	~~0.91~~	~~105~~	~~1924~~	~~14~~	~~2031~~	~~17~~	~~2137~~	~~33~~
~~66661_TRA_Data~~	~~66661~~	~~21~~	~~1225475~~	~~260~~	~~3~~	~~732~~	~~0.004~~	~~0.1181~~	~~0.0009~~	~~5.674~~	~~0.108~~	~~0.349~~	~~0.006~~	~~0.91~~	~~100~~	~~1927~~	~~14~~	~~1927~~	~~16~~	~~1928~~	~~30~~
~~66658_TRA_Data~~	~~66658~~	~~6~~	~~1730548~~	~~367~~	~~3~~	~~1034~~	~~0.003~~	~~0.1182~~	~~0.0009~~	~~5.673~~	~~0.108~~	~~0.348~~	~~0.006~~	~~0.91~~	~~100~~	~~1929~~	~~14~~	~~1927~~	~~16~~	~~1925~~	~~30~~
~~66605_TRA_Data~~	~~66605~~	~~131b~~	~~1483338~~	~~354~~	~~371~~	~~859~~	~~0.431~~	~~0.1197~~	~~0.0009~~	~~5.797~~	~~0.110~~	~~0.351~~	~~0.006~~	~~0.91~~	~~100~~	~~1951~~	~~14~~	~~1946~~	~~16~~	~~1942~~	~~31~~
~~66654_TRA_Data~~	~~66654~~	~~13a~~	~~273367~~	~~61~~	~~24~~	~~151~~	~~0.160~~	~~0.1201~~	~~0.0010~~	~~6.226~~	~~0.119~~	~~0.376~~	~~0.007~~	~~0.90~~	~~103~~	~~1957~~	~~15~~	~~2008~~	~~17~~	~~2058~~	~~32~~
~~66606_TRA_Data~~	~~66606~~	~~148c~~	~~2035864~~	~~432~~	~~3~~	~~1195~~	~~0.003~~	~~0.1204~~	~~0.0010~~	~~5.761~~	~~0.109~~	~~0.347~~	~~0.006~~	~~0.91~~	~~99~~	~~1963~~	~~14~~	~~1941~~	~~16~~	~~1920~~	~~30~~
~~66615_TRA_Data~~	~~66615~~	~~155b~~	~~1584264~~	~~336~~	~~4~~	~~974~~	~~0.004~~	~~0.1204~~	~~0.0009~~	~~5.518~~	~~0.104~~	~~0.332~~	~~0.006~~	~~0.91~~	~~97~~	~~1963~~	~~14~~	~~1903~~	~~16~~	~~1850~~	~~29~~
~~66641_TRA_Data~~	~~66641~~	~~50~~	~~18800~~	~~220~~	~~151~~	~~563~~	~~0.269~~	~~0.1216~~	~~0.0010~~	~~5.901~~	~~0.111~~	~~0.352~~	~~0.006~~	~~0.91~~	~~99~~	~~1980~~	~~14~~	~~1961~~	~~16~~	~~1942~~	~~31~~
~~66638_TRA_Data~~	~~66638~~	~~65~~	~~479783~~	~~107~~	~~36~~	~~258~~	~~0.141~~	~~0.1225~~	~~0.0010~~	~~6.479~~	~~0.123~~	~~0.384~~	~~0.007~~	~~0.91~~	~~102~~	~~1994~~	~~14~~	~~2043~~	~~17~~	~~2093~~	~~33~~
~~66622_TRA_Data~~	~~66622~~	~~93~~	~~138205~~	~~37~~	~~61~~	~~73~~	~~0.833~~	~~0.1228~~	~~0.0010~~	~~6.553~~	~~0.126~~	~~0.387~~	~~0.007~~	~~0.90~~	~~103~~	~~1997~~	~~15~~	~~2053~~	~~17~~	~~2109~~	~~33~~
~~66616_TRA_Data~~	~~66616~~	~~158c~~	~~1059843~~	~~230~~	~~33~~	~~591~~	~~0.056~~	~~0.1240~~	~~0.0010~~	~~6.268~~	~~0.119~~	~~0.367~~	~~0.007~~	~~0.91~~	~~100~~	~~2015~~	~~14~~	~~2014~~	~~16~~	~~2013~~	~~32~~
~~66651_TRA_Data~~	~~66651~~	~~18~~	~~1344869~~	~~287~~	~~9~~	~~766~~	~~0.012~~	~~0.1241~~	~~0.0010~~	~~6.232~~	~~0.118~~	~~0.364~~	~~0.007~~	~~0.91~~	~~100~~	~~2016~~	~~14~~	~~2009~~	~~16~~	~~2003~~	~~31~~
~~66642_TRA_Data~~	~~66642~~	~~76~~	~~174225~~	~~53~~	~~123~~	~~104~~	~~1.178~~	~~0.1268~~	~~0.0010~~	~~6.045~~	~~0.115~~	~~0.346~~	~~0.006~~	~~0.90~~	~~97~~	~~2054~~	~~15~~	~~1982~~	~~16~~	~~1915~~	~~30~~
~~66636_TRA_Data~~	~~66636~~	~~103b~~	~~61559~~	~~14~~	~~11~~	~~33~~	~~0.319~~	~~0.1272~~	~~0.0012~~	~~6.652~~	~~0.129~~	~~0.379~~	~~0.007~~	~~0.88~~	~~100~~	~~2060~~	~~16~~	~~2066~~	~~17~~	~~2072~~	~~33~~
~~66639_TRA_Data~~	~~66639~~	~~69~~	~~861595~~	~~189~~	~~40~~	~~486~~	~~0.081~~	~~0.1287~~	~~0.0010~~	~~6.494~~	~~0.123~~	~~0.366~~	~~0.007~~	~~0.91~~	~~98~~	~~2080~~	~~14~~	~~2045~~	~~17~~	~~2011~~	~~32~~
~~66659_TRA_Data~~	~~66659~~	~~27~~	~~704527~~	~~162~~	~~82~~	~~402~~	~~0.204~~	~~0.1300~~	~~0.0010~~	~~6.539~~	~~0.124~~	~~0.365~~	~~0.007~~	~~0.91~~	~~98~~	~~2098~~	~~14~~	~~2051~~	~~17~~	~~2005~~	~~31~~
~~66618_TRA_Data~~	~~66618~~	~~97a~~	~~134503~~	~~31~~	~~16~~	~~62~~	~~0.264~~	~~0.1350~~	~~0.0012~~	~~8.285~~	~~0.161~~	~~0.445~~	~~0.008~~	~~0.89~~	~~105~~	~~2163~~	~~16~~	~~2263~~	~~17~~	~~2374~~	~~37~~
~~66663_TRA_Data~~	~~66663~~	~~1b~~	~~408275~~	~~101~~	~~91~~	~~202~~	~~0.451~~	~~0.1367~~	~~0.0011~~	~~7.925~~	~~0.151~~	~~0.421~~	~~0.008~~	~~0.91~~	~~102~~	~~2185~~	~~14~~	~~2223~~	~~17~~	~~2263~~	~~35~~
~~66614_TRA_Data~~	~~66614~~	~~153b~~	~~994003~~	~~234~~	~~109~~	~~486~~	~~0.224~~	~~0.1790~~	~~0.0014~~	~~10.305~~	~~0.195~~	~~0.418~~	~~0.008~~	~~0.91~~	~~91~~	~~2644~~	~~13~~	~~2463~~	~~17~~	~~2250~~	~~35~~
~~66650_TRA_Data~~	~~66650~~	~~56~~	~~99625~~	~~26~~	~~17~~	~~37~~	~~0.449~~	~~0.2020~~	~~0.0017~~	~~15.362~~	~~0.295~~	~~0.552~~	~~0.010~~	~~0.90~~	~~100~~	~~2842~~	~~14~~	~~2838~~	~~18~~	~~2832~~	~~42~~
~~66656_TRA_Data~~	~~66656~~	~~11~~	~~789~~	~~437~~	~~283~~	~~651~~	~~0.435~~	~~0.2040~~	~~0.0015~~	~~15.622~~	~~0.269~~	~~0.546~~	~~0.010~~	~~0.90~~	~~98~~	~~2858~~	~~12~~	~~2854~~	~~16~~	~~2809~~	~~42~~

Strike through: data not used
Yellow: younger population
Black: older population

Appendix 3: Monazite U-Pb analysis results

file	sample	Pb	Th	U	206/204Pb	207Pb/206Pb	1s	207Pb/235U	1s	206Pb/238U	1s	r	% Concordance	207Pb/206Pb	1s	207Pb/235U	1s	206Pb/238U	1s
66764_TRA_Data	75	4839	28225	5430	118104	0.1092	0.0006	4.7697	0.0960	0.3167	0.0064	0.96	99	1787	10	1780	17	1773	31
66755_TRA_Data	87b	4474	32410	4076	85681	0.1093	0.0006	4.7200	0.0950	0.3133	0.0063	0.96	98	1787	10	1771	17	1757	31
66765_TRA_Data	76	4237	24333	5086	127781	0.1093	0.0006	4.6610	0.0938	0.3092	0.0062	0.96	97	1789	10	1760	17	1737	31
66745_TRA_Data	110b	4196	27607	4426	99465	0.1095	0.0006	4.8449	0.0975	0.3208	0.0065	0.96	100	1791	10	1793	17	1794	32
66753_TRA_Data	101b	4207	30250	3955	85385	0.1095	0.0006	4.7314	0.0952	0.3133	0.0063	0.96	98	1792	10	1773	17	1757	31
66769_TRA_Data	69	4920	29172	5466	81184	0.1097	0.0006	4.8070	0.0967	0.3178	0.0064	0.96	99	1795	10	1786	17	1779	31
66771_TRA_Data	71	5165	34116	5341	92619	0.1100	0.0006	4.8346	0.0973	0.3189	0.0064	0.96	99	1799	10	1791	17	1784	31
66772_TRA_Data	85	4691	31569	4690	61546	0.1100	0.0006	4.8401	0.0974	0.3190	0.0064	0.96	99	1800	10	1792	17	1785	31
66763_TRA_Data	61	4502	32263	4175	88768	0.1100	0.0006	4.7486	0.0955	0.3130	0.0063	0.96	97	1800	10	1776	17	1755	31
66754_TRA_Data	87a	4525	32453	4202	92708	0.1101	0.0006	4.7485	0.0955	0.3128	0.0063	0.96	97	1801	10	1776	17	1755	31
66746_TRA_Data	107a	4133	24332	4714	145794	0.1101	0.0006	4.8826	0.0982	0.3216	0.0065	0.96	100	1801	10	1799	17	1797	32
66751_TRA_Data	105b	4451	26108	5047	108250	0.1104	0.0006	4.8547	0.0977	0.3189	0.0064	0.96	99	1806	10	1794	17	1784	31
66752_TRA_Data	101a	4223	30311	3870	110395	0.1105	0.0006	4.8057	0.0967	0.3155	0.0064	0.96	98	1807	10	1786	17	1768	31
66750_TRA_Data	105a	4706	29036	5177	108656	0.1105	0.0006	4.8107	0.0968	0.3158	0.0064	0.96	98	1807	10	1787	17	1769	31
66766_TRA_Data	77	4812	17104	4962	117911	0.1105	0.0006	4.9314	0.0993	0.3237	0.0065	0.96	100	1808	10	1808	17	1808	32
66747_TRA_Data	107b	4581	27933	5091	94089	0.1105	0.0006	4.8780	0.0982	0.3200	0.0065	0.96	99	1808	10	1798	17	1790	31
66773_TRA_Data	86	4301	26612	4673	107937	0.1107	0.0006	4.8388	0.0974	0.3171	0.0064	0.96	98	1811	10	1792	17	1775	31
66767_TRA_Data	79	4264	27967	4237	71450	0.1107	0.0006	4.9145	0.0989	0.3220	0.0065	0.96	99	1811	10	1805	17	1800	32
66770_TRA_Data	83	3998	27029	3880	79042	0.1108	0.0006	4.9263	0.0991	0.3225	0.0065	0.96	99	1812	10	1807	17	1802	32
66749_TRA_Data	93b	4858	28776	5609	10264924	0.1108	0.0006	4.8256	0.0971	0.3159	0.0064	0.96	98	1812	10	1789	17	1770	31
66748_TRA_Data	93a	5285	30073	6212	113490	0.1109	0.0006	4.8280	0.0971	0.3157	0.0064	0.96	97	1815	10	1790	17	1769	31
66744_TRA_Data	110a	5097	31385	5696	78692	0.1112	0.0006	4.8105	0.0968	0.3137	0.0063	0.96	97	1819	10	1787	17	1759	31
~~66768_TRA_Data~~	~~68~~	~~5743~~	~~31763~~	~~0~~	~~119263~~	~~#VALUE!~~	~~#VALUE!~~	~~#VALUE!~~	~~#VALUE!~~	~~#VALUE!~~	~~#VALUE!~~	~~#VALUE!~~	~~#VALUE!~~	~~#NUM!~~	~~#NUM!~~	~~#VALUE!~~	~~#VALUE!~~	~~#VALUE!~~	~~#VALUE!~~

Strike through: data not used

Appendix 4: Micro-XRF elemental mappings. The element and its colour indicated in the lower left corner of each figure.